Goal-Oriented Adaptivity using Unconventional Error Representations

Vincent Darrigrand

Supervised by *David Pardo* and *Hélène Barucq*

Co-tutelage between *UPV-EHU* and *UPPA*

May 2017

Acknowledgements

First of all, my entire gratitude goes to Prof. Fernando Cossio, President of Ikerbasque[1] who made this Ph.D. possible. In particular, I welcome his courage for his help towards me and others during a tough period.

I am extremely thankful for Prof. David Pardo's outstanding advisor-ship. I especially enjoyed learning from his experience and intuition that had almost never failed. He gave me many opportunities to enjoy my journey through the elaboration of this Ph.D. dissertation. I greet him for the access to his wide network of worldwide collaborations. As a result, I was able to work in Valparaíso, Chile, for half a year, which has been one of the highlights of my Ph.D. training period.

I also thank Dr. Hélène Barucq for her support and help, especially during my one-year ATER position stay at the University of Pau. I had several enlightening conversations with Dr. Barucq and her collaborators, and my stay at Univ. of Pau was greatly rewarding both from a personal and a professional point of view.

I am grateful to Prof. Ignacio Muga for his involvement in the scientific work presented in this document and for his warm and helpful welcoming in Valparaíso. I enjoyed the work times as much as the "barbacoa/carrete" times.

I express my gratitude to Prof. Serge Prudhomme and Albert Romkes for the fruitful ongoing scientific discussions on the topic of this work.

Finally, I wish to thank all the colleagues from the various teams I have been part of, from the M^{2}SI group to the INRIA Magique 3D team, and to Valparaíso IMA for their friendship and support. In particular, I thank Dr. Ángel Rodríguez-Rozas for his inestimable help and patience solving my coding struggles, as well as Dr. Théophile Chaumont-Frelet for his coding strict policies and his endless advice "on the fly"; Florian Fauchet for the discussions on Tikz/PGF graphics puzzles that ended in the creation of the short course "How to improve scientific drawings with Tikz/pgf"; Dr. Julen Alvarez for his help and support on many aspects during the whole period.

This dissertation would not have been possible without the financial support of the following projects: Projects of the Spanish Ministry of Economy and Competitiveness with reference MTM2013-40824-P, MTM2016-76329-R

[1] `http://www.ikerbasque.net`

(AEI/FEDER, EU), MTM2016-81697-ERC and the Basque Government Consolidated Research Group Grant IT649-13 on "Mathematical Modeling, Simulation, and Industrial Applications (M2SI)"; BCAM "Severo Ochoa" accreditation of excellence SEV-2013-0323 and the Basque Government through the BERC 2014-2017 program; the European Union's Horizon 2020, research and innovation program under the Marie Sklodowska-Curie grant agreement Nº 644202.

Abstract

In Goal-Oriented Adaptivity (GOA), the error in a Quantity of Interest (QoI) is represented using global error functions of the direct and adjoint problems. This error representation is subsequently bounded above by element-wise error indicators that are used to drive optimal refinements.

In this work, we propose to replace, in the error representation, the adjoint problem by an alternative operator. The main advantage of the proposed approach is that, when judiciously selecting such alternative operator, the corresponding upper bound of the error representation becomes sharper, leading to a more efficient GOA.

These representations can be employed to design novel h, p, and hp energy-norm and goal-oriented adaptive algorithms.

While the method can be applied to a variety of problems, in this Dissertation we first focus on one-dimensional (1D) problems, including Helmholtz and steady state convection-dominated diffusion problems.

Numerical results in 1D show that for the Helmholtz problem, it is advantageous to select the Laplace operator for the alternative error representation. Specifically, the upper bounds of the new error representation are sharper than the classical ones used in both energy-norm and goal-oriented adaptive methods, especially when the dispersion (pollution) error is significant.

The 1D steady state convection-dominated diffusion problem with homogeneous Dirichlet boundary conditions exhibits a boundary layer that produces a loss of numerical stability. The new error representation based on the Laplace operator delivers sharper error upper bounds. When applied to a p-GOA, the alternative error representation captures earlier the boundary layer, despite the existing spurious numerical oscillations.

We then focus on the two- and three-dimensional (2D and 3D) Helmholtz equation. We show via extensive numerical experimentation that the upper bounds provided by the alternative error representations are sharper than the classical ones. When using the alternative error indicators, a naive p-adaptive process converges, whereas under the same conditions, the classical method fails and requires the use of the so-called Projection Based Interpolation (PBI) operator or some other technique to regain convergence. We also provide guidelines for finding operators delivering sharp error representation upper bounds.

Abstract

Similar results stand for a 2D convection-dominated diffusion problem as well as for 2D problems with discontinuous material coefficients. Finally, we consider a sonic Logging While Drilling (LWD) problem to illustrate the applicability of the proposed method.

Resumen

En un contexto de adaptatividad orientada a un objetivo, el error en una cantidad de interés está representado a través de los errores globales de los problemas directo y adjunto. Esta representación del error se acota superiormente por una suma de indicadores de error de cada elemento. Estos se utilizan para producir refinamientos óptimos.

En este trabajo, proponemos representar el error del problema adjunto utilizando un operador alternativo. La principal ventaja de nuestro enfoque es que cuando se elige correctamente dicho operador alternativo, la correspondiente cota superior se vuelve más cercana al error en la cantidad de interés, lo que permite una adaptatividad más eficiente.

Estas representaciones pueden ser utilizadas para diseñar algoritmos adaptativos en h, p o hp, basados en la norma de la energía o para aproximar una cantidad de interés específica.

Aunque el método propuesto se puede aplicar a una amplia gama de problemas, en esta tesis doctoral nos centramos primero en problemas unidimensionales (1D), tales como el problema de Helmholtz y el problema estacionario de convección-difusión con convección dominante.

Los resultados numéricos en 1D muestran que, para los problemas de propagación de ondas, las ventajas de este método son notorias cuando se considera el operador de Laplace para la representación del error. Específicamente, las cotas superiores derivadas de la nueva representación son más cercanas a la cantidad de interés que las del método convencional. Esto es cierto tanto para la norma de la energía global como para una cantidad de interés particular, especialmente cuando el error de dispersión es significativo.

El problema estacionario 1D de convección-difusión con convección dominante y con condiciones de Dirichlet homogéneas tiene una capa límite que produce una pérdida de estabilidad numérica. La nueva representación del error proporciona cotas superiores más cercanas a la cantidad de interés. Cuando se aplica a un algoritmo adaptativo en p orientado a un objetivo, la representación alternativa del error captura antes la capa límite, a pesar de las existentes oscilaciones numéricas no físicas.

En esta tesis doctoral, también nos centramos en la ecuación de Helmholtz en dos y tres dimensiones (2D y 3D). Mostramos a través de múltiples experimentos numéricos que las cotas superiores proporcionadas por las representaciones

alternativas del error son más cercanas a la cantidad de interés que cuando uno considera la representación clásica. Al utilizar los indicadores alternativos del error, un algoritmo adaptativo en p sencillo converge, mientras que en las mismas condiciones, el método convencional falla y requiere el uso de operadores de proyección o de otras técnicas para recuperar la convergencia. En este trabajo, también determinamos operadores que proporcionan representaciones del error que inducen cotas superiores más ajustadas.

Establecemos resultados similares tanto para el problema estacionario de convección-difusión con convección dominante en 2D como para problemas 2D con materiales discontinuos. Finalmente, se considera un problema sónico en pozos petrolíferos para ilustrar la aplicabilidad del método propuesto.

Résumé

Dans un contexte d'adaptabilité ciblée, l'erreur commise sur une quantité d'intérêt peut être représentée grâce aux erreurs globales des problèmes direct et adjoint. Cette représentation de l'erreur est majorée par la somme des indicateurs d'erreurs élémentaires. Ces derniers sont alors utilisés pour produire des raffinements de maillage optimaux.

Dans ces travaux, nous proposons de représenter l'erreur du problème adjoint via un opérateur alternatif. L'avantage principal de notre approche est que lorsque l'on choisit correctement l'opérateur alternatif, la majoration correspondante de l'erreur à la quantité d'intérêt devient plus précise, pour autant l'adaptabilité issue de l'utilisation de ces nouveaux indicateurs s'en trouve améliorée.

Ces représentations peuvent être employées pour concevoir des algorithmes adaptatifs en espace (h), en ordre d'approximation (p) ou les deux (hp), basés sur la norme d'énergie ou bien ciblés sur une quantité d'intérêt.

Bien que la méthode puisse être appliquée à une large gamme de problèmes, nous nous concentrons tout d'abord sur des problèmes unidimensionnels (1D), comme le problème d'Helmholtz et le problème de convection-diffusion stationnaire à convection dominante.

Les résultats numériques en 1D montrent que, pour les problèmes de propagation d'ondes, les avantages de notre méthode sont notoires lorsque l'on considère l'opérateur de Laplace pour la représentation de l'erreur. Plus précisément, les majorations issues de la nouvelle représentation sont plus précises que celles provenant de la méthode classique et ce si l'on considère l'énergie globale ou bien une quantité d'intérêt particulière. Le phénomène est d'autant plus notable lorsque l'erreur de dispersion (pollution) est significative.

Le problème 1D de convection-diffusion stationnaire à convection dominante avec des conditions limites de Dirichlet homogènes présente une couche limite qui produit une perte de stabilité numérique. La nouvelle représentation d'erreur délivre des majorations plus précises. Lorsqu'appliquée à une p-adaptabilité ciblée, la représentation d'erreur alternative permet une capture plus efficace la couche limite, malgré les oscillations numériques parasites existantes.

Devant ces résultats encourageants, nous nous penchons sur l'équation d'Helmholtz à deux et trois dimensions (2D et 3D). Nous montrons, au travers

de multiples simulations numériques, que les majorations fournies par les représentations d'erreur alternatives sont plus précises que celle de la représentation classique. Lorsque l'on utilise les indicateurs d'erreur alternatifs, un processus naïf de p-adaptabilité ciblée converge, tandis que dans les mêmes conditions, la méthode classique échoue et requiert l'utilisation d'un opérateur de projection ou d'autre techniques pour récupérer la convergence. Dans ce travail, nous fournissons également des directives pour déterminer les opérateurs qui fournissent des représentations d'erreur induisant de majorations précises.

Des résultats similaires sont aussi établis tant pour un problème 2D de convection-diffusion stationnaire à convection dominante que pour des problèmes 2D ayant des coefficients de matériaux discontinus. Nous considérons un problème de diagraphie ultra-sonique en cours de forage pour illustrer l'applicabilité de la méthode proposée.

Contents

List of Figures

1. Introduction

In Finite Element Methods (FEMs), it is often necessary to design meshes with a large number of Degrees of Freedom (DoF) to obtain highly accurate solutions. Since computational resources are limited, it is customary to build discretizations that require the smallest possible number of DoF to achieve a given tolerance error. As a result, mesh-adaptive finite element algorithms arose during the last decades for solving various engineering problems (e.g., [1, 2, 3]).

While adaptive algorithms were first designed to accurately approximate the energy-norm of a problem [4, 5], many engineering applications require a good approximation of a specific Quantity of Interest (QoI). An energy-norm driven self-adaptive strategy can still be used for that purpose, although it often becomes sub-optimal and unable to provide an accurate solution for the required QoI in a reasonable amount of time.

For example, in [6, 7] authors deal with a problem in which electromagnetic fields are measured at a receiver antenna in a lossy media. In that situation, the amplitude of the measurement is several orders of magnitude smaller at the receiver than at the source, because of the energy dissipation through the medium. Thus, a small relative error of the solution in the energy-norm may not imply a small relative error at the receiver. Examples in [6, 7] show that the classical energy-norm adaptive approach may procure relative errors of the QoI surpassing 15%, whereas the global energy-norm error is below 0.01%.

1.1. Developments and Applications of Goal-Oriented Adaptivity

The origin of the Goal-Oriented Adaptivity (GOA) is in the works of Rannacher et al. [8, 9, 10] followed by the works of Peraire, Patera et al. [11, 12, 13, 14, 15, 16] on *a posteriori* error estimates of the error in the QoI. The works of Prudhomme and Oden [17, 18, 19, 20] formulated the goal-oriented error estimation procedure based on representing the error in the QoI in terms of global functions defined over the entire computational domain. This error representation is subsequently bounded by the sum of local indicators that are used for the adaptive process.

There exist numerous engineering applications that motivate the use of GOA, including electromagnetics [21, 7, 22, 23, 24], structural problems and viscoelasticity [25, 26, 27, 28, 29], fluid-structure interactions [30, 31, 32], and control theory [33, 34, 35]. Apart from these applications, convergence properties of GOA have also been recently studied in [36, 37, 38, 39, 40]. In the following, we detail some of the main developments of GOA concerning these applications.

1.1.1. Application to structural problems

The first applications of the method to structural problems were published in 2000 and 2001 by J.T. Oden and K.S. Vemaganti in [41, 42], and they were based on the previous works of J.T. Oden & S. Prudhomme [17, 19]. Authors developed the theory and methodologies of goal-oriented adaptive modeling of heterogeneous materials. From there, J.T. Oden and his collaborators, S. Prudhomme, D. Fuentes, D. Littlefield, A. Romkes developed a series of applications on structural problems: In [43], authors extended the GOA to discrete lattices models. In [44], authors considered a class of problems with axisymmetric deformations of layered elastomer-reinforced shells-of-revolution subjected to shock loading, and an extension of [41, 42] to problems in elastostatics of heterogeneous materials was published in [45], where the material properties are given as functions of random variables with known probability distribution density functions.

P. Ladevèze and his collaborators, L. Chamoin, J. Panetier, J. Waeytens, F. Pled developed tools (based on constitutive relation error) for the GOA in the scope of structural problems such as viscoelasticity, fracture mechanics, and transient viscodynamics: they developed error bounds of outputs of interest for linear viscoelasticity [46, 47, 48]. Consequently, they obtained a "non-intrusive" technique to solve the adjoint problem through a partition of unity method [49, 50]. A strategy to handle nonlinear point-wise QoI to obtain strict error bounds without linearization was developed in [51] and extended to fracture mechanics problems solved by means of XFEM [25], and to transient viscodynamics [26]. They also revisited and improved the bounding techniques with tools that lean on the Saint-Venant principle [52].

In 2012, C. Jhurani and L. Demkowicz developed and implemented a framework for numerical homogenization and GOA for nonlinear lattice elasticity problems. The method requires the Moore-Penrose pseudo-inverse of element stiffness matrices [27, 28].

1.1.2. Application to electroacoustic and electromagnetic problems

A *hp* GOA strategy was developed by P. Solin and L. Demkowicz in [53]. Its first use in [54] provided not only an application to electromagnetics but also a verification of the method. D. Pardo, L. Demkowicz, C. Torres-Verdín, L. Tabarovsky, M. Paszynski and C. Michler applied it to electrostatics and electrodynamics in the works [21, 7, 22]. They simulated measurements obtained by an alternate current resistivity logging instrument in a borehole environment surrounded by steel casing for the assessment of rock formation properties. In [55], authors combined the Perfectly Matched Layer (PML) with the GOA in the same framework. They showed that this combination enables to significantly reduce the size of the computational domain with substantial savings in computer time and memory. In the same framework, [56, 57] developed an *hp*-GOA with shared data structures and a parallel multi-frontal direct solver.

In 2007, *hp*-GOA was applied to the simulation of electromagnetic waveguides in [58, 59]. [60] provided a comparison between energy-norm and goal-oriented based automatic *hp*-adaptive processes. [61] presented the same work but in the context of open region electromagnetic problems. A multigoal-oriented adaptive strategy for *hp*-FEM was developed in [23]. This adaptive strategy delivered a single optimal *hp*-grid intended to approximate simultaneously the solution of multiple QoI and has been applied to invert magnetotelluric measurements [24]. K. Key and J. Ovall developed a parallel goal-oriented adaptive FEM that can be used to rapidly compute highly accurate solutions for 2.5D controlled-source electromagnetic and 2D magnetotelluric problems [62]. L. M. Steffens et al. illustrated in [63] a new refinement strategy for the Helmholtz equation based on *a posteriori* estimations of the numerical wave number developed in [64].

1.1.3. Applications to fluid-structure interactions

Among the first works that introduced the GOA to simulate and explain fluid-structure interactions, we find [65, 66]. K.G. Van der Zee developed his Ph.D. dissertation on this subject [67]. In collaboration with E. H. Van Brummelen, P. W. Fick, C.V. Verhoosel, and J.T. Oden, among others, K.G. Van der Zee explored different aspects of the integration of the GOA by considering problems of fluid-structure interactions. In [68], they developed a goal-oriented error estimator for finite element discretizations of a fluid-structure interaction problem: the steady Stokes flow in a 2D channel where part of the channel wall is flexible. They addressed, in [69], a complication in the application of

GOA to fluid-structure interaction problems: the treatment of the interface conditions has non-trivial consequences for the properties of the dual problem. They also used goal-oriented error estimation and adaptivity in the scope of free-boundary problems [70, 71]. In [32], they considered goal-oriented error estimation in the scope of free-boundary problems using isogeometric analysis. They developed *a posteriori* estimates of errors in the QoI for the nonlinear system of evolution equations embodied in the Cahn-Hilliard model of binary phase transition [31]. Finally, [30] presented rigorous derivations of exact linearized adjoints for a coupled fluid-structure problem. This allows the direct application of the established goal-oriented error estimation framework.

1.1.4. Application to control theory

In the scope of optimal control of Partial Differential Equations (PDEs), the goal-oriented dual weighted approach was applied to unconstrained problems in [72, 73], to control constrained ones in [74, 75, 76] and to state constrained problems in [77, 75]. More recent works have been published about the Dual Weighted approach and the application to control theory: (a) [78] developed a combined *a posteriori* analysis for the discretization and iteration errors in the computation of finite element approximations to elliptic boundary value problems. The emphasis was on the multi-grid method. The underlying theoretical framework was that of the Dual Weighted Residual (DWR) method for goal-oriented error estimation; (b) [79] presented a general strategy for designing adaptive space-time finite element discretizations of the non-stationary Navier-Stokes equations; (c) [80] developed, analyzed and implemented the goal-oriented weighted dual approach to mixed control-state constrained distributed optimal control problems for linear second order elliptic boundary value problems; (d) [35] derived primal-dual weighted goal-oriented a posteriori error estimates for point-wise state constrained optimal control problems for second order elliptic partial differential equations. (e) [34] studied a DWR approach for goal-oriented adaptive finite elements for a class of optimal control problems for elliptic variational inequalities. The development is based on the concept of C-stationarity; (f) [33] developed an adaptive algorithm for solving elliptic optimal control problems with simultaneously appearing state and control constraints.

1.1.5. Convergence analysis

In 2009, goal-oriented adaptive methods were usually not proven to converge. An exception is a method from [81], in which adaptivity was purely driven by the minimization of the energy-norm of the error in the dual problem.

Another exception is the goal-oriented method from [82]. Few works have been produced since then: (a) In [39], an adaptive finite element method was analyzed for approximating functionals of the solution of symmetric elliptic second order boundary value problems. (b) [38] developed a convergence theory for a class of goal-oriented adaptive finite element algorithms for second order non-symmetric linear elliptic equations. (c) [37] developed a convergence theory for a class of goal-oriented adaptive finite element algorithms for second order semilinear elliptic equations. These last two results were gathered in S. Pollock's thesis [36]. One of the most recent developments on the topic was due to M. Feischl, D. Praetorius and K.G. Van Der Zee [40], who performed an abstract analysis of optimal GOA.

1.2. Goal Oriented Adaptive algorithms

GOA algorithms iterate along the following steps. Given an initial coarse mesh, they estimate the error either using an *a posteriori* error technique [11, 13, 14, 15, 16, 83, 84, 12, 14] or by approximating it over a finer mesh [55, 85, 55, 23, 56]. Then, the error in the QoI is represented via the global error functions of the original and adjoint problems. Such global representation expresses how much the error in a particular point is affecting to the error in the QoI. The exact solution of the adjoint problem (*influence function*) alone is insufficient to drive refinements since an enrichment (refinement) on the discrete space does not guarantee a decrease of the influence function error at any particular point. However, one may build an element-wise based upper bound in terms of local norms whose energy decreases as refinements occur. This upper bound can be used to drive refinements: one simply enriches those elements that will reduce most that upper bound per added DoF. In this way, the next coarse grid is built, and the entire process is iterated until a given tolerance error is reached.

For symmetric and positive definite problems, the energy-norm approach becomes a particular case of the goal-oriented one that corresponds to the situation in which the QoI and the load vector of the original problem coincide, as it occurs in several waveguide problems, e.g. [60, 58].

Different strategies were devised to obtain sharp upper bounds of an error representation. For example, in [17], authors introduced a scalar parameter intended to improve the sharpness of the bound. In [86], the author introduced dual estimators of the functional error that are based on dual residual weighting and on dual error estimate weighting. These estimators are asymptotically exact with respect to the error in the QoI.

1.3. Main contribution

In this work, we start with the methodology presented in [17], referred to as the *classical* GOA method. It employs the dual residual to derive upper bounds of the error in the QoI, and thus, indicators for the adaptive process. However, we depart from the classical approach by introducing an alternative dual operator exhibiting better properties than the original one (e.g. positive definiteness) for the representation of the error in the QoI, so the corresponding error upper bounds (sum of indicators) become sharper than the classical ones. This new methodology generalizes the classical one. In particular, when the alternative dual operator coincides with the adjoint operator, we recover the error upper bounds of the classical goal-oriented method.

The main contribution of this dissertation is to demonstrate that a proper choice of such alternative operator may improve the upper bounds of the error representation. As a result, the adaptive algorithm arising from the new error representation is more efficient when compared to a classical one. Extensive numerical results in 1D, 2D, and 3D are illustrated using uniform h- and p-refinements, as well as a simple self-adaptive goal-oriented p-refinement strategy.

This dissertation merges the results from our publications [87, 88, 89]. In [87], we described the method for general 1D, 2D, and 3D problems, and we illustrated it numerically with a 1D-Helmholtz example. A convergent p-adaptive algorithm was obtained either: (a) by combining the classical indicators and the Projection Based Interpolation (PBI) [90, 91, 85], or (b) by using the alternative indicators (with or without PBI). We selected the Helmholtz equation for several reasons: this equation is widely used in applications having a transmitter-receiver structure where goal-oriented strategies are often needed; the traditional weak Helmholtz bilinear form is not positive definite; and the discrete solution is known to be numerically unstable for high wavenumber because of dispersion errors and pollution effects [92, 93, 94, 95, 1, 96, 97, 98, 99].

In [88], we extended those results to the case of 1D convection-dominated diffusion problems, where numerical instabilities occur due to the presence of a boundary layer [100, 2]. Thus, the main contribution of this publication was to study the effect of the alternative error representation for the case of 1D convection-dominated diffusion problems with the classical FEM. It is well-known that the rapid capture of boundary layers is essential to regain stability, e.g. [101, 102, 103, 104, 105]. Numerical results show that our proposed strategy captures such layers faster than the classical GOA method.

Finally, in [89], we extended our numerical results to the 2D and 3D cases and applied them to Helmholtz and convection-dominated diffusion problems

for continuous and discontinuous coefficients. We also showed that finding, in general, the operator that provides the sharpest possible bound is prohibitively expensive, and we provided a feasible alternative operator that delivers quite sharp upper bounds. Finally, a sonic Logging While Drilling (LWD) problem was selected to illustrate the applicability of the proposed method.

1.4. Organization of the dissertation

The remainder of the dissertation is organized as follows: Chapter 2 formulates our new methodology and compare it to the classical approach. Chapter 3 describes the adaptive algorithms used to produce the numerical results. Chapter 4 is devoted to numerical results for the 1D case, both for a Helmholtz problem and a convection-dominated diffusion problem. Chapter 5 analyzes multiple 2D and 3D numerical results for Helmholtz and convection-dominated diffusion problems with continuous and discontinuous material coefficients. A sonic geophysical borehole application is described in Chapter 6. The main achievements are described in chapter 7 and the main conclusions and future works are stated in Chapter 8. This dissertation also contains Appendix A that describe a reformulation of the proposed error representations in terms of bilinear forms.

Part I.

Description of the error representations and algorithms

2. Abstract formulation and unconventional error representations

In this chapter, we first introduce the notations and the abstract formulation used in the rest of the document. Then, we describe the classical goal-oriented error representation, which allows us to introduce an unconventional error representation by selecting an alternative operator. We discuss the challenges that arise when searching for the optimal alternative operator. Finally, we introduce the general model problem that will be used for the numerical experiments.

2.1. General abstract setting

Given a domain $D \subset \mathbb{R}^n$, $\mathbb{H}(D)$ denotes a Hilbert space of functions defined over D, endowed with the norm $\|\cdot\|_{\mathbb{H}(D)}$.

Let $\Omega \subset \mathbb{R}^n$ be the physical domain of our problem of interest. Let $\mathcal{T}$ be a partition of Ω into open elements K such that $\bar{\Omega} = \bigcup_{K\in\mathcal{T}} \bar{K}$.

We work with a Hilbert space $\mathbb{H}(\Omega)$ having the following property: If $w \in \mathbb{H}(\Omega)$, then its restriction w_K to any open element $K \in \mathcal{T}$ satisfies $w_K \in \mathbb{H}(K)$. We define the restriction $R_K : \mathbb{H}(\Omega) \to \mathbb{H}(K)$ such that $R_K(v) = v_K, \forall v \in \mathbb{H}(\Omega)$. From now on, we will use the simplified notation $\mathbb{H} := \mathbb{H}(\Omega)$ and $\mathbb{H}_K := \mathbb{H}(K)$. We denote by $\mathbb{H}^*$ the space of continuous linear forms from $\mathbb{H}$ to $\mathbb{K}$ ($\mathbb{R}$ or $\mathbb{C}$) and $\mathbb{H}_K^*$ the space of continuous linear forms from $\mathbb{H}_K$ to $\mathbb{K}$.

A bounded linear operator $B \in \mathcal{L}(\mathbb{H}, \mathbb{H}^*)$ is said to be localizable if, for any $K \in \mathcal{T}$, there exists $B_K \in \mathcal{L}(\mathbb{H}_K, \mathbb{H}_K^*)$ such that:

$$\langle Bw, v\rangle_{\mathbb{H}^*,\mathbb{H}} = \sum_{K\in\mathcal{T}} \langle B_K \circ R_K w, R_K v\rangle_{\mathbb{H}_K^*,\mathbb{H}_K} = \sum_{K\in\mathcal{T}} \langle B_K w_K, v_K\rangle_{\mathbb{H}_K^*,\mathbb{H}_K} .$$

In other words, $B = \sum_{K\in\mathcal{T}} R_K^* \circ B_K \circ R_K$ where R_K^* is the adjoint of R_K.

Remark: It is straightforward to show that if $B : \mathbb{H} \to \mathbb{H}^*$ is localizable, then the formal adjoint operator $B^* : \mathbb{H} \to \mathbb{H}^*$ is also localizable and $B^* = \sum_{K\in\mathcal{T}} R_K^* \circ B_K^* \circ R_K$.

2.2. Formulation of the error representations

2.2.1. Classical goal-oriented formulation

Consider a loading form $f \in \mathbb{H}^*$ and a Quantity of Interest (QoI) $l \in \mathbb{H}^*$. Let $\mathbb{H}_h \subset \mathbb{H}$ be a conforming finite element subspace associated with partition $\mathcal{T}$. Let $B \in \mathcal{L}(\mathbb{H}, \mathbb{H}^*)$ be a localizable operator such that there exists a unique solution for both continuous and discrete direct and dual problems:

> Find $u \in \mathbb{H}$ and $u_h \in \mathbb{H}_h$ such that
>
> $$Bu = f \quad \text{in } \mathbb{H}^* \tag{2.1}$$
> $$\langle Bu_h, w_h \rangle_{\mathbb{H}^*,\mathbb{H}} = \langle f, w_h \rangle_{\mathbb{H}^*,\mathbb{H}}, \quad \forall w_h \in \mathbb{H}_h. \tag{2.2}$$

and

> Find $v \in \mathbb{H}$ and $v_h \in \mathbb{H}_h$ such that
>
> $$B^*v = l \quad \text{in } \mathbb{H}^* \tag{2.3}$$
> $$\langle B^*v_h, w_h \rangle_{\mathbb{H}^*,\mathbb{H}} = \langle l, w_h \rangle_{\mathbb{H}^*,\mathbb{H}}, \quad \forall w_h \in \mathbb{H}_h. \tag{2.4}$$

The errors in the approximations of the direct and adjoint problems are defined as $e = u - u_h$ and $\varepsilon = v - v_h$, respectively. One can also represent these errors as solutions of the following variational problems:

> - Find $e \in \mathbb{H}$ such that
>
> $$Be = f - Bu_h =: \mathcal{R}_p(u_h). \tag{2.5}$$
>
> - Find $\varepsilon \in \mathbb{H}$ such that
>
> $$B^*\varepsilon = l - B^*v_h =: \mathcal{R}_d(v_h). \tag{2.6}$$

Functionals $\mathcal{R}_p(u_h), \mathcal{R}_d(v_h) \in \mathbb{H}^*$ are known as the primal and dual residuals, respectively.

Evaluating (2.6) at e, using Galerkin's orthogonality and the localization property of B, we obtain

$$\langle l\,, e \rangle_{\mathbb{H}^*,\mathbb{H}} = \langle \mathcal{R}_d(v_h)\,, e \rangle_{\mathbb{H}^*,\mathbb{H}} = \langle B^*\varepsilon\,, e \rangle_{\mathbb{H}^*,\mathbb{H}} = \sum_{K \in \mathcal{T}} \langle B_K^*\varepsilon_K\,, e_K \rangle_{\mathbb{H}_K^*,\mathbb{H}_K} \tag{2.7}$$

Thus, an upper bound of the error in the QoI is given as follow:

$$\left|\langle l\,,e\rangle_{\mathbb{H}^*,\mathbb{H}}\right| \leqslant \sum_{K\in\mathcal{T}}\left|\langle B_K^*\varepsilon_K\,,e_K\rangle_{\mathbb{H}_K^*,\mathbb{H}_K}\right| = \sum_{K\in\mathcal{T}}\eta_K =: \eta_{\mathcal{T}}, \tag{2.8}$$

where $\eta_K := \left|\langle B_K^*\varepsilon_K\,,e_K\rangle_{\mathbb{H}_K^*,\mathbb{H}_K}\right|$. This bound will be referred to as the *classical bound*.

2.2.2. Alternative representations

The key idea proposed here is to use alternative representations of the residuals $\mathcal{R}_d(v_h)$ or $\mathcal{R}_p(u_h)$. Let $\widetilde{B}\in\mathcal{L}(\mathbb{H},\mathbb{H}^*)$ be a localizable invertible operator. We define the alternative dual error representation as the solution of the linear equation:

> Find $\widetilde{\varepsilon}\in\mathbb{H}$ such that
>
> $$\widetilde{B}\,\widetilde{\varepsilon} = \mathcal{R}_d(v_h). \tag{2.9}$$

Analogously, we define the alternative primal error representation as the solution of the linear equation:

> Find $\widetilde{e}\in\mathbb{H}$ such that
>
> $$\widetilde{B}\,\widetilde{e} = \mathcal{R}_p(u_h). \tag{2.10}$$

For simplicity, we use the same operators for the construction of the alternative direct and dual errors. However, it is possible to select different representations for each error. Following the same procedure as in Eqs. (2.7) and (2.8), we obtain the alternative bound of the error in the QoI,

$$\left|\langle l\,,e\rangle_{\mathbb{H}^*,\mathbb{H}}\right| \leqslant \sum_{K\in\mathcal{T}}\left|\left\langle \widetilde{B}_K\widetilde{\varepsilon}_K\,,e_K\right\rangle_{\mathbb{H}_K^*,\mathbb{H}_K}\right| = \sum_{K\in\mathcal{T}}\widetilde{\eta}_K =: \widetilde{\eta}_{\mathcal{T}} \tag{2.11}$$

where $\widetilde{\eta}_K := \left|\left\langle \widetilde{B}_K\widetilde{\varepsilon}_K\,,e_K\right\rangle_{\mathbb{H}_K^*,\mathbb{H}_K}\right|$. One can alternatively make use of the primal error representation $\widetilde{e}$ to obtain the bound:

$$\left|\langle l\,,e\rangle_{\mathbb{H}^*,\mathbb{H}}\right| \leqslant \sum_{K\in\mathcal{T}}\left|\left\langle \widetilde{B}_K\widetilde{e}_K\,,\varepsilon_K\right\rangle_{\mathbb{H}_K^*,\mathbb{H}_K}\right|. \tag{2.12}$$

The method presented here is indeed a generalization of the classical Goal-Oriented Adaptivity (GOA), that is recovered by simply selecting $\widetilde{B} = B^*$ in Eq. (2.11) or $\widetilde{B} = B$ in Eq. (2.12).

Numerical results (see Figure 5.7) show that upper bounds given by Eqs. (2.11) and (2.12) are often similar. Hence and for simplicity, in the following we will consider Eq. (2.11), disregarding Eq. (2.12).

An interesting case occurs when $\widetilde{B}$ defines a scalar product on $\mathbb{H}$, then the alternative error representation is the *Riesz representation* of the residual. Additionally, if each local counterpart $\widetilde{B}_K$ of $\widetilde{B}$ is self-adjoint and semi-positive definite, operator $\widetilde{B}_K$ defines a semi-inner product on $\mathbb{H}_K$ and we can take additional Cauchy-Schwarz inequalities on (2.11), i.e.,

$$\widetilde{\eta}_{\mathcal{T}} \leqslant \sum_{K\in\mathcal{T}} \sqrt{\left\langle \widetilde{B}_K \widetilde{\varepsilon}_K \,,\, \widetilde{\varepsilon}_K \right\rangle_{\mathbb{H}_K^*,\mathbb{H}_K}} \sqrt{\left\langle \widetilde{B}_K e_K \,,\, e_K \right\rangle_{\mathbb{H}_K^*,\mathbb{H}_K}}. \tag{2.13}$$

From the mathematical standpoint, using upper bounds $\eta_{\mathcal{T}}$ or $\widetilde{\eta}_{\mathcal{T}}$ is controversial. First, because in the "Classical bound" (2.8), the operator of the problem can be indefinite, as for the Helmholtz equation, and one cannot ensure that uniform grid refinements will monotonically reduce that bound unless, in the case of a Helmholtz problem, the grid is assumed to be sufficiently small with respect to the wavenumber, so the problem at the element level becomes positive semi-definite. Even in this last situation, the associated cosine of the angle between e and ε can still behave erratically under mesh refinements. A similar problem can be diagnosed with bound (2.11) since the cosine of the angle between e and $\widetilde{\varepsilon}$ cannot be controlled under mesh refinements.

Stable upper bounds can be easily derived, as shown in Eq. (2.13). However, practitioners often employ error bound (2.8) (despite the fact that it is mathematically unstable), since it is sharper than the stable upper bounds and frequently provides better results [21, 22]. In here, we follow this practical approach, and we compare upper bounds (2.8) vs (2.11).

In the remainder of this dissertation, we will display the error values and their upper bounds relatively to $\langle l \,,\, u \rangle_{\mathbb{H}^*,\mathbb{H}}$ in percent (unless specified).

2.2.3. Optimal alternative operator

The sharpest bound is obtained by an operator for which the triangle inequality in Equation (2.11) becomes an equality, namely:

$$\left| \langle l \,,\, e \rangle_{\mathbb{H}^*,\mathbb{H}} \right| = \left| \sum_{K\in\mathcal{T}} \left\langle \widetilde{B}_K \widetilde{\varepsilon}_K \,,\, e_K \right\rangle_{\mathbb{H}_K^*,\mathbb{H}_K} \right| = \sum_{K\in\mathcal{T}} \left| \left\langle \widetilde{B}_K \widetilde{\varepsilon}_K \,,\, e_K \right\rangle_{\mathbb{H}_K^*,\mathbb{H}_K} \right|. \tag{2.14}$$

This implies that for all elements $K \in \mathcal{T}$, the complex quantities

$$\left\langle \widetilde{B}_K \widetilde{\varepsilon}_K \, , e_K \right\rangle_{\mathbb{H}_K^*, \mathbb{H}_K}$$

are sharing the same angle. Moreover, each estimator needs to share the same angle of $\langle l \, , e \rangle_{\mathbb{H}^*, \mathbb{H}}$. To simplify, let us assume that they are all positive real numbers. Then, we have to find an operator $\widetilde{B}$ such that the element-wise application $\widetilde{B}_K \widetilde{\varepsilon}_K \in \mathbb{H}_K^*$ has to compensate the variations of e_K in order to obtain a positive real number after integration. The consequence is that operator $\widetilde{B} = \sum_{K \in \mathcal{T}} R_K^* \circ \widetilde{B}_K \circ R_K$ has to be defined on each element according to e_K. It will probably occur that, if it exists, $\widetilde{B}$ will not be a conventional variational form, which will make much more complex the implementation of the method. Thus, in this work, rather than searching for the optimal operator, we shall concentrate on finding the best possible operator within a preset family via numerical experimentation.

2.3. Model problem: convection, diffusion, reaction

In this document, we illustrate the use of the error estimators presented above on a problem governed by a diffusion-convection-reaction equation. We consider the following general model problem. Let Ω be a domain of dimension $d \in \{1, 2, 3\}$.

> Find u such that, for $\beta \in (L^2(\Omega))^d$, $\alpha, \gamma \in L^2(\Omega)$,
>
> $$- \nabla(\alpha \cdot \nabla u) + \beta \cdot \nabla u + \gamma u = g \quad \text{on } \Omega. \tag{2.15}$$

In particular, for $\beta = 0$ and $\gamma < 0$, we obtain Helmholtz equation and for $\gamma = 0$, $\|\alpha\|_{L^2(\Omega)} \ll \|\beta\|_{L^2(\Omega)^d}$, we recover a convection-dominated diffusion problem. The boundary conditions will be specified for each particular case.

3. Goal-oriented algorithm

In this chapter, we describe the goal-oriented algorithm we employed to obtain numerical results. First, we describe the main structure of the adaptive algorithm, and then we detail its variations employed to compute the fine meshes, the errors, and the element marking strategies.

3.1. Goal-Oriented Adaptivity (GOA) algorithm

The GOA algorithm is sketched in Figure 3.1. We start the iterative mesh-adaptation algorithm by defining an initial coarse mesh with a given element size h and polynomial order p set globally. In order to estimate the error functions, we approximate it by considering a fine (reference) mesh. There are various ways to define the fine mesh; we postpone this discussion to Section 3.2. We approximate errors e and ε (resp. $\widetilde{\varepsilon}$) of the direct (2.1) and the adjoint (2.3) (resp. alternative adjoint (2.9)) problems on the fine mesh. In the following, we refer to the approximation on the fine mesh of the errors by the notations e and ε (resp. $\widetilde{\varepsilon}$). Further details on the errors computations are provided in Section 3.3. Then, we compute the element-wise contributions of the error $(\eta_K)_{K\in\mathcal{T}}$ given by Eq. (2.8) (resp. $(\widetilde{\eta}_K)_{K\in\mathcal{T}}$ given by Eq. (2.11)) and select ("mark") some elements for refinement.We describe the employed marking strategies in Section 3.4. After performing those refinements, we obtain an updated coarse mesh, which constitutes the initial mesh for the subsequent adaptive iteration. We repeat this process until we reach the required precision.

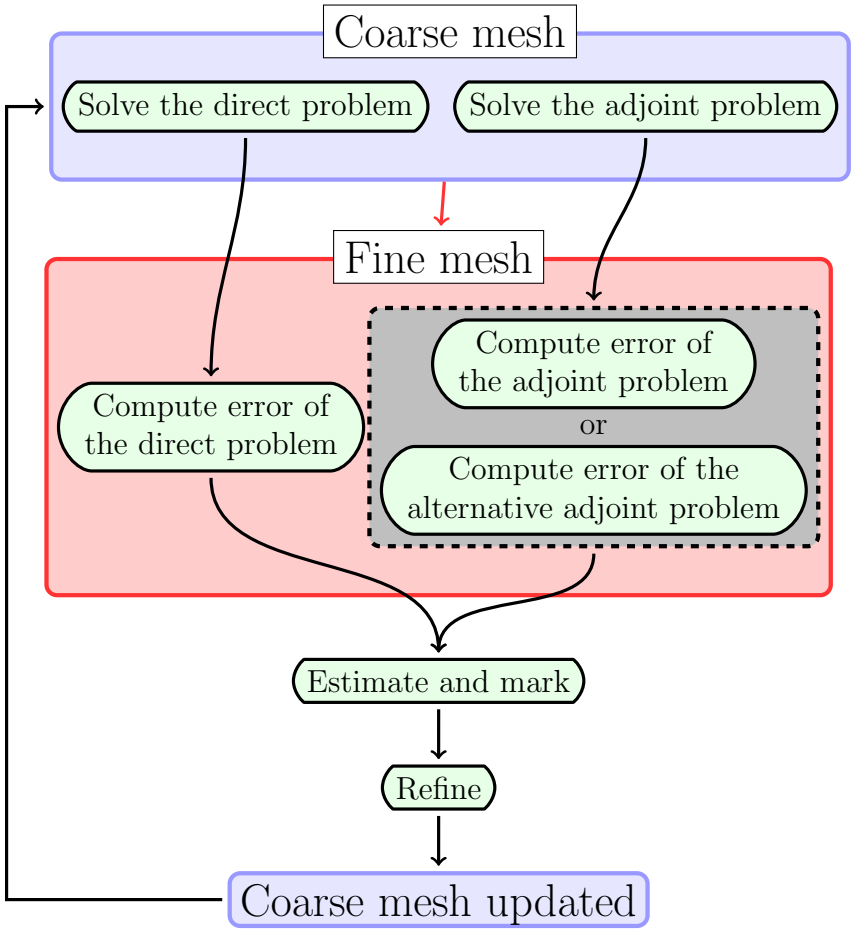

Figure 3.1.: Goal-Oriented Adaptivity algorithm.

3.2. Fine meshes construction

Given a Cartesian coarse mesh with a given element size h and approximation order p, we construct the fine mesh by either (a) selecting a reference element size $h_{\text{ref}} < h$, or (b) uniformly increasing the polynomial order by $\Delta p = 2$.

This increment in p is somehow arbitrary, and one could select a different value, taking into account that a larger value will significantly increase the computational cost, while the lower value $\Delta p = 1$ may be insufficient to accurately estimate the error. Although in some cases the fine mesh should be finer in space in order to better estimate the error, the high regularity of the solutions of our model problem justifies such choice of fine mesh. Note that for the Helmholtz problem, the value of Δp is not as crucial as for the convection-dominated diffusion problem, where the behavior of the upper bounds depends on Δp since the features of the solution are localized unlike in the solution of

the Helmholtz problem.

A fine grid based on a reference element size $h_{ref} < h$ has been considered only in an early version of the uniform h-refinements 1D algorithm implemented in MATLAB (Algorithm 1). In this algorithm, we set the following input parameters: the number of elements of the discretization N and the uniform polynomial order of approximation p. We set the wavenumber k such that for a given N and p, the minimum number of Degrees of Freedom (DoF) per wavelength is small (below three). Then, we select a set of N_{mesh} structured meshes until we reach a number of DoF per wavelength close to 100. We consider the finest mesh as our reference mesh.

Algorithm 1: Uniform h-refinements in 1D

Input: N, p

for $i \in \{1, \cdots, N_{mesh}\}$ **do**

  $h_i = \frac{1}{N \cdot 2^i}$

  $u_{h_i}, v_{h_i} = \text{solve}(h_i, p)$ `// Solve the direct and adjoint problems`

$u_{ref} \longleftarrow u_{h_{N_{\text{mesh}}}}$

$v_{ref} \longleftarrow v_{h_{N_{\text{mesh}}}}$

for $i \in \{1, \cdots, N_{mesh} - 1\}$ **do**

  $\mathfrak{I}_{h_i}$`// compute mesh injections onto the finest mesh`

  $\widetilde{\varepsilon}_{h_i} = \text{alternative\_residual\_dual}(h_{N_{\text{mesh}}}, p, \mathfrak{I}_{h_i} v_{h_i})$ `// Solve the unconventional dual error problem`

  $e_{h_i} = u_{ref} - \mathfrak{I}_{h_i} u_{h_i}$`// Estimate the errors`

  $\varepsilon_{h_i} = v_{ref} - \mathfrak{I}_{h_i} v_{h_i}$

The fine mesh based on increasing uniformly the order of approximation by two has been employed to perform numerical experiments related to p-uniform refinements and p-adaptivity. The resulting algorithm (Algorithm 2) has been implemented in Fortran90 using PETSc libraries [106] for the resolution of the finite element systems. Due to the use of hierarchical basis functions, the corresponding injection operator is trivially implemented by simply adding zeros to the coefficients associated with the $p + 1$ and $p + 2$ DoF, leaving the remaining coefficients unchanged.

Algorithm 2: p-adaptivity

Input: $\mathcal{T}_{h,p_{\text{init}}} = \bigcup_{K_{p_{init}}} K_{p_{init}}$ // Initialize coarse mesh

$\mathcal{T}_{h,p_{\text{init}}+2}$ // Construct the fine mesh

$relative\_error = \text{tol}$ // Initialize variable *relative_error*

while $relative\_error \geqslant tol$ **do**

  u_h, v_h // Compute the coarse mesh solutions

  $\mathfrak{I}_p(u_h)$, $\mathfrak{I}_p(v_h)$ // Inject the coarse solutions into the fine mesh

  e, ε (resp. $\widetilde{\varepsilon}$) // Compute errors using Eqs. (2.5), (2.6) (resp. (2.9)), based on the residuals

  $\forall K_p \in \mathcal{T}_{h,p}$, η_{K_p} (resp. $\widetilde{\eta}_{K_p}$) // Compute estimators

  $relative\_error = \dfrac{|\langle l\,, e\rangle|}{|\langle l\,, (e - u_h)\rangle|} \cdot 100$ // Update the relative error

  forall $K_p \in \mathcal{T}_{h,p}$ **do**

    if $\frac{\eta_{K_p}}{\Delta\text{DoF}_{K_p}} \geqslant (\max_{K_p} \frac{\eta_{K_p}}{\Delta\text{DoF}_{K_p}}) \times \beta$ *(resp.* $\frac{\widetilde{\eta}_{K_p}}{\Delta\text{DoF}_{K_p}} \geqslant (\max_{K_p} \frac{\widetilde{\eta}_{K_p}}{\Delta\text{DoF}_{K_p}}) \times \beta$*)* **then**

      Mark element's interior, faces, and edges

  $K_p \longleftarrow K_{p+1}$ // Refine each marked element, face, and edge

  $\mathcal{T}_{h,p}$ // Update the mesh and ensure the minimum rule

3.3. Error computations

As mentioned in Section 2.2, errors e and ε of the direct and adjoint problems can be approximated either by computing the difference between the coarse and fine mesh solutions (Algorithm 1) or by solving for the residuals, as shown in Eqs. (2.6) and (2.5) (Algorithm 2). Both methods are equivalent. However, when it comes to the alternative error $\widetilde{\varepsilon}$, the coarse mesh solution of the alternative operator is unavailable. Thus, and in order to keep a generic approach for all problems, we solve the residual based equations (2.6), (2.5), and (2.9).

3.4. Marking strategies and refinements

Once all error functions are estimated globally, we compute the element-wise error contributions leading to the error estimators η_K and $\widetilde{\eta}_K$ given by Eqs. (2.8) and (2.11). Those contributions are ponderated by the number of DoF that would need to be added (ΔDoF_K) in the case of refinement.

To determine which elements need to be refined, we select those whose error estimator is larger than a given percentage of the largest estimator $\max_K(\frac{\eta_K}{\Delta\text{DoF}_K})$ and $\max_K(\frac{\widetilde{\eta}_K}{\Delta\text{DoF}_K})$, respectively. In this work, unless explicitly mentioned, we set that percentage to $\beta = 0.4$. We isotropically increase by $\Delta p = 1$ the polynomial orders of interior, faces, and edges of the selected elements.

The uniform refinements algorithms are particular cases of the adaptive strategy, where the mesh is globally refined either in h or p (i.e., the selected percentage is equal to $\beta = 0$).

Once an updated mesh has been generated, we ensure that the minimum rule [91] is respected by increasing the polynomial order of those element interiors whose boundary nodes (faces and/or edges) exhibit a larger order of approximation.

This adaptive approach can be trivially implemented, and we use it here to illustrate the advantages and limitations of using alternative error representations. More sophisticated and effective adaptive processes can be used, e.g., [67, 107, 108, 109, 110, 111].

3.5. Projection Based Interpolation (PBI)

Following [91, 53], we have implemented the PBI in order to analyze its performance in the context of GOA when considering our proposed alternative error representations. It ensures, for instance, almost optimal convergence rates for the classical p-adaptive algorithm (up to a logarithmic factor, see [112]). The

PBI projects the fine mesh solutions u and v into the coarse grid by combining interpolation with a local minimum energy projection. We denote those projections by $\Pi_h(u)$ and $\Pi_h(v)$. The error representations (2.8) and (2.11) then become error indicators as follow,

$$\eta^{\Pi_h} = \sum_{K\in\mathcal{T}} \eta_K^{\Pi_h} = \sum_{K\in\mathcal{T}} \left| \left\langle B_K \varepsilon_K^{\Pi_h} , e_K^{\Pi_h} \right\rangle_{\mathbb{H}_K^*,\mathbb{H}_K} \right| \tag{3.1}$$

$$\widetilde{\eta}^{\Pi_h} = \sum_{K\in\mathcal{T}} \widetilde{\eta}_K^{\Pi_h} = \sum_{K\in\mathcal{T}} \left| \left\langle \widetilde{B}_K \widetilde{\varepsilon}_K^{\Pi_h} , e_K^{\Pi_h} \right\rangle_{\mathbb{H}_K^*,\mathbb{H}_K} \right| \tag{3.2}$$

where $e^{\Pi_h}, \varepsilon^{\Pi_h}, \widetilde{\varepsilon}^{\Pi_h} \in \mathbb{H}$ are solutions of the following variational problems.

- Find $e^{\Pi_h} \in \mathbb{H}$ such that

$$B e^{\Pi_h} = \mathcal{R}_p(\Pi_h(u)). \tag{3.3}$$

- Find $\varepsilon^{\Pi_h} \in \mathbb{H}$ such that

$$B^* \varepsilon^{\Pi_h} = \mathcal{R}_d(\Pi_h(v)). \tag{3.4}$$

- Find $\widetilde{\varepsilon}^{\Pi_h} \in \mathbb{H}$ such that

$$\widetilde{B}\, \widetilde{\varepsilon}^{\Pi_h} = \mathcal{R}_d(\Pi_h(v)). \tag{3.5}$$

Note that values (3.1) and (3.2) computed using the PBI are no longer bounds of the error in the Quantity of Interest (QoI) $\langle l , e\rangle_{\mathbb{H}^*,\mathbb{H}}$. They are referred to as *error indicators* in the literature (cf. [97]).

Construction of the 2D Projection Based Interpolation (PBI) The PBI follows three "rules": (a) "locality", (b) "global continuity", and (c) "optimality". "Locality" means that the PBI is computed element-wise; "global continuity" imposes the global continuity across the elements; and "optimality" means that, since the order of approximation will decrease, we seek to minimize the loss of information using a projection.

Given an element K, we compute the coefficients $(u_i^{\Pi})_i$ of $\Pi_h(u)$, interpolant of u on K. We consider the coefficients of $\Pi_h(u)$ according to the type of associated basis function: first, the ones associated with the basis functions that are not null on the vertexes $(\phi_v)_v$; then, the ones associated with the basis function that are not null on the edges but zero on the vertices (edge

bubble functions, $((\phi_{e,i})_i)_e)$, and finally the ones that are associated with the basis functions that are non-zero only on the interior of the element (element bubble basis function $(\phi_{K,i})_i$).

$$\Pi_h(u) = \sum_v u_v^\Pi \phi_v + \sum_e \sum_i u_{e,i}^\Pi \phi_{e,i} + \sum_i u_{K,i}^\Pi \phi_{K,i}. \tag{3.6}$$

To determine the coefficients, we follow these steps:

(a) u_v^Π is the coefficient of the vertex v connected to the element K and set as

$$u_v^\Pi = u_v. \tag{3.7}$$

(b) For each edge e, we consider the basis functions $(\phi_{e,i})_i$ that are bubble basis functions of this edge and we compute $(u_{e,i}^\Pi)_i$ by minimizing the quantity

$$\left\| \sum_i u_{e,i}^\Pi \phi_{e,i} - \left(u - \sum_v u_v^\Pi \phi_v \right) \right\|_{H_{00}^{1/2}(e)} \tag{3.8}$$

where $H_{00}^{1/2}(e)$ is the subspace of $H^{1/2}(e)$ of the functions vanishing at the endpoints of the edge e. In practice, we do not computing the $H_{00}^{1/2}$ semi-norm. As in [91], we approximated it by a geometrically weighted H^1-norm

$$\|u\|^2_{H_{00}^{1/2}(e)} \simeq \int_e \left| \frac{\partial u}{\partial s} \right|^2 \frac{ds}{d\xi} ds, \tag{3.9}$$

where $\frac{ds}{d\xi}$ is the line integral Jacobian of the parametrization of the edge e into the master element.

(c) Finally, for the coefficients corresponding to the bubble element basis functions $(\phi_{K,i})_i$, as for the edges, we compute $(u_{K,i}^\Pi)_i$ by minimizing the quantity

$$\left\| \sum_i u_{K,i}^\Pi \phi_{K,i} - \left((u - \sum_v u_v^\Pi \phi_v + \sum_e \sum_i u_{e,i}^\Pi \phi_{e,i} \right) \right\|_{H^1(K)}. \tag{3.10}$$

We refer to [112, 91] for further details.

3.6. Computation of the alternative operator

In order to compute the alternative error estimator, we need to build and factorize the matrix associated with the alternative operator. Thus, we cannot

reuse the same matrix for the computation of both the direct and the alternative adjoint errors. This is a drawback of our method, hopefully, compensated by achieving an adaptive process that requires fewer DoF to reach its goal.

Part II.

Numerical results

4. 1D problems

In this chapter, we present numerical results for two types of one-dimensional (1D) problems: Helmholtz and convection-dominated diffusion problems.

Let $\Omega = (0,1)$ be the domain. We denote by $L^2(\Omega)$ the space of square integrable functions on Ω, $H^1(\Omega)$ the Sobolev space of functions with $L^2(\Omega)$ first derivatives on Ω and by $H_0^1(\Omega)$ the subspace of functions from $H^1(\Omega)$ that vanish on the boundaries and $\langle \cdot\,, \cdot \rangle_{L^2}$ is the standard L^2-inner product.

4.1. 1D Helmholtz equation

4.1.1. Model problem

Given $k > 0$, let us consider the following problem:

Find u such that,

$$\begin{cases} -\left(\dfrac{d^2}{dx^2} + k^2\right) u = 1 & \text{in } (0,1), \\ u(0) = 0, \dfrac{du}{dx}(1) = -\dfrac{1}{2}. \end{cases} \tag{4.1}$$

We set $\mathbb{H} := \{v \in H^1(0,1), v(0) = 0\}$. Then, for any $\phi, \psi \in \mathbb{H}$,

$$\langle B\phi\,, \psi \rangle_{\mathbb{H}^*,\mathbb{H}} = \left\langle \frac{d\phi}{dx}\,, \frac{d\psi}{dx} \right\rangle_{L^2(0,1)} - k^2 \langle \phi\,, \psi \rangle_{L^2(0,1)}\,, \tag{4.2}$$

$$\langle f\,, \phi \rangle_{\mathbb{H}^*,\mathbb{H}} = \langle 1\,, \phi \rangle_{L^2(0,1)} - \frac{\phi(1)}{2}. \tag{4.3}$$

For illustrative purposes, we define the following linear output functional (Quantity of Interest (QoI)):

$$\langle l\,, \phi \rangle_{\mathbb{H}^*,\mathbb{H}} = \langle 1\,, \phi \rangle_{L^2(2/5,4/5)} \quad \forall \phi \in \mathbb{H}. \tag{4.4}$$

We set the 1D-Laplacian as the alternative operator $\widetilde{B}$, that is:

$$\left\langle \widetilde{B}\phi\,, \psi \right\rangle_{\mathbb{H}^*,\mathbb{H}} = \left\langle \frac{d\phi}{dx}\,, \frac{d\psi}{dx} \right\rangle_{L^2(0,1)} \quad \forall \phi, \psi \in \mathbb{H}. \tag{4.5}$$

There exist several ways to numerically compute the errors. One is to use the analytical solution and the approximated solution on $\mathbb{H}_h$. In our case, we know the analytical solution of the direct problem (4.1):

$$u(x) = \mathfrak{R}e\left(\alpha e^{ikx} + \beta e^{-ikx} - \frac{1}{k^2}\right), \tag{4.6}$$

where

$$\alpha = \frac{2k - 2e^{ki}i + k^2 e^{ki}i}{2k^3\left(e^{2ki}+1\right)} \qquad \text{and} \qquad \beta = -\frac{e^{ki}\left(k^2 - 2 + 2ke^{ki}i\right)i}{2k^3\left(e^{2ki}+1\right)}.$$

However, we have not derived the exact solution of the adjoint problem (2.3) nor the solution of our alternative problem (2.9). Thus, we work with two approximation spaces: "coarse" and "fine", as described in Chapter 3.

4.1.2. Numerical results

4.1.2.1. Uniform p-refinements

We first consider the case $l \equiv f$. The direct and adjoint problems coincide, so do their errors $e = \varepsilon$ and $\widetilde{e} = \widetilde{\varepsilon}$. This is the choice corresponding to classical energy-norm adaptive algorithms [60, 59].

Figure 4.1 shows numerically that the alternative bound provides a sharper estimation of the error in the QoI, $\langle l\,, e\rangle_{\mathbb{H}^*,\mathbb{H}}$ when performing uniform p-refinements. We also distinguish two different regimes: (a) the pre-asymptotic one, where the alternative upper bound is significantly sharper than the classical one, and (b) the asymptotic regime, where both upper bounds are almost identical.

We now represent the L^2-norm and H^1-semi-norm of the errors e and $\widetilde{e}$. That last quantity is obtained by solving the problem:

> Find $\widetilde{e} \in \mathbb{H}$ such that:
>
> $$\left\langle \widetilde{B}\widetilde{e}\,, \phi \right\rangle_{\mathbb{H}^*,\mathbb{H}} = \left\langle \widetilde{B}e\,, \phi \right\rangle_{\mathbb{H}^*,\mathbb{H}} \quad \forall \phi \in \mathbb{H}. \tag{4.7}$$

Figure 4.2 shows that the norms of the error associated with the alternative operator version are smaller than those corresponding to the traditional operators in the pre-asymptotic regime and approximate each other in the asymptotic regime. Intuitively, it seems that the alternative representation softens (or eliminates) the pollution effect. This observation may explain why we obtain sharper estimates using $\widetilde{e}$. A second interesting fact is that $\|\nabla e\|_{L^2(0,1)}$

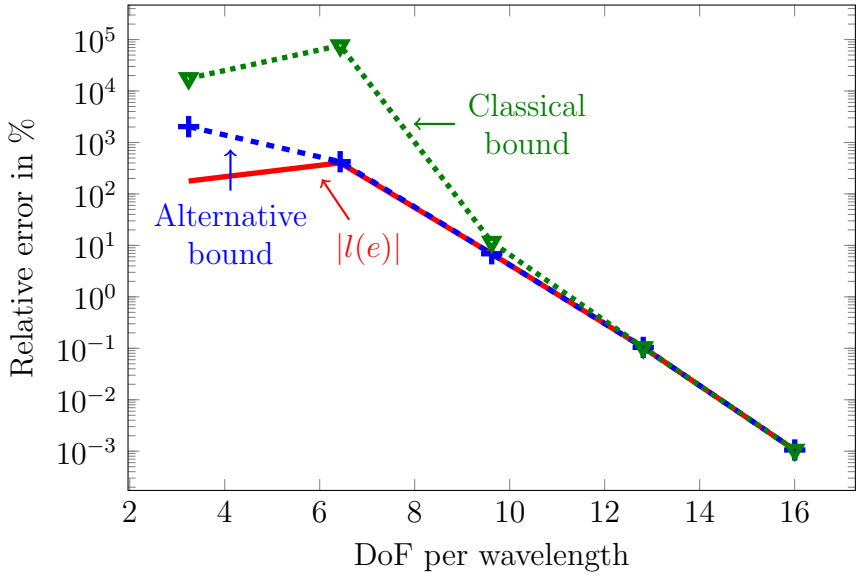

Figure 4.1.: 1D Helmholtz problem. Upper energy-norm bounds with uniform p-refinements, $l \equiv f$, $k = 128$.

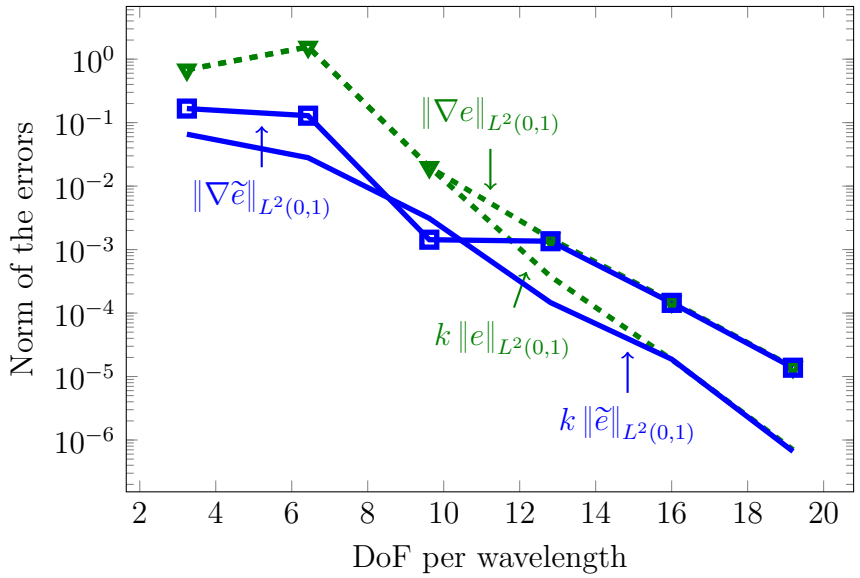

Figure 4.2.: 1D Helmholtz problem. Norm of the errors for uniform energy-norm p-refinements, $k = 128$.

and $k\,\|e\|_{L^2(0,1)}$ are of the same order in the pre-asymptotic regime. This does not occur for the alternative error representations.

As previously mentioned, one reason for observing better results with the al-

ternative upper bounds seems to be the reduction of the pollution error. This idea is further confirmed by the numerical results presented in Figure 4.3, showing that for few Degrees of Freedom (DoF) per wavelength (in the pre-asymptotic range, Figures [4.3a, 4.3b, 4.3c]), $\widetilde{e}$ is less affected than e by the pollution effect that arises when increasing the wavenumber k. When we consider a larger number of DoF per wavelength so that we enter into the asymptotic regime (here 13 DoF per wavelength is enough for that, Figure 4.3d), the pollution disappears and both upper bounds become almost identical.

It is remarkable that the alternative upper bounds are sharper than the classical ones just when it is needed, that is, in the pre-asymptotic regime when the number of DoF per wavelength is below 13. In the asymptotic regime, Helmholtz equation over a single element behaves like Laplace equation (a simple scaling argument shows that the L^2-term becomes negligible), and the corresponding upper bounds coincide, as expected.

Figure 4.4 shows upper bounds for the case corresponding to the output functional l defined in Eq. 4.4. The observed behavior is similar as in the previous example. Figure 4.4 displays the upper bounds compared to the QoI. Figure 4.5 describes the norms of the errors and Figures 4.6 and 4.7 show how the errors ε and $\widetilde{\varepsilon}$ are affected by pollution. The conclusions of the previous case still apply here. Additionally, we observe that the errors of the dual problems are smaller than those of the original problem (see Figure 4.5) because the right-hand side is now localisable. Finally, Figures 4.6c and 4.6d show that the errors of the 1D Laplace equation $\widetilde{\epsilon}$ are null at the nodes of the mesh, as expected, which implies that the pollution error disappears.

4.1.2.2. Uniform h-refinements

We now consider the case of uniform h-refinements (see Algorithm 1). As in the previous cases, Figure 4.8 shows that the alternative bound provides a sharper estimation of the error in the QoI $\langle l\,, e\rangle_{\mathbb{H}^*,\mathbb{H}}$ also when performing uniform h-refinements. Indeed, this figure exhibits a similar behavior as that corresponding to the p-uniform refinements case (Figure 4.4). The alternative estimate is sharper than the classical one. We also distinguish a different behavior for the pre-asymptotic and asymptotic regimes.

Figure 4.9 displays the L^2-norm and H^1-semi-norm of the errors ε, e, $\widetilde{\varepsilon}$, and $\widetilde{e}$. We observe similar results as those shown in Figure 4.2, i.e., we obtain smaller errors for the alternative representation of the error in the pre-asymptotic regime and similar results for the asymptotic regime.

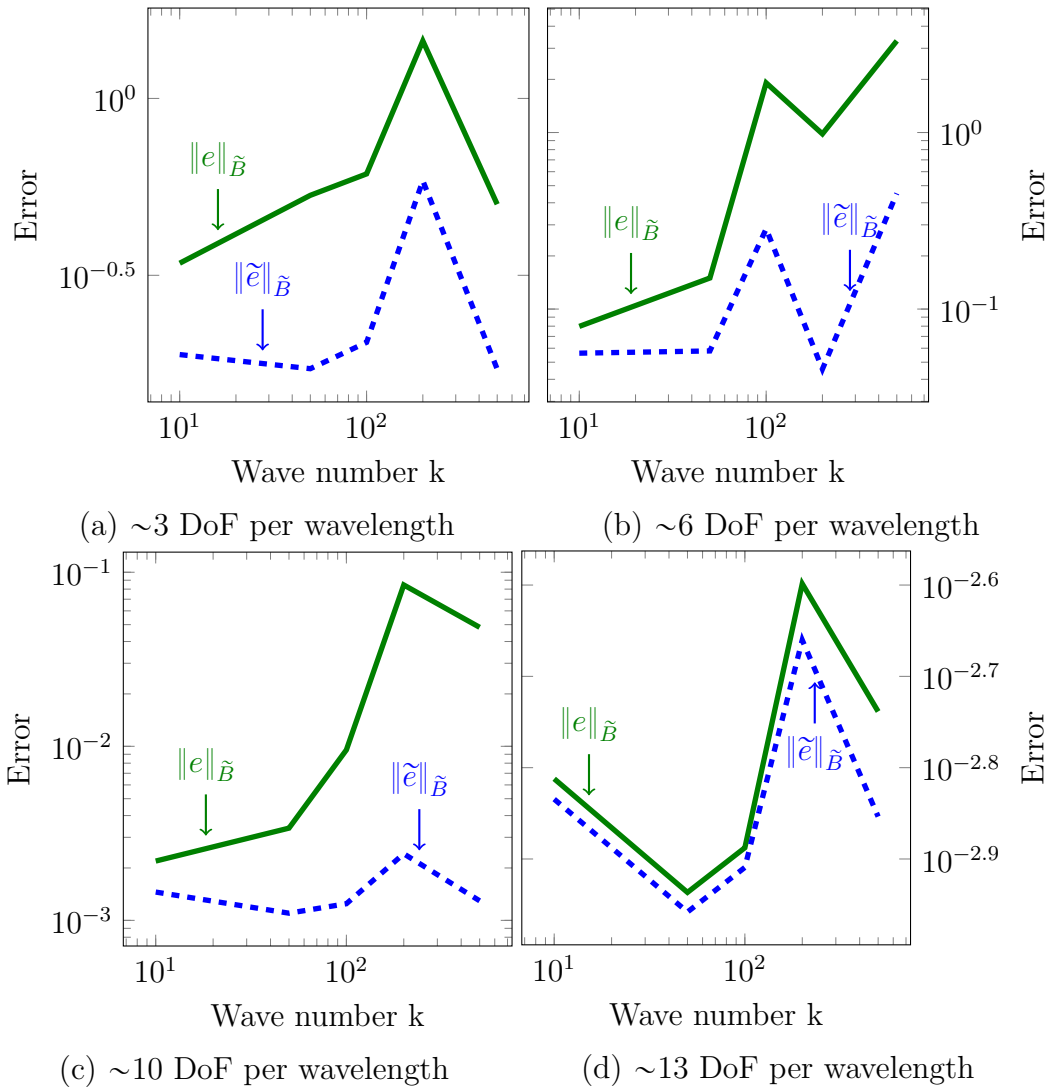

(a) ∼3 DoF per wavelength (b) ∼6 DoF per wavelength

(c) ∼10 DoF per wavelength (d) ∼13 DoF per wavelength

Figure 4.3.: 1D Helmholtz problem. Norm of the errors e and $\tilde{e}$ when increasing the wavenumber k with $\tilde{B}$ being the Laplace operator using uniform p-refinements.

4.1.2.3. p-adaptivity

We now consider the p-adaptive strategy described in Algorithm 2 with the following parameters: the wavenumber $k = 128$, the error tolerance on the QoI used as stopping criterion $tol = 10^{-4}$. The number of elements ensures that the minimum number of DoF per wavelength is three so we satisfy the Nyquist rate. We also impose a minimum of five elements in total to avoid rare cases.

Figure 4.10 displays the upper bounds computed with and without the

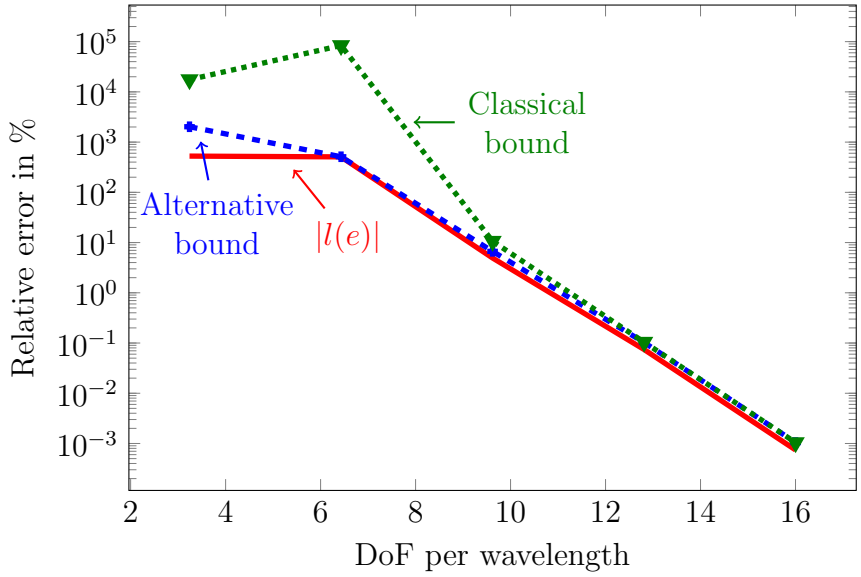

Figure 4.4.: 1D Helmholtz problem. Upper bounds for uniform p-refinements for $k = 128$ and $h = 0.0154$.

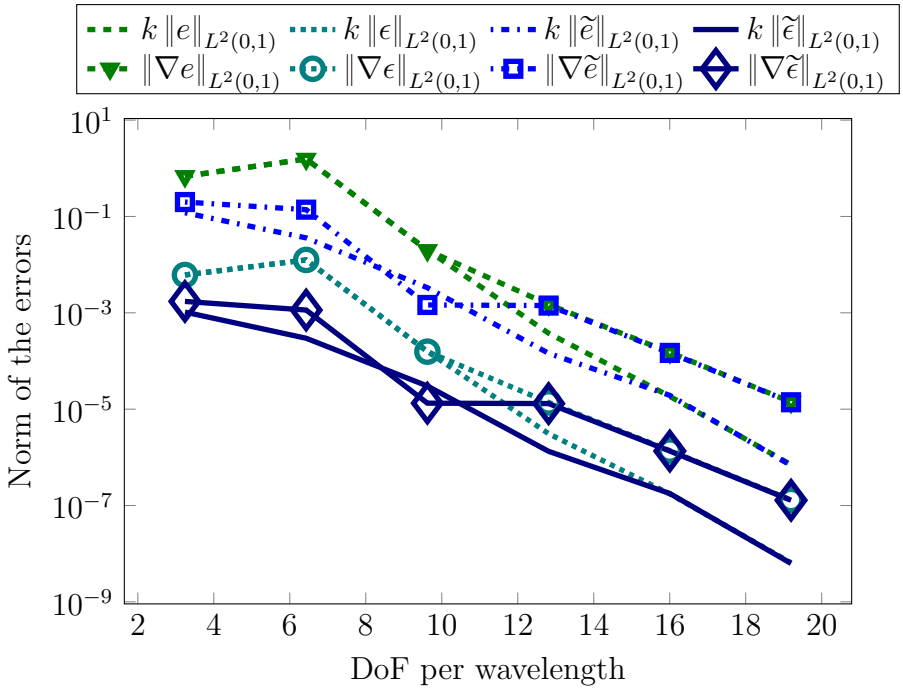

Figure 4.5.: 1D Helmholtz problem. Norm of the errors for uniform goal-oriented p-refinements, $k = 128$.

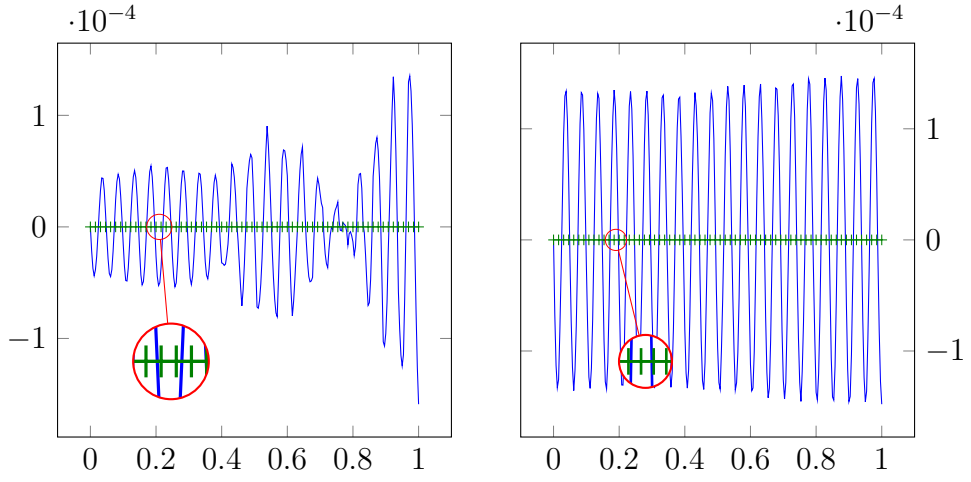

(a) ε_h with ∼3 DoF per wavelength (b) ε_h with ∼6 DoF per wavelength

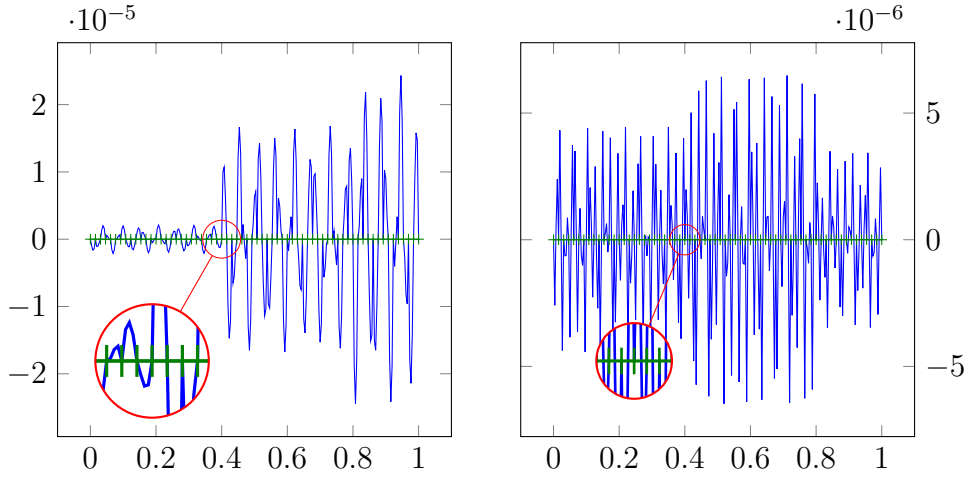

(c) $\widetilde{\varepsilon}_h$ with ∼3 DoF per wavelength (d) $\widetilde{\varepsilon}_h$ with ∼6 DoF per wavelength

Figure 4.6.: 1D Helmholtz problem. Error functions ε_h and $\widetilde{\varepsilon}_h$ with $\widetilde{B}$ being the Laplace operator using uniform p-refinements, $k = 128$.

Projection Based Interpolation (PBI). When considering a p-adaptive algorithm without projections, the classical error representation provides a non-convergent algorithm (see Figure 4.10a). Projectors are introduced to ensure convergence (see Figure 4.10b). With the alternative error representation, we recover convergence even without using the projected errors, as shown in Figures 4.10c and 4.10d. We believe that this behavior is strongly linked to properties of the 1D-Laplace operator. Notice that the projected error is built so that its value is null at the nodes of the mesh, thus, minimizing the pollution effect. The 1D-Laplace operator has the same property. We expect to loose

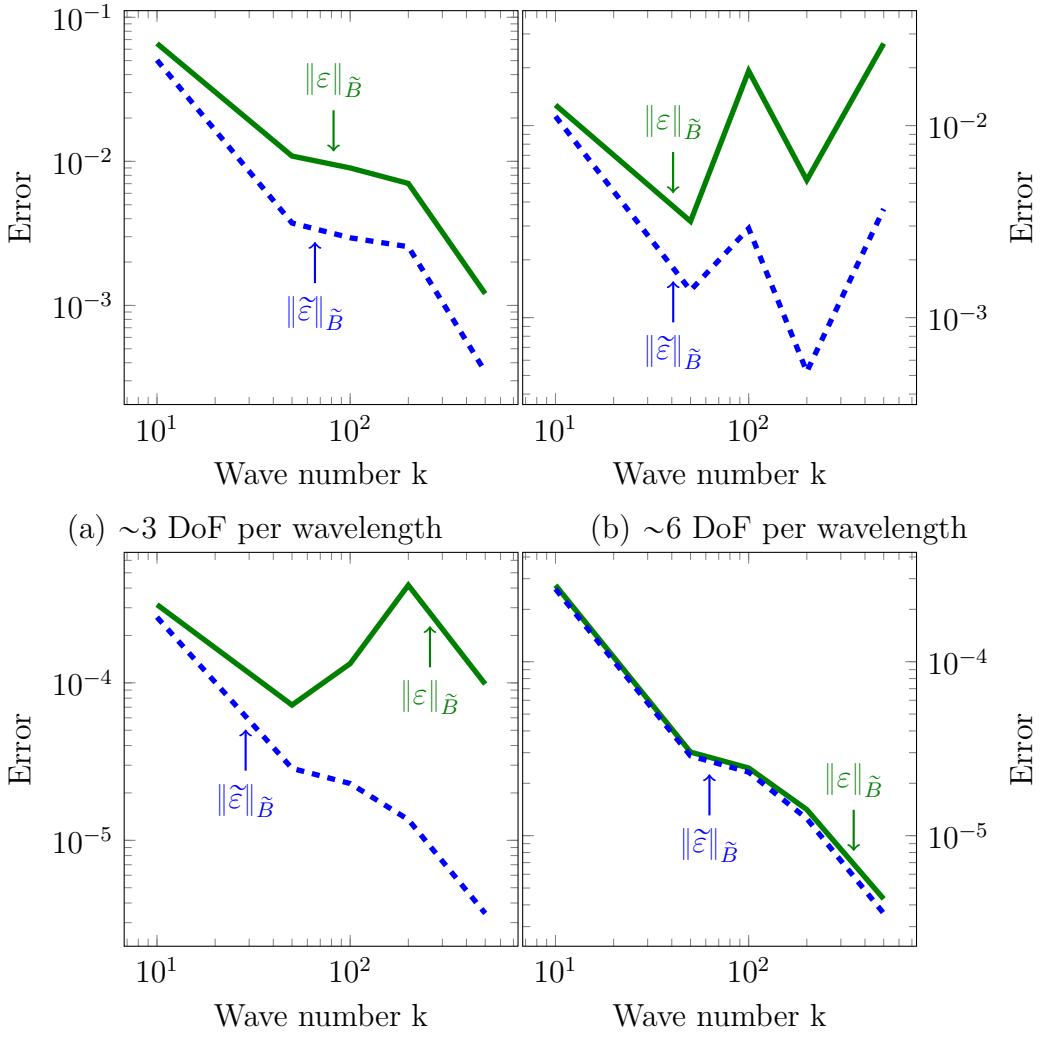

(a) ∼3 DoF per wavelength (b) ∼6 DoF per wavelength

(c) ∼10 DoF per wavelength (d) ∼13 DoF per wavelength

Figure 4.7.: 1D Helmholtz problem. Norm of the errors ε_h and $\widetilde{\varepsilon}_h$ when increasing the wavenumber k with $\widetilde{B}$ being the Laplace operator using uniform p-refinements.

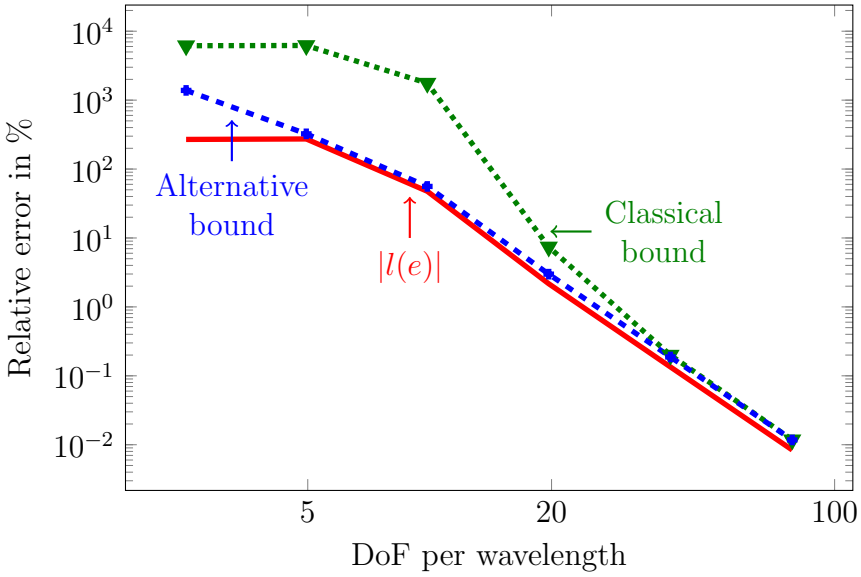

Figure 4.8.: 1D Helmholtz problem. Upper bounds for uniform h-refinements with $k = 128$ and $p = 2$.

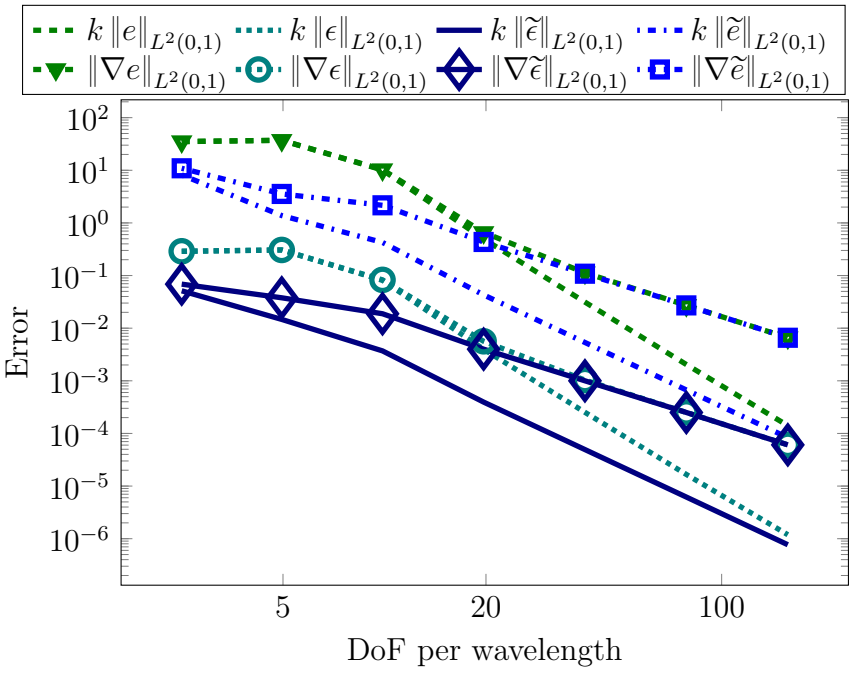

Figure 4.9.: 1D Helmholtz problem. Norms of the errors for uniform h-refinements with $k = 128$ and $p = 2$.

this property when using other operators for $\widetilde{B}$.

In all cases, the upper bounds behave in the same way than for the uniform refinements in the sense that the alternative upper bounds are sharper than the classical ones during the pre-asymptotic regime and similar to each other in the asymptotic regime.

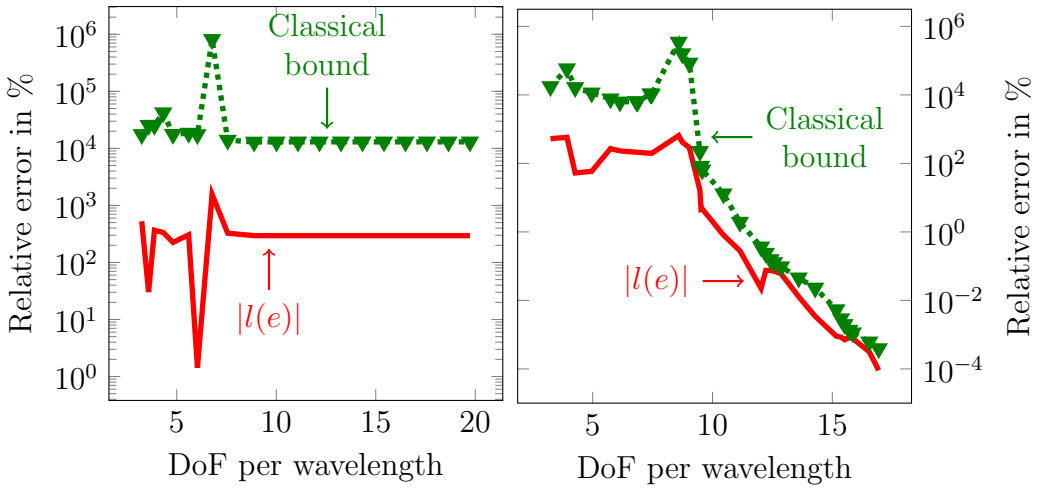

(a) Without PBI, adaptivity with classical criterion

(b) With PBI, adaptivity with classical criterion

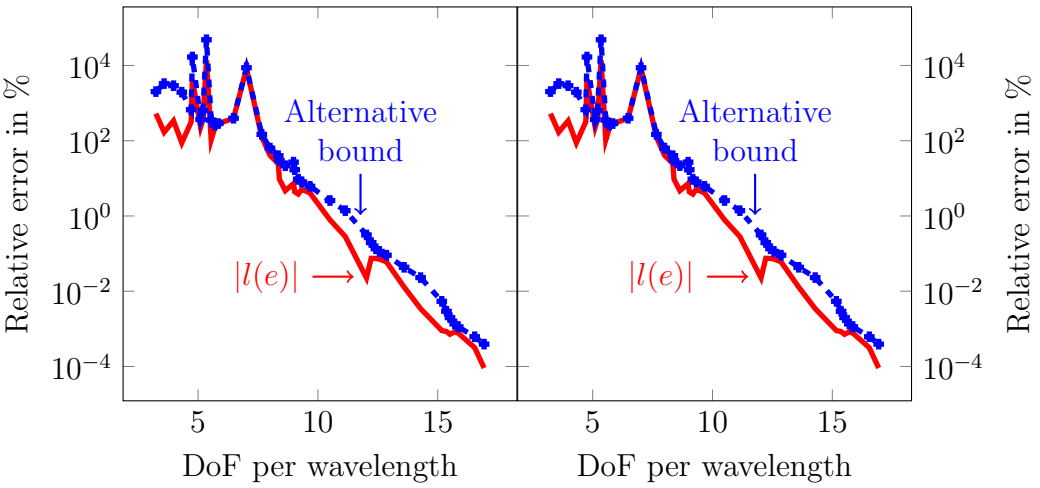

(c) Without PBI, adaptivity with alternative criterion

(d) With PBI, adaptivity with alternative criterion

Figure 4.10.: 1D Helmholtz problem. Upper bounds for p-refinements with $k = 128$ and $h = 0.0154$.

4.1.2.4. Modifying the alternative operator

One feature of the proposed method is that we can select the alternative operator $\widetilde{B}$. One could expect that the sharpness of the upper bounds will depend strongly on such choice. Figure 4.11 describes the upper bounds obtained when employing the L^2 inner product

$$\left\langle \widetilde{B}u\,,v\right\rangle_{\mathbb{H}^*,\mathbb{H}} = \langle u\,,v\rangle_{L^2(0,1)} \tag{4.8}$$

for computing the error representation compared to the bound obtained when using the Laplacian. We display the upper bounds both for h-uniform and p-uniform refinements. We observe that: (a) the upper bounds are sharper in the pre-asymptotic range than the classical ones, and (b) the upper bounds corresponding to the Laplace operator are the sharpest in all cases.

Similarly, we now select the operator

$$\left\langle \widetilde{B}u\,,v\right\rangle_{\mathbb{H}^*,\mathbb{H}} = \langle \nabla u\,,\nabla v\rangle_{L^2(0,1)} + k^2\,\langle u\,,v\rangle_{L^2(0,1)}\,. \tag{4.9}$$

Figure 4.12 shows the upper bounds for the case of p-uniform refinements. We obtain similar results and conclusions as before, namely: (a) the alternative upper bound is sharper than the classical one, and (b) the upper bounds computed using the Laplace operator are the sharpest of all. We note that the upper bound computed with the positive Helmholtz operator given by Eq. (4.9) is sharper than the one computed using the L^2 scalar product given by Eq. (4.8), Figure 4.11b.

Figure 4.13 illustrates how the pollution seems to affect the errors e and $\widetilde{e}$ when considering the positive Helmholtz operator given by Eq. (4.9). Results are similar to the Laplacian case. However, we now observe that error $\widetilde{e}$ is more affected by the pollution than in the Laplacian case. Indeed, the error function is no longer null at the nodes. Figures 4.14a and 4.14b display the corresponding error functions for three and six DoF per wavelength, respectively.

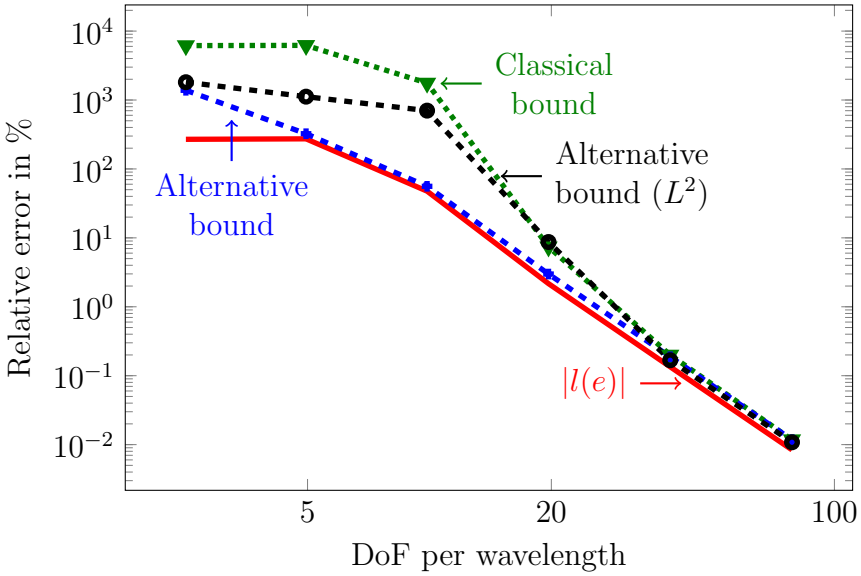

(a) Uniform h-refinements

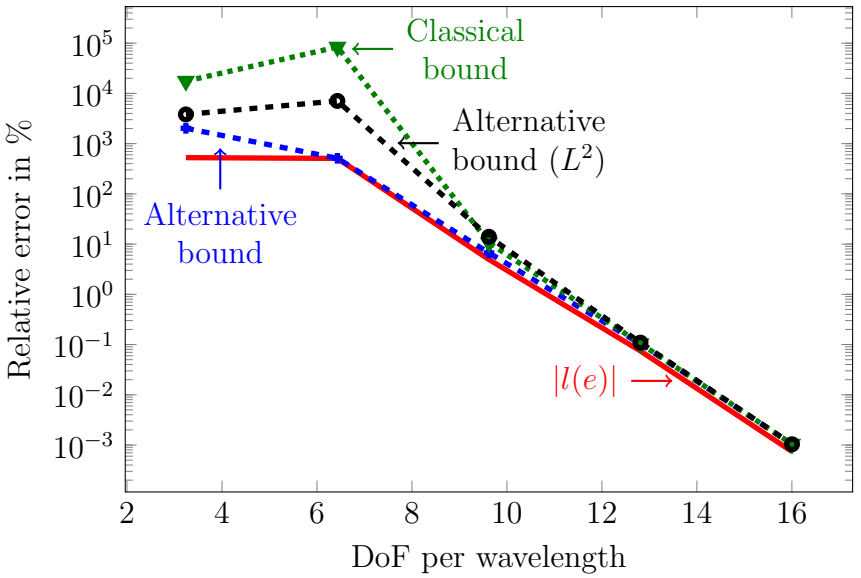

(b) Uniform p-refinements

Figure 4.11.: 1D Helmholtz problem. Alternative upper bounds for uniform h- and p-refinements using $\left\langle \widetilde{B}u\,,v\right\rangle_{\mathbb{H}^*,\mathbb{H}} = \langle u\,,v\rangle_{L^2(0,1)}$, $k = 128$.

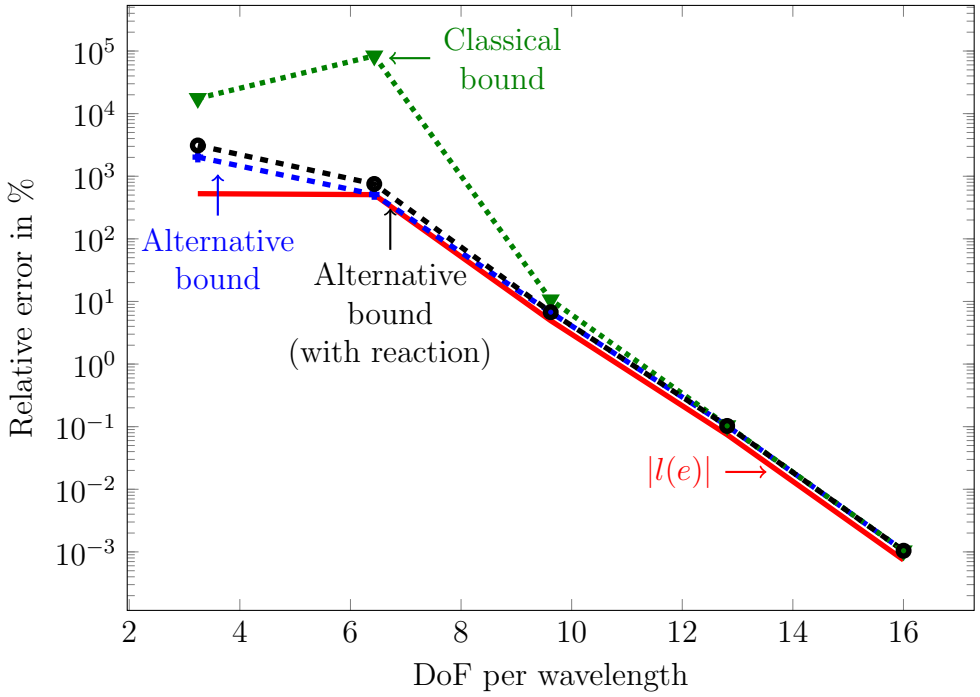

Figure 4.12.: 1D Helmholtz problem. Alternative upper bounds for uniform $p-$refinements using $\left\langle \tilde{B}u\,,v\right\rangle_{\mathbb{H}^*,\mathbb{H}} = \langle \nabla u\,,\nabla v\rangle_{L^2(0,1)} + k^2\,\langle u\,,v\rangle_{L^2(0,1)}$, $k = 128$.

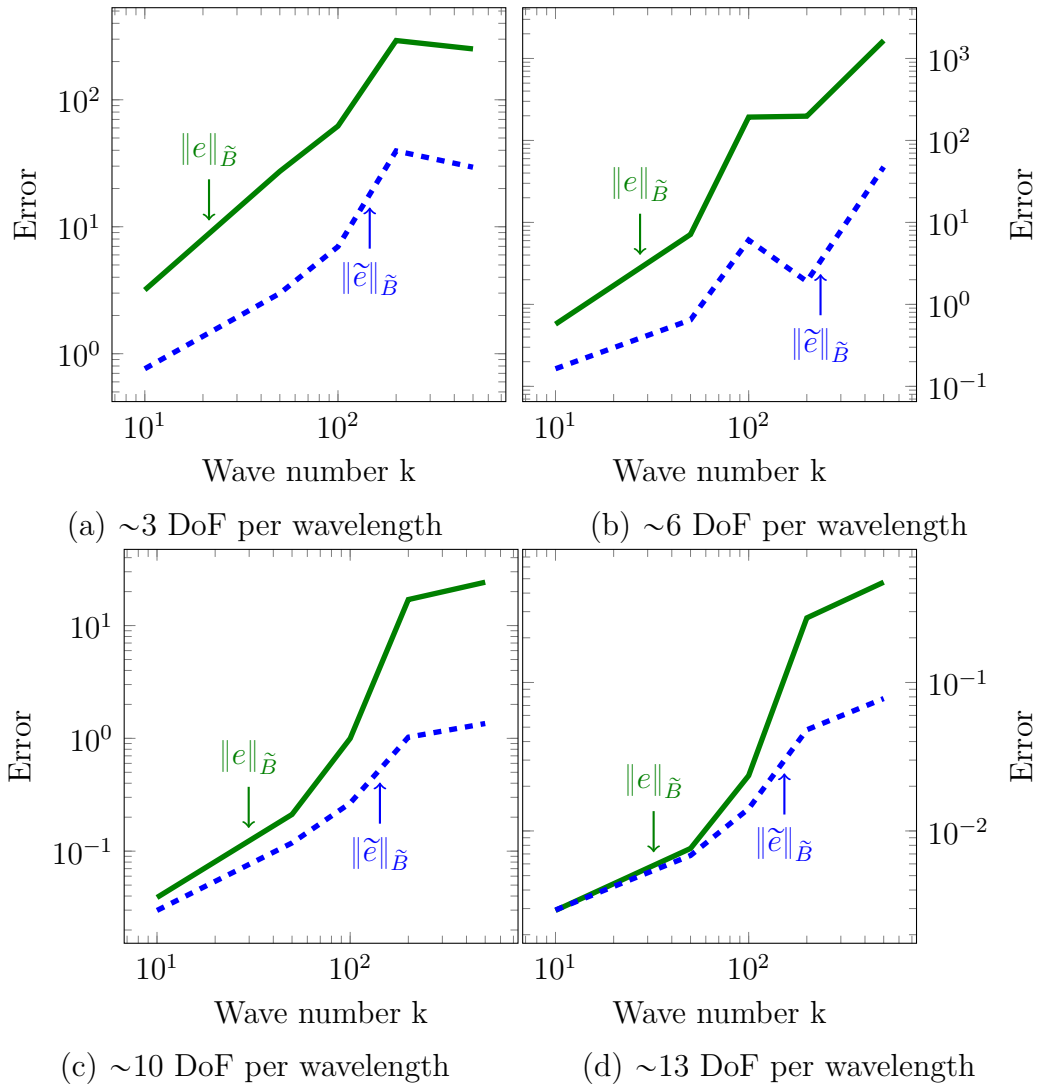

(a) ∼3 DoF per wavelength (b) ∼6 DoF per wavelength

(c) ∼10 DoF per wavelength (d) ∼13 DoF per wavelength

Figure 4.13.: 1D Helmholtz problem. Norm of the errors when increasing the wavenumber k with $\widetilde{B}$ being the positive Helmholtz operator using uniform p-refinements.

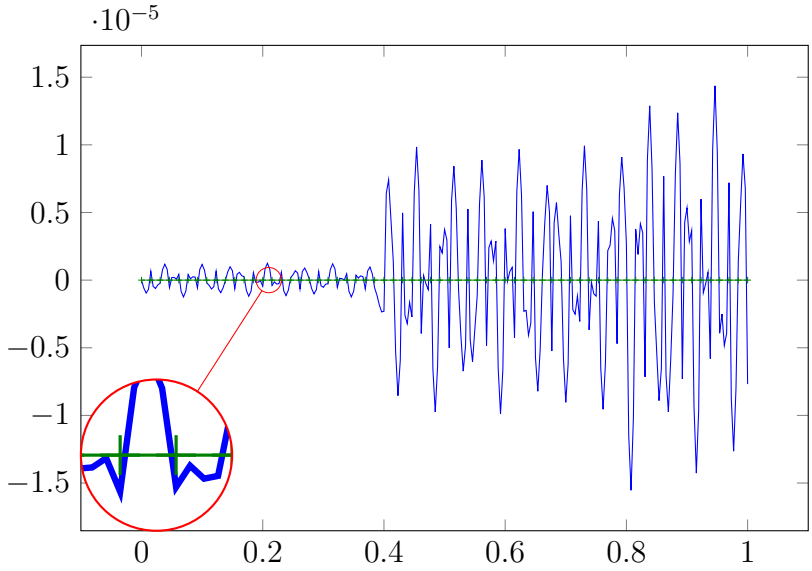

(a) $\widetilde{\varepsilon}_h$ with ∼3 DoF per wavelength

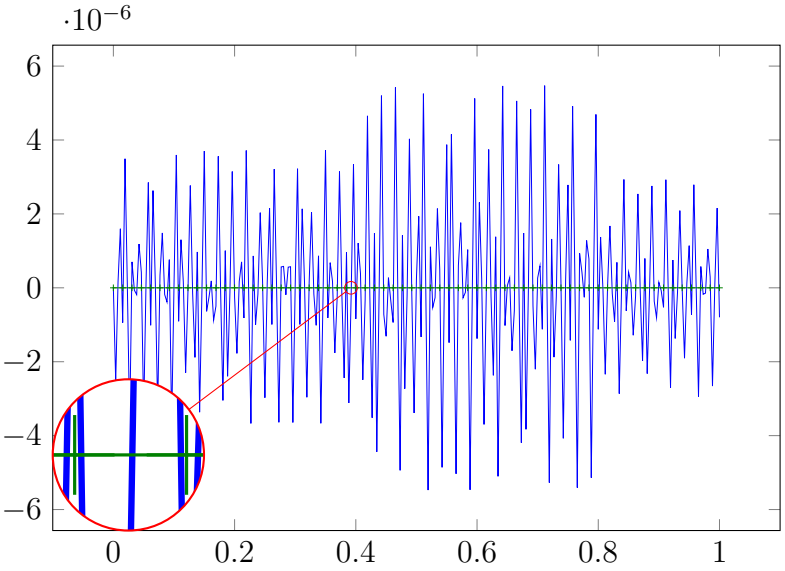

(b) $\widetilde{\varepsilon}_h$ with ∼6 DoF per wavelength

Figure 4.14.: 1D Helmholtz problem. Error function $\widetilde{\varepsilon}_h$ with $\widetilde{B}$ being the positive Helmholtz operator using uniform p-refinements, $k = 128$. Error functions do not vanish at the nodes.

4.2. 1D steady state convection-dominated diffusion problem

4.2.1. Model problem

We consider the following 1D steady state convection-dominated diffusion problem with homogeneous Dirichlet conditions:

> For a given source $F \in L^2(0,1)$ and $0 < \alpha \ll 1$, find u such that,
>
> $$\begin{cases} \left(-\alpha \dfrac{d^2}{dx^2} - \dfrac{d}{dx}\right) u = F(x) \quad \text{on } (0,1), \\ u(0) = u(1) = 0. \end{cases} \tag{4.10}$$

The associated variational formulation is: For $\mathbb{H} = H_0^1(0,1)$

> Find $u \in \mathbb{H}$ such that,
>
> $$\langle Bu\,,\phi\rangle_{\mathbb{H}^*,\mathbb{H}} = \langle f\,,\phi\rangle_{\mathbb{H}^*,\mathbb{H}}\,, \quad \forall \phi \in \mathbb{H}, \tag{4.11}$$

where B is defined as

$$\langle Bu\,,v\rangle_{\mathbb{H}^*,\mathbb{H}} = \alpha\,\langle \partial_x u\,,\partial_x v\rangle_{L^2(0,1)} - \langle \partial_x u\,,v\rangle_{L^2(0,1)}\,, \quad \forall u,v \in \mathbb{H}.$$

We again select the alternative operator as the one associated with the Laplace operator, i.e.:

$$\left\langle \widetilde{B}u\,,v\right\rangle_{\mathbb{H}^*,\mathbb{H}} = \langle \partial_x u\,,\partial_x v\rangle_{L^2(0,1)}\,, \quad \forall u,v \in H_0^1(0,1). \tag{4.12}$$

4.2.2. Numerical results

The initial coarse mesh contains 100 elements uniformly distributed on the log scale between 0 and 1 with a uniform polynomial order $p_{init} = 1$ and the smallest element size being equal to 10^{-4}. We define the source $F \equiv 1$ over the domain and the QoI as the integration of the i-th derivative ($i = 0$ or $i = 1$) on a subset that includes the boundary layer, specifically $(0, 0.05) \subset (0,1)$. That is, $\forall \phi \in H_0^1(0,1)$,

$$\langle f\,,\phi\rangle_{\mathbb{H}^*,\mathbb{H}} = \langle F\,,\phi\rangle_{L^2(0,1)} = \langle 1\,,\phi\rangle_{L^2(0,1)}\,, \tag{4.13}$$

$$\langle l_i\,,\phi\rangle_{\mathbb{H}^*,\mathbb{H}} = \frac{1}{0.05}\left\langle 1\,,\phi^{(i)}\right\rangle_{L^2(0,0.05)}\,, \tag{4.14}$$

where $\phi^{(i)}$ is the i-th derivative of ϕ. We set the diffusion coefficient to $\alpha = 10^{-6}$. The bilinear form we use to compute the alternative upper bounds is the one derived from the Laplace equation with homogeneous Dirichlet boundary conditions given by Equation (4.12).

4.2.2.1. Uniform p-refinement

Figures 4.15 and 4.16 illustrate the behavior of the error upper bounds when performing uniform p-refinements. Figure 4.15 shows that the alternative bound coincides with the error in the QoI when considering l_0. The sign of every estimator is the same, and thus, the triangular inequality that provides the element-wise upper bound generates no loss. Figure 4.16 illustrates the behavior of the upper bounds when considering l_1. In both cases, the alternative bound is sharper than the classical one. Consequently, we expect the adaptive process driven by the alternative error estimators to be more efficient. In the following, we only consider l_0 as QoI.

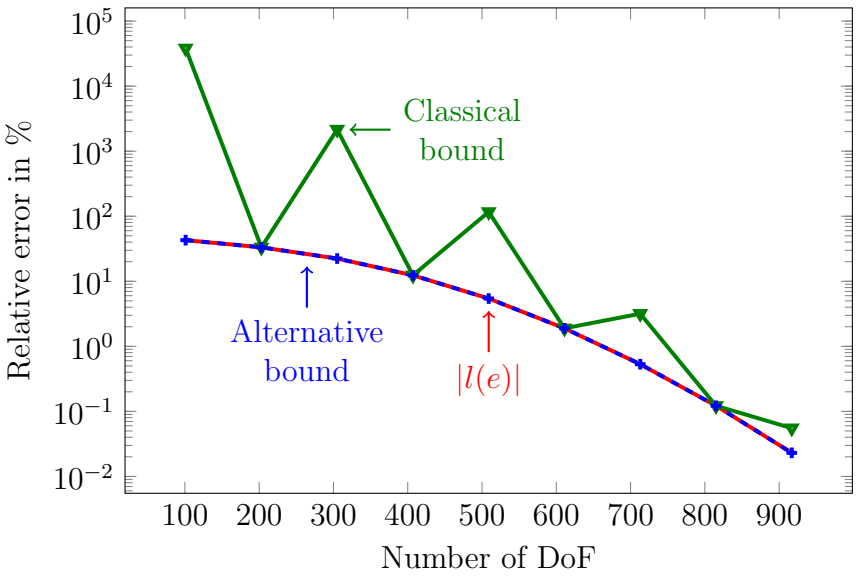

Figure 4.15.: 1D convection-dominated diffusion problem. Upper bounds obtained using uniform p-refinements when the QoI is l_0

4.2.2.2. p-adaptivity

Since the exact solution is almost linear everywhere except on the proximity of the boundary layer, we expect that the optimal mesh will select a large value of p on the element(s) contained in the boundary layer, and it will be $p = 1$

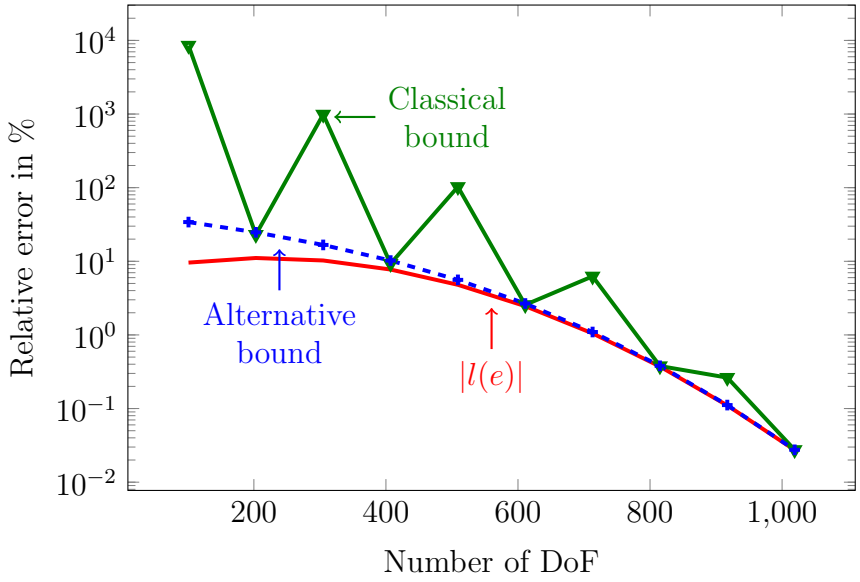

Figure 4.16.: 1D convection-dominated diffusion problem. Upper bounds obtained using uniform p-refinements when the QoI is l_1

elsewhere. Furthermore, since the alternative adjoint error $\widetilde{\varepsilon}$ is zero at the nodes due to the choice of Laplace equation as the alternative dual operator (see [87] and Section 4.1 for details), we would expect to solve the linear part exactly when considering the exact solution as the reference one. However, the selected fine mesh is not particularly adapted to this kind of problem, since the initial mesh is coarse and does not match the boundary layer, as it occurs in practical problems. Thus, the algorithm starts in the pre-asymptotic regime.

We executed the adaptive processes described in Chapter 3 with a stopping tolerance in the QoI of 0.01% and a maximum approximation order of 27. Figures 4.17 and 4.18 track the error evolution on the QoI throughout the adaptive process with the ratio used for the marking process (see Algorithm 2) set to $\beta = 0.4$ and $\beta = 0.99$. The alternative estimators employ less DoF than both the classical adaptive process and uniform p-refinements.

We have plotted the final meshes (see Figure 4.19) for the cases $\beta = 0.4$ (Figure 4.19a) and $\beta = 0.99$ (Figure 4.19b). The respective direct solutions computed on those meshes are displayed in Figure 4.20.

We observe that the classical algorithm fails at eliminating the spurious oscillations in both cases, especially, when $\beta = 0.99$. It is completely miss driven by the spurious oscillations. Also, the alternative method identifies the boundary layer more efficiently than the classical one. Indeed, for the case $\beta = 0.4$, the algorithm with the classical estimators executes more refinements

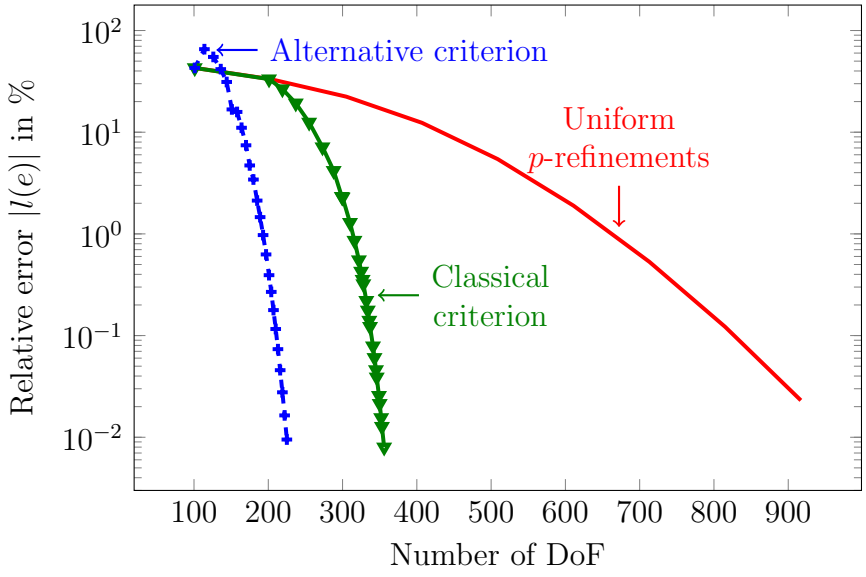

Figure 4.17.: 1D convection-dominated diffusion problem. Error in the QoI for adaptive p-refinements, $\beta = 0.4$

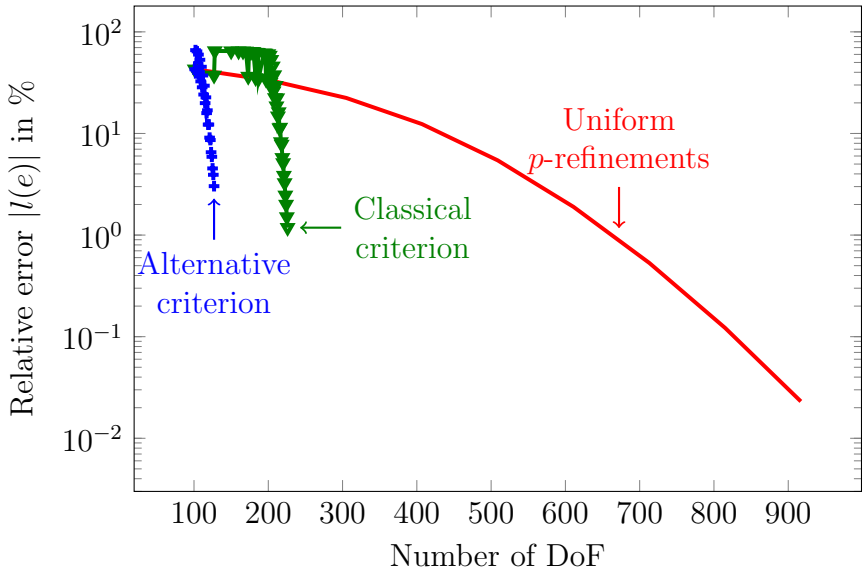

Figure 4.18.: 1D convection-dominated diffusion problem. Error in the QoI for adaptive p-refinements, $\beta = 0.99$

in the linear part of the solution, while the alternative estimator refines more intensively around the boundary layer. For $\beta = 0.99$, the classical method fails to catch both the boundary layer and the QoI, producing thus an erroneous

solution, whereas the alternative method succeeds at eliminating almost all oscillations by computing a quasi-optimal mesh. Note that the classical method concentrates refinements around the point 0.05, where the QoI ends.

In Figure 4.20, we have employed an "overkilling solution" over a highly refined mesh (containing around 800 elements) for illustrative purposes.

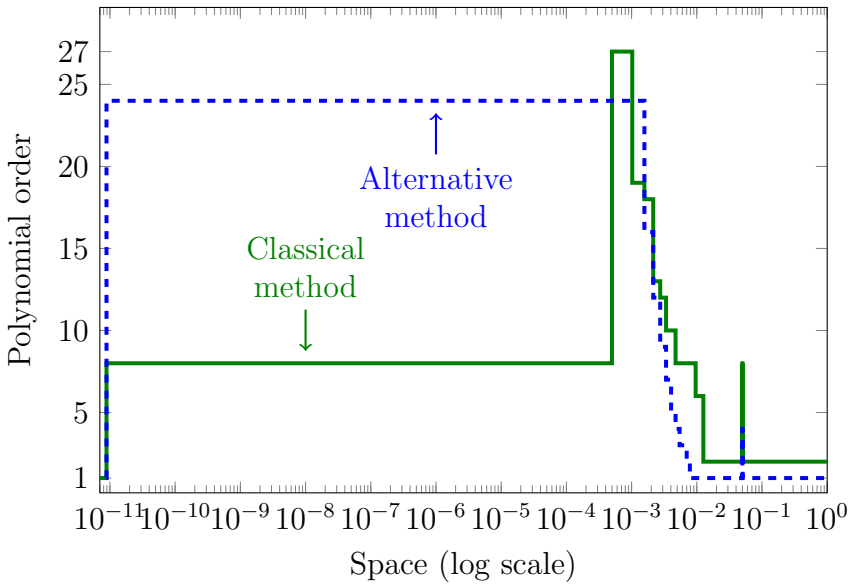

(a) $\beta = 0.4$

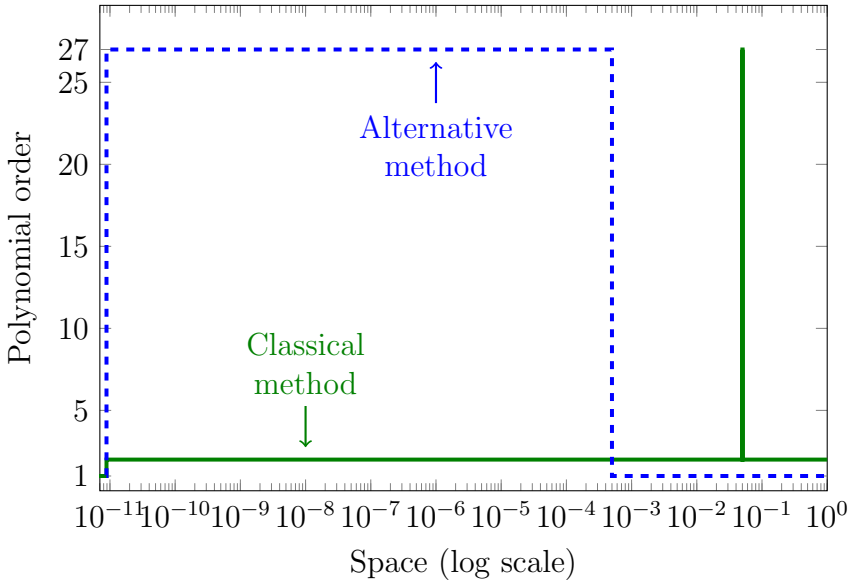

(b) $\beta = 0.99$

Figure 4.19.: 1D convection-dominated diffusion problem. Final adapted coarse meshes after the p-adaptive process for different refinement ratios β.

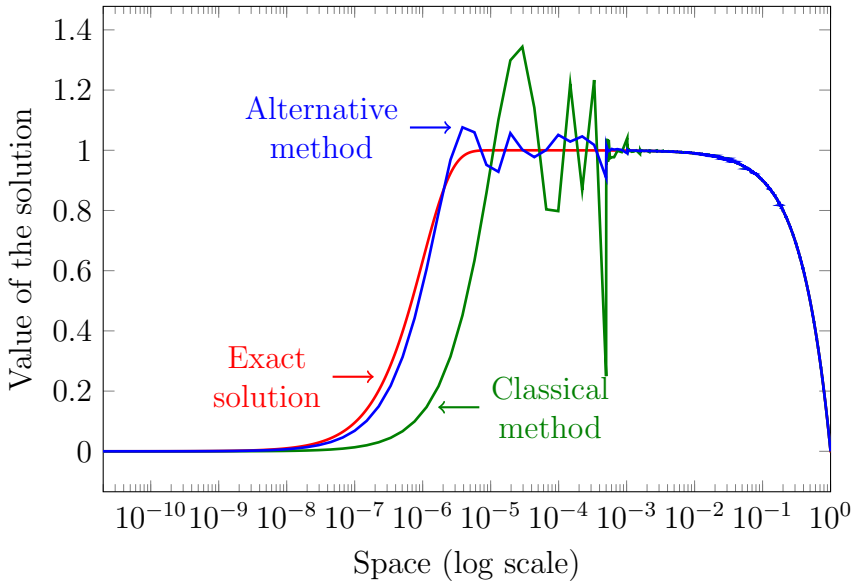

(a) $\beta = 0.4$

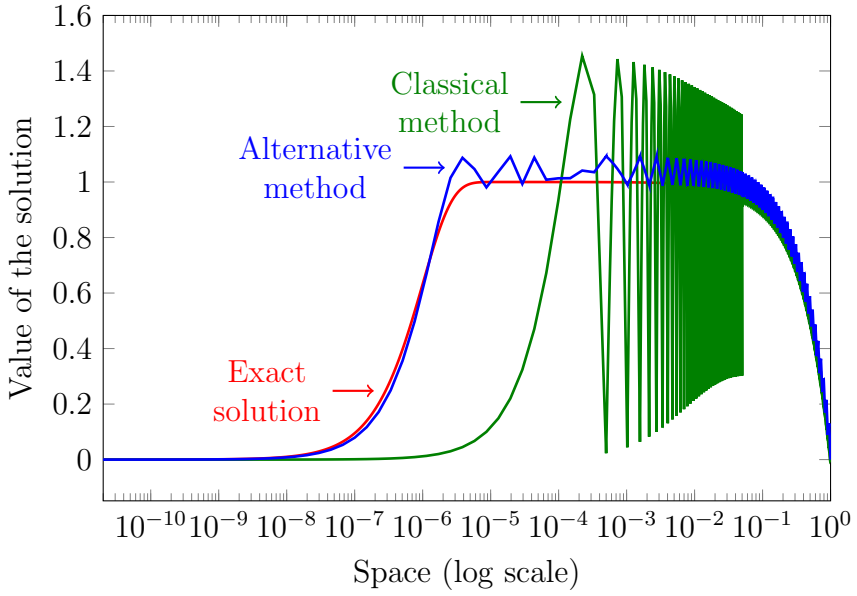

(b) $\beta = 0.99$

Figure 4.20.: 1D convection-dominated diffusion problem. Solution of the direct problem on the adapted coarse mesh for different refinements ratios β.

5. 2D and 3D problems

In this chapter, we present numerical results for two- and three-dimensional (2D and 3D) Helmholtz and convection-dominated diffusion problems.

5.1. Helmholtz equation

5.1.1. Model problem

We consider the following problem with mixed boundary conditions: for $\Omega = (0,1)^d$, a domain of dimension $d = 2$ or 3, $\bar{\Gamma}_D \bigcup \bar{\Gamma}_I = \partial\Omega$, $\mathring{\Gamma}_D \bigcap \mathring{\Gamma}_I = \varnothing$, a partition of the domain boundary $\partial\Omega$,

Find u such that, for $k > 0$,

$$\begin{cases} -\Delta u - k^2 u = 1 & \text{in } \Omega, \\ u = 0 & \text{on } \Gamma_D, \\ \partial_{\vec{n}} u + iku = 0 & \text{on } \Gamma_I, \end{cases} \tag{5.1}$$

where $\vec{n}$ is the outgoing normal unit vector. We set $\mathbb{H} \coloneqq \{u \in H^1(\Omega), u_{|\Gamma_D} = 0\}$ and $\langle \cdot\,, \cdot \rangle_{L^2}$ the standard L^2 sesquilinear product. We define the Quantity of Interest (QoI) as the linear functional in $\mathbb{H}^*$ corresponding to the integral of $w \in \mathbb{H}$ on a portion Γ_{QoI} of the boundary Γ_I, which is given by the functional

$$\langle l\,, w \rangle_{\mathbb{H}^*,\mathbb{H}} = \langle 1\,, w \rangle_{L^2(\Gamma_{\text{QoI}})} \quad \forall w \in \mathbb{H}.$$

Operator $B \in \mathcal{L}(\mathbb{H}, \mathbb{H}^*)$ associated with the above problem is defined as follows,

$$\langle Bw\,, z \rangle_{\mathbb{H}^*,\mathbb{H}} = \langle \nabla w\,, \nabla z \rangle_{L^2(\Omega)} - k^2 \langle w\,, z \rangle_{L^2(\Omega)} + ik \langle w\,, z \rangle_{L^2(\Gamma_I)}\,, \quad \forall w, z \in \mathbb{H}. \tag{5.2}$$

Notice that the above problem is numerically unstable for high wavenumbers, see e.g. [92, 93, 94, 95, 1, 96, 113, 63, 64].

For the 2D case, $d = 2$, the boundaries are set as

$$\Gamma_D := \big([0,1] \times \{0\}\big) \bigcup \big(\{0\} \times [0,1]\big), \tag{5.3}$$

$$\Gamma_I := \big([0,1] \times \{1\}\big) \bigcup \big(\{1\} \times [0,1]\big), \tag{5.4}$$

$$\Gamma_{\text{QoI}} := \{1\} \times (0.75, 1), \tag{5.5}$$

as illustrated in Figure 5.1.

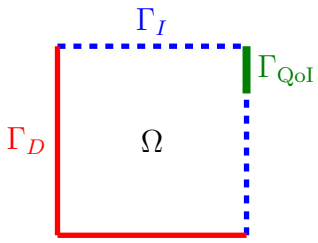

Figure 5.1.: Computational domain for Helmholtz problem in 2D.

For the 3D case, $d = 3$, we set the boundaries as follows (see Figure 5.2): A Dirichlet boundary condition is set on the three faces whose intersection is $(0,0,0)$ and an impedance boundary condition is set on the three faces whose intersection is $(1,1,1)$.

$$\Gamma_D := \big([0,1] \times [0,1] \times \{0\}\big) \bigcup \big([0,1] \times \{0\} \times [0,1]\big) \tag{5.6}$$

$$\bigcup \big(\{0\} \times [0,1] \times [0,1]\big) \tag{5.7}$$

$$\Gamma_I := \big([0,1] \times [0,1] \times \{1\}\big) \bigcup \big([0,1] \times \{1\} \times [0,1]\big) \tag{5.8}$$

$$\bigcup \big(\{1\} \times [0,1] \times [0,1]\big) \tag{5.9}$$

$$\Gamma_{\text{QoI}} := \big([0.75,1] \times [0.75,1] \times \{1\}\big) \bigcup \big([0.75,1] \times \{1\} \times [0.75,1]\big) \tag{5.10}$$

$$\bigcup \big(\{1\} \times [0.75,1] \times [0.75,1]\big). \tag{5.11}$$

5.1.2. Numerical results

5.1.2.1. Selection of the alternative operator

Let B be the 2D Helmholtz operator defined by (5.2) with $k \in \mathbb{R}^+$, a source $f \in \mathbb{H}^*$, and a QoI $l \in \mathbb{H}^*$, as defined in Section 5.1.1. We set the wavenumber

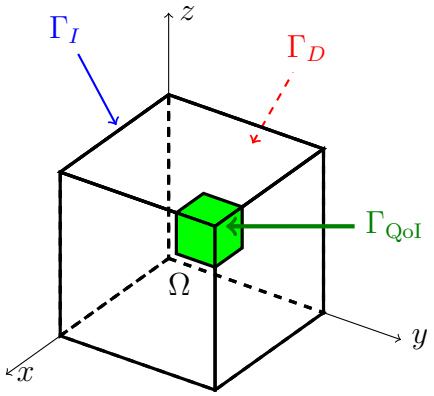

Figure 5.2.: Computational domain for our 3D Helmholtz problem.

to $k = 17\pi$. We analyze the behavior of $\widetilde{\eta}_{\mathcal{T}}$ of Eq. 2.11 when varying the alternative operator $\widetilde{B}_\alpha$, for a given discretization $\mathcal{T}$, over the family $\mathcal{U}$:

$$\mathcal{U} := \left\{ \widetilde{B}_\alpha,\ \alpha \in \mathbb{C} \right\} \tag{5.12}$$

where

$$\left\langle \widetilde{B}_\alpha \cdot, \cdot \right\rangle_{\mathbb{H}^*,\mathbb{H}} = \langle \nabla \cdot, \nabla \cdot \rangle_{L^2(\Omega)} + \alpha \langle \cdot, \cdot \rangle_{L^2(\Omega)} + i\sqrt{|\alpha|} \langle \cdot, \cdot \rangle_{L^2(\Gamma_I)} . \tag{5.13}$$

Boundary conditions for $\widetilde{B}_\alpha$ are selected to be the same as those of the original operator B.

Figures 5.3 and 5.4 show the evolution of $\widetilde{\eta}_{\mathcal{T}}$ with respect to α and along specific directions: in Figure 5.3 the parameter α is real, whereas in Figure 5.4 the parameter α is purely imaginary.

The sharpest upper bounds are obtained for $\alpha = 0$ (Laplace operator) in most cases. When α is real (see Figure 5.3), the Laplace operator is not delivering exactly the sharpest bound, but it is very close to it.

The top panel of Figure 5.3 shows that for large $|\alpha|$ ($\geqslant 10^5$), the behavior of the alternative operator is almost equivalent to that of the L^2-sesquilinear product. If $\alpha > 0$, $\widetilde{B}_\alpha$ is self-adjoint and positive definite. For both cases ($\alpha \geqslant 10^5$ and $\alpha \leqslant -10^5$), the alternative upper bounds are sharper than the classical ones. If $\alpha < 0$, then we are dealing with a Helmholtz operator. To numerically resolve Equation (2.9), we need to satisfy the Nyquist rate. When $\alpha < -k^2$ (the red area), the Nyquist rate criterion is compromised, and the numerical resolution is untrustworthy. Thus, we restrict the analysis to $\alpha \in [-k^2, 0]$. The middle panel of Figure 5.3 zooms on this area. We observe that bound $\widetilde{\eta}_{\mathcal{T}}$ is slightly oscillating as α becomes more negative, probably

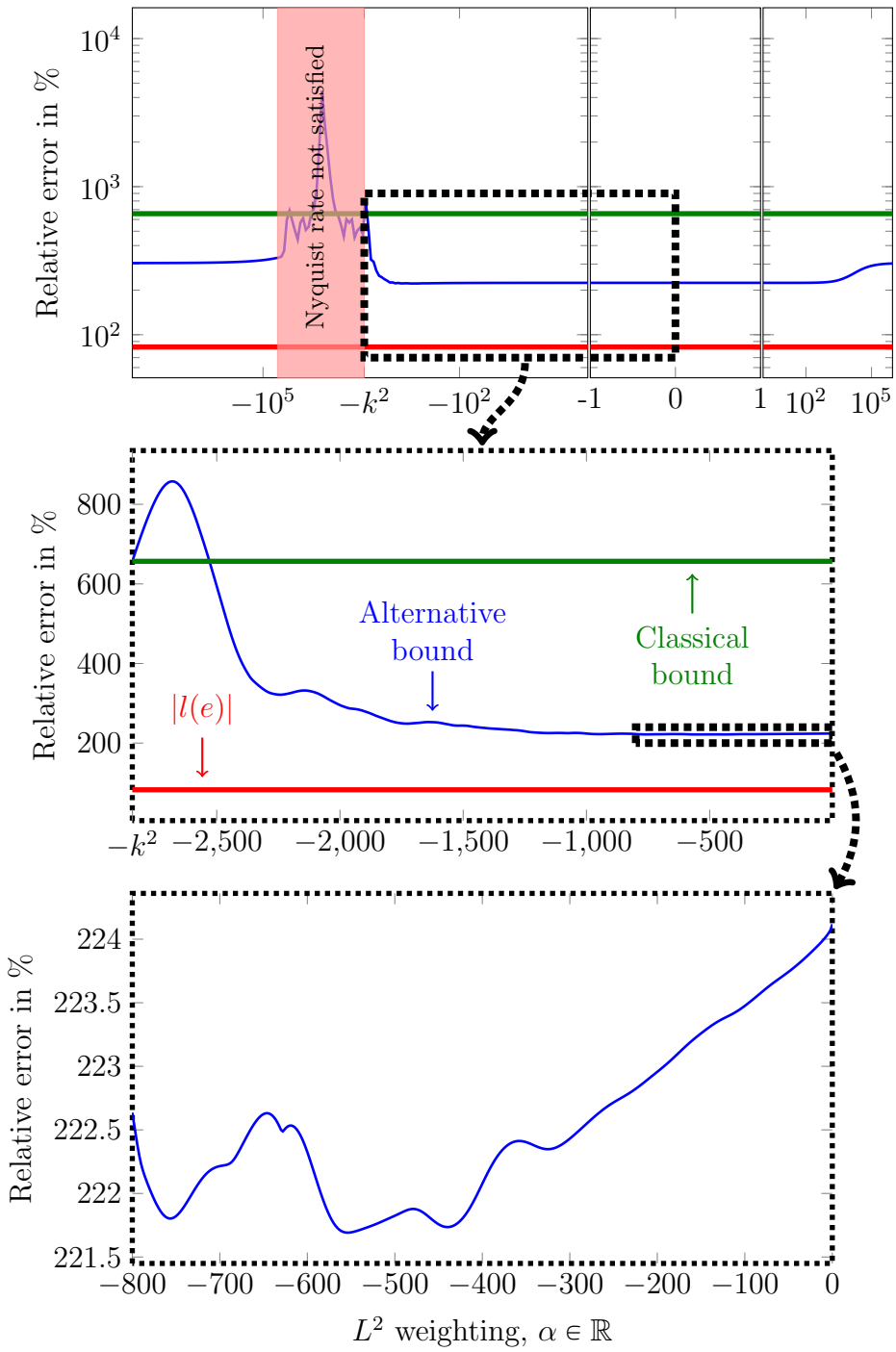

Figure 5.3.: 2D Helmholtz problem, $\widetilde{\eta}_{\mathcal{T}}$ versus α for $\alpha \in \mathbb{R}$, $k = 2\pi \times 8.5 = 17\pi \simeq 53$, and approx. 3 DoF per wavelength (with uniform $p = 3$).

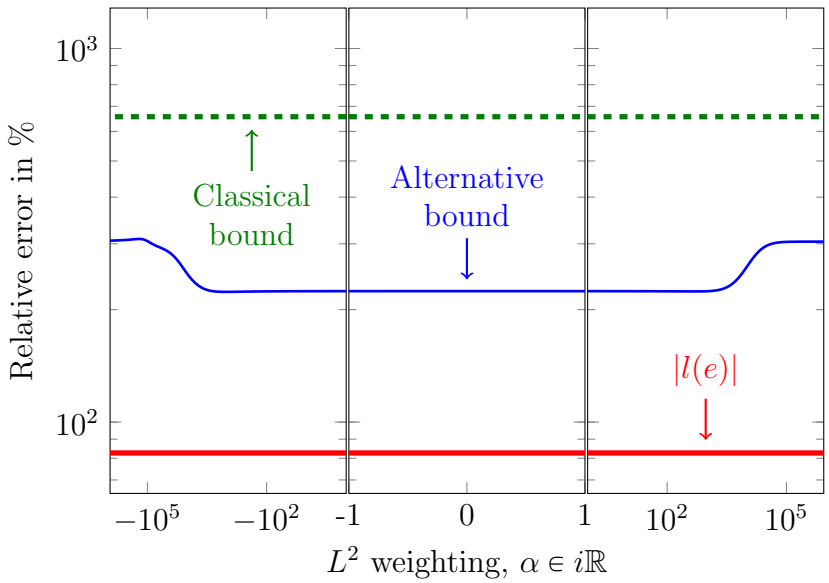

Figure 5.4.: 2D Helmholtz problem, $\widetilde{\eta}_{\mathcal{T}}$ versus α for $\alpha \in i\mathbb{R}$, $k = 17\pi$, and approx. 3 DoF per wavelength (with uniform $p = 3$).

because the number of DoF per wavelength is getting smaller and dispersion effect is stronger. The almost flat area for $\alpha > -800$ is rescaled in Figure 5.3 (bottom panel) in order to determine whether or not the Laplacian is the operator that provides the sharpest bound. We observe that the minimum is not reached for $\alpha = 0$, but the relative difference between the minimum (around 222% for $\alpha \simeq 550$) and the value of $\widetilde{\eta}_{\mathcal{T}}$ for $\alpha = 0$, $\widetilde{\eta}_{\mathcal{T}} \simeq 224\%$ is negligible. Thus, for approximation space $\mathbb{H}_h$, it seems advantageous to use the Laplace operator as the alternative operator.

Figure 5.5 shows the evolution of $\widetilde{\eta}_{\mathcal{T}}$ as a function of α under the same conditions than in Figure 5.3 but, in here, we modify the approximation space $\mathbb{H}_h$ by increasing the polynomial order p by one. These results show the robustness of the selected alternative operator (namely, the Laplacian) with respect to the choice of discrete space $\mathbb{H}_h$.

From those numerical results, it appears that the stability of the alternative operator plays a key role on the sharpness (or not) of the upper bounds. Indeed, unlike the Helmholtz operator, the Laplace one does not generate any dispersion error. Thus, in the remainder of this section, we select the Laplace operator as our alternative operator.

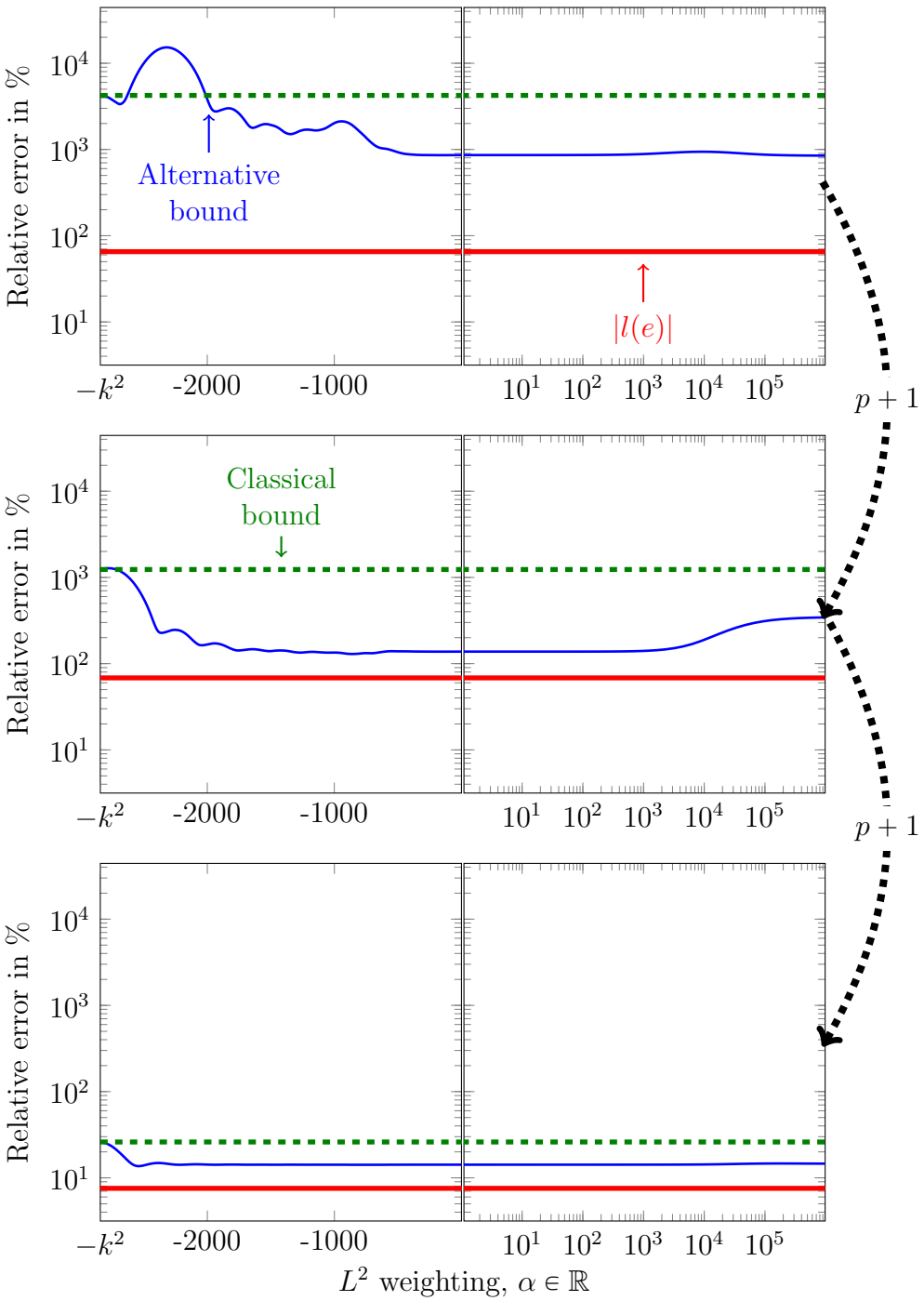

Figure 5.5.: 2D Helmholtz problem, $\widetilde{\eta}_{\mathcal{T}}$ versus α for $\alpha \in [-k^2, +\infty)$, $k = 17\pi$. The top graph is produced for 3 DoF per wavelength (with uniform $p = 2$). The subsequent plots are obtained by increasing the approximation order p. The Laplace operator provides a quasi-optimal upper bound for all cases.

5.1.2.2. 2D numerical results: refinements and adaptivity

Figures 5.6 and 5.7 show the upper bounds of the algorithm 2 when performing uniform h-refinements (Figure 5.6) and uniform p-refinements (Figure 5.7). As mentioned in Section 2.2, Figure 5.7 shows that using $\widetilde{e}$ or $\widetilde{\varepsilon}$ leads to almost identical results. Thus, we restrict ourselves to the use of $\widetilde{\varepsilon}$, and the representation of the dual residual $\mathcal{R}_d(v_h)$.

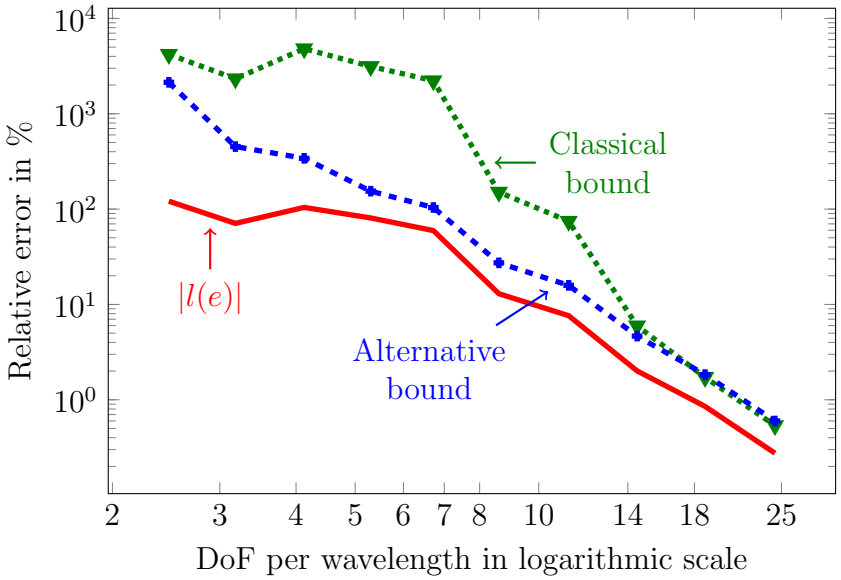

Figure 5.6.: 2D Helmholtz problem, $k = 17\pi$. Uniform h-refinements, $p = 2$. Error evolution in the QoIand upper bounds given by the different error representations

In all cases, the element size h of the initial mesh is selected to enforce that the discretization exhibits always at least 2.5 DoF per wavelength ($p_{\text{init}} = 1$, uniformly). In this way, the Nyquist criterion is satisfied, and the pollution error eventually decays at an exponential rate with respect to p, since $2p_{\text{init}} + 1 > kh + \beta(kh)^{1/3}$ for some $\beta > 0$ (see [114, 97]). Once the pollution error vanishes, the expected rate of convergence is h^{2p} (see [67]) for smooth enough solutions. Figure 5.7 shows that the convergence rates obtained for this example when using uniform p-refinements are smaller than expected probably due to the loss of smoothness caused by the non-smooth squared shape of the domain and the lack of regularity of the right-hand side.

From these graphics, we observe that the alternative bound (2.11) is significantly sharper in the pre-asymptotic regime than the classical one (2.8), and both upper bounds coincide when the error in the QoI is around 1% or below (asymptotic regime).

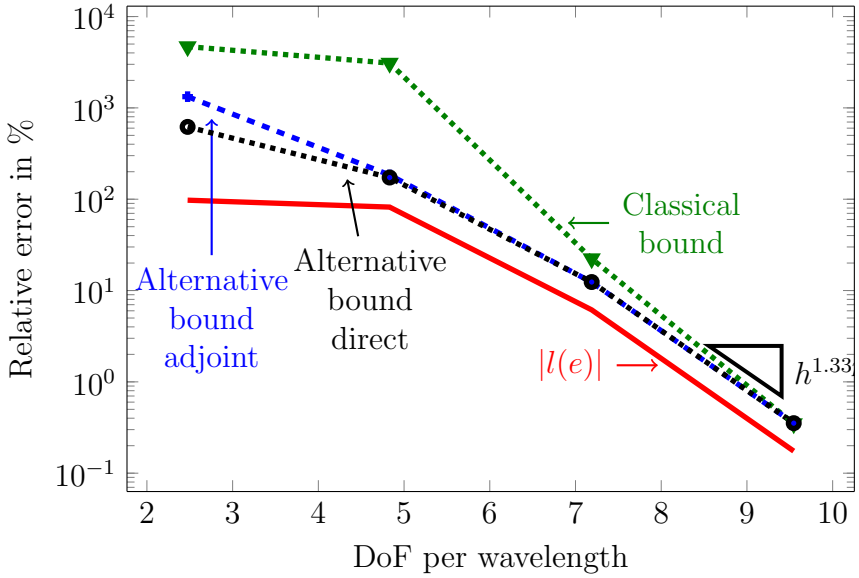

Figure 5.7.: 2D Helmholtz problem, $k = 17\pi$. Uniform p-refinements, $hk \gg 1$. Error evolution in the QoI and upper bounds given by the different error representations, namely, the classical bound (2.8), the alternative bound using the residual dual $\mathcal{R}_d(v_h)$ (2.11), and the alternative bound using the residual primal $\mathcal{R}_p(u_h)$ (2.11).

Figures 5.8 and 5.9 show that with the alternative error representation, the p-adaptive algorithm converges without the need to introduce the Projection Based Interpolation (PBI) operator. When using the PBI, both algorithms converge with a similar behavior, as illustrated in Figure 5.8.

When convergence occurs, errors exhibit almost identical convergence rates as those observed for the uniform p-refinements, see Figure 5.9. Indeed, since the solution of our model is highly regular and of uniform amplitude, quasi-optimal meshes are obtained via uniform p-refinements and the final adapted meshes (displayed in Figures 5.10b, 5.10c, and 5.10d) are almost p-uniform. We remark that the classical criterion does not converge because it selects inappropriate p-refinements that do not decrease the error, and the algorithm stops due to the limit of $p = 14$ set on the approximation order; see Figure 5.10a.

With the alternative error representation (where $\widetilde{B}$ is the weak Laplace operator) without PBI, we achieve similar results as those obtained with the classical estimate with PBI. Thus, in this case, we can substitute the PBI, which complicates the implementation, by the alternative dual problem.

Figure 5.11 shows the distribution map of the element error estimators

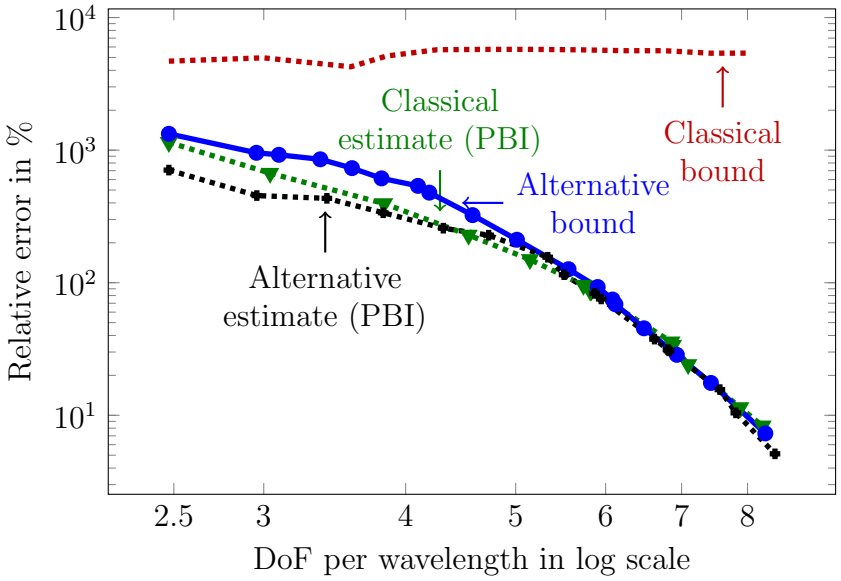

Figure 5.8.: 2D Helmholtz problem, $k = 17\pi$, $hk \gg 1$. Error representation associated to the criterion selected for p-adaptivity.

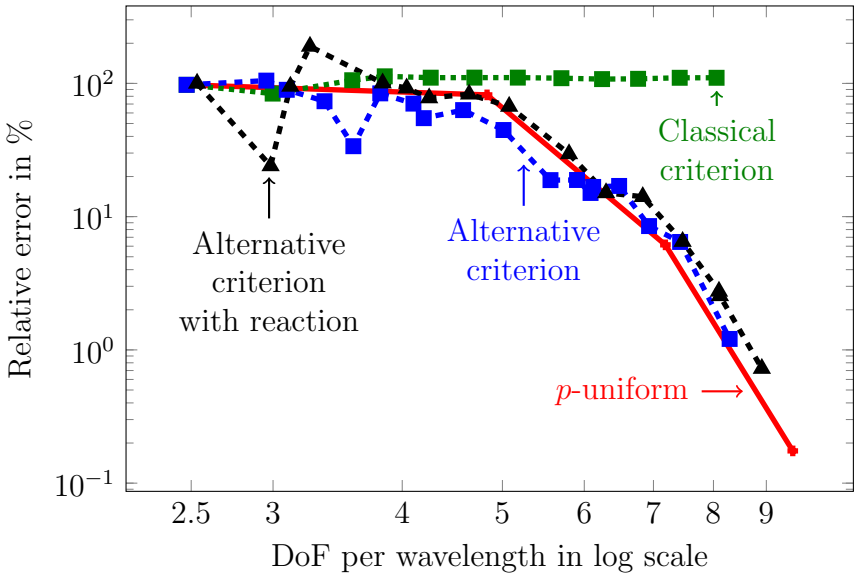

Figure 5.9.: 2D Helmholtz problem, $k = 17\pi$, $hk \gg 1$. Relative error in % in the QoI, $|l(e)|$ depending on the selected adaptive criterion.

η_K (2.8) and $\widetilde{\eta_K}$ (2.11). We observe that the maximum error is about one order of magnitude larger for the classical estimators than for the alternative ones, which corroborates the results described in Figures 5.6 and 5.7. The al-

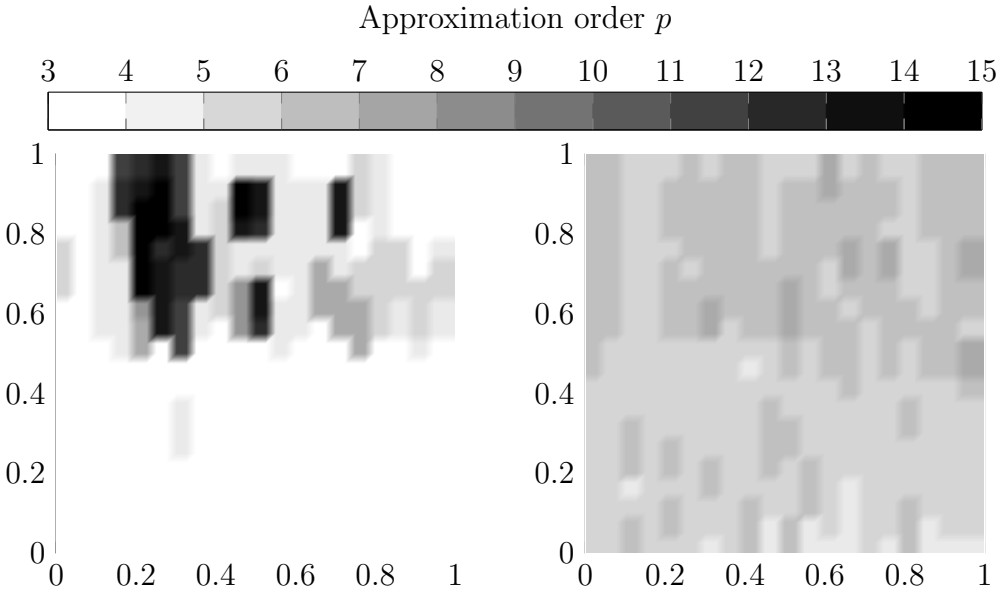

(a) Classical criterion without PBI (b) Alternative criterion without PBI

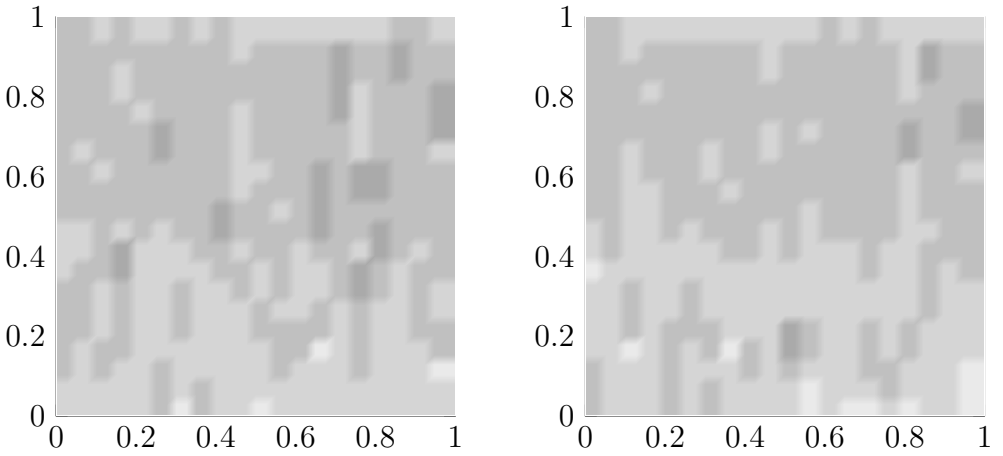

(c) Classical criterion with PBI (d) Alternative criterion with PBI

Figure 5.10.: 2D Helmholtz problem, $k = 17\pi$, $hk \gg 1$. Final adapted fine meshes after p-adaptivity.

ternative method concentrates the largest errors close to the QoI, which seem to rapidly decay as we move below the line $(0,1) \times \{0.75\}$. This observation is coherent with the fact that the error $\widetilde{\varepsilon}$ is the solution of a diffusive problem that takes as a source the residual of the adjoint problem. Conversely, the classical method exhibits large errors in a region that seems unrelated to the QoI. Figure 5.10a confirms that refinements occur in the aforementioned region. Apart from the extreme values, the error distribution is quite uniform, which is consistent with the nature of both e and ε, which are solutions of Helmholtz residual problems.

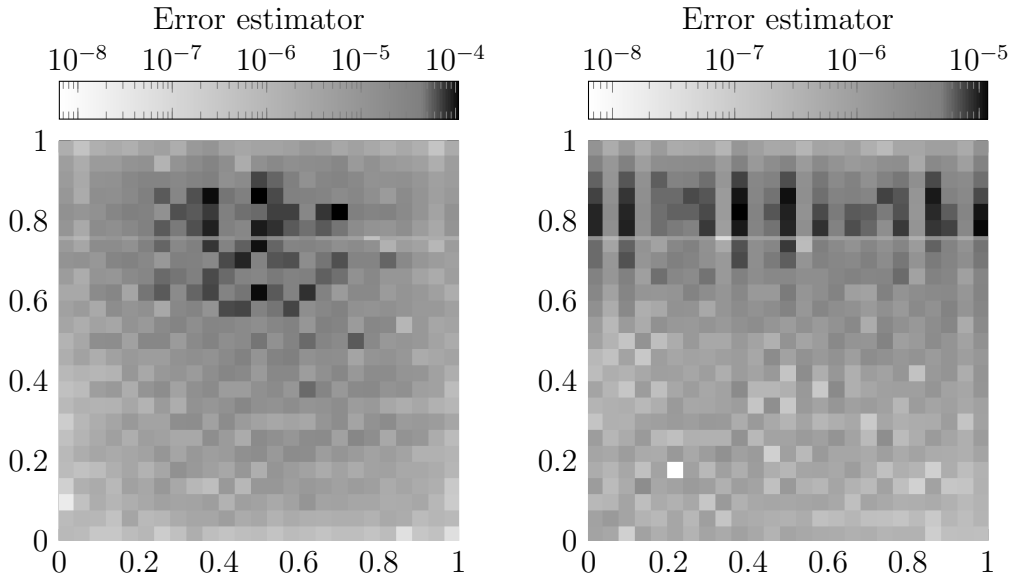

(a) Classical estimators (b) Alternative estimators

Figure 5.11.: 2D Helmholtz problem, $k = 17\pi$, $p = 1$ uniformly, $hk \gg 1$. Error map representations. We select a logarithmic scale of the error for selecting the color. The gray color has been set to separate between the elements that are to be refined (those with darker tones) and those that will be unrefined (brighter tones).

Increasing the wavenumber. We now increase the wavenumber k of operator B. We employ a constant number of DoF per wavelength in order to compare the behavior of the classical and the alternative upper bounds. Figure 5.12 shows that the alternative bound is significantly less affected by pollution than the classical one and stays closer to the error in the QoI. The observed oscillations are due to the selected QoI and they depend upon the total number of wavelengths in the computational domain.

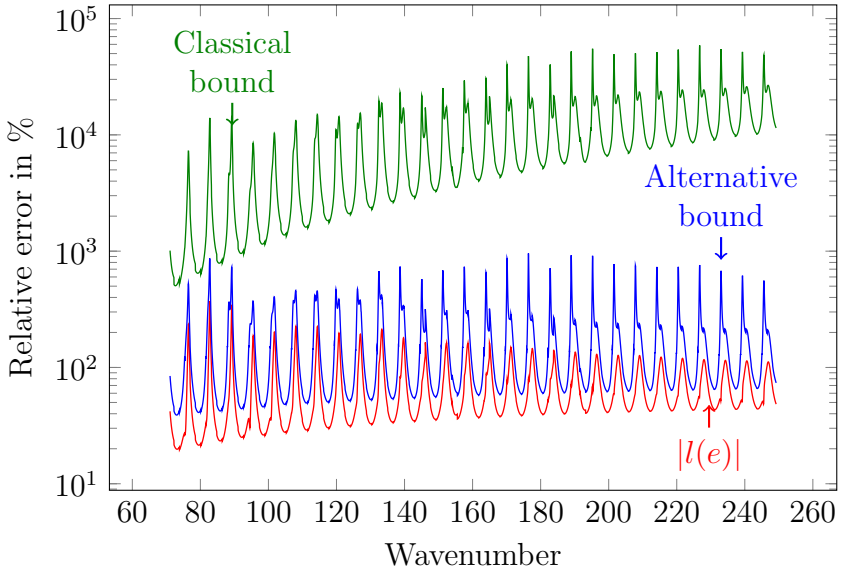

Figure 5.12.: 2D Helmholtz problem, uniform $p = 2$; h is determined in order to ensure a fixed number of (approx. eight) DoF per wavelength. Error evolution in the QoI and upper bounds for the error representation of the QoI when the wavenumber is increasing from 71 to 250. $\widetilde{B}$ is the Laplace operator.

Gradient of the solution as Quantity of Interest. We now show the robustness of the method by considering a different kind of QoI (similar to that used, for instance, in [115]). For this purpose, we consider the 2D problem described in Section 5.1.1 with the following QoI:

$$\langle l\,,w\rangle_{\mathbb{H}^*,\mathbb{H}} = \langle 1\,,\nabla w\rangle_{L^2(\Omega_{\mathrm{QoI}})} \qquad \forall w \in \mathbb{H}.$$

where $\Omega_{\mathrm{QoI}} := (0.75, 1)^2$. Figure 5.13 shows that the bound provided by the alternative representation is sharper than the classical one in the pre-asymptotic regime, as expected.

5.1.2.3. 3D numerical results: refinements and adaptivity

Figure 5.14 shows numerical results corresponding to uniform p-refinements. Again, our method provides sharper upper bounds in the pre-asymptotic regime than those obtained with the classical method. The p-adaptive algorithm also exhibits a behavior similar to that observed in the 2D case (see Figure 5.15). The alternative bound is driving the convergence more efficiently than the classical one.

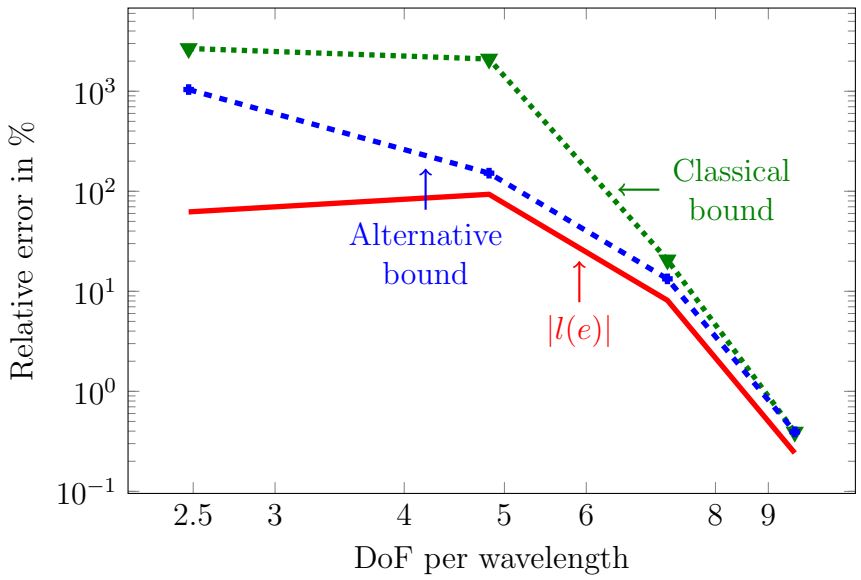

Figure 5.13.: 2D Helmholtz problem, $k = 17\pi$, $hk \gg 1$, uniform p-refinements. Error evolution in the QoI and upper bounds for the error representation in the QoI when the QoI is the average of the gradient on a subdomain of Ω.

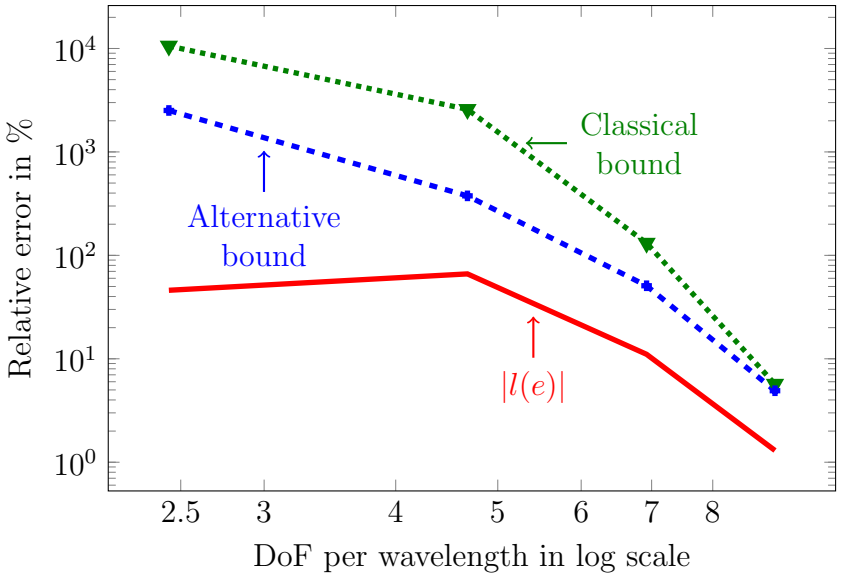

Figure 5.14.: 3D Helmholtz problem, $k = 6\sqrt{3}\pi \simeq 32.64$. Uniform p-refinements.

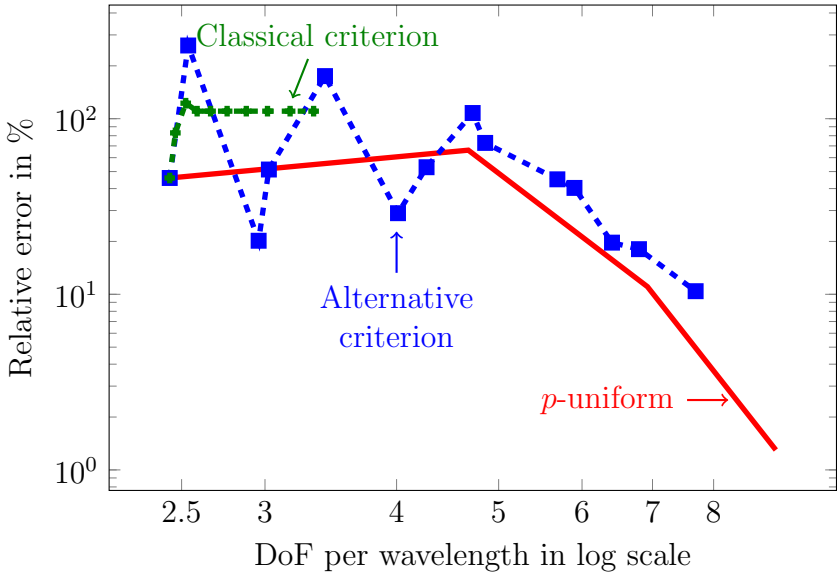

Figure 5.15.: 3D Helmholtz problem, $k = 6\sqrt{3}\pi \simeq 32.64$. Error evolution in the QoI depending on the p-adaptive criterion.

5.2. Convection-dominated diffusion problem

5.2.1. Model problem

We consider the following model problem based on a convection-dominated diffusion equation. For $\Omega = (0,1)^2$,

> Find u such that, for $\nu > 0$,
>
> $$\begin{cases} -\nu\Delta u + (1,1)\cdot\nabla u = 1 & \text{in } \Omega, \\ u = 0 & \text{on } \partial\Omega. \end{cases} \tag{5.14}$$

We set $\mathbb{H} = \{u \in H^1(\Omega), u = 0 \text{ on } \partial\Omega\}$ and $\langle \cdot\,,\cdot \rangle_{L^2}$ the standard L^2 scalar product. We define the QoI as the integral over $\Omega_{\text{QoI}} \subset \Omega$ of $w \in \mathbb{H}$, which is given by the functional

$$\langle l\,, w\rangle_{\mathbb{H}^*,\mathbb{H}} = \langle 1\,, w\rangle_{L^2(\Omega_{\text{QoI}})} \quad \forall w \in \mathbb{H}.$$

Operator $B \in \mathcal{L}(\mathbb{H}, \mathbb{H}^*)$ is defined as follows,

$$\langle Bw\,, z\rangle_{\mathbb{H}^*,\mathbb{H}} = \nu\,\langle \nabla w\,, \nabla z\rangle_{L^2(\Omega)} + \langle (1,1)\cdot\nabla w\,, z\rangle_{L^2(\Omega)}\,, \quad \forall w, z \in \mathbb{H}. \tag{5.15}$$

We define the alternative operator:

$$\left\langle \widetilde{B}w\,,z\right\rangle_{\mathbb{H}^*,\mathbb{H}} = \langle \nabla w\,,\nabla z\rangle_{L^2(\Omega)} \quad \forall w,z\in\mathbb{H}, \tag{5.16}$$

which is associated with the Laplace equation with homogeneous Dirichlet boundary condition on $\partial\Omega$. We set the QoI domain to $\Omega_{\text{QoI}} = (0.75,1)^2$ which includes a portion of the boundary layer.

5.2.2. Numerical results

We perform uniform p- and h-refinements starting from a quasi-uniform initial mesh with 11×11 elements. Figure 5.16 shows the behavior of the upper bounds with respect to diffusion parameter ν. As parameter ν decreases, the upper bounds increase, as expected.

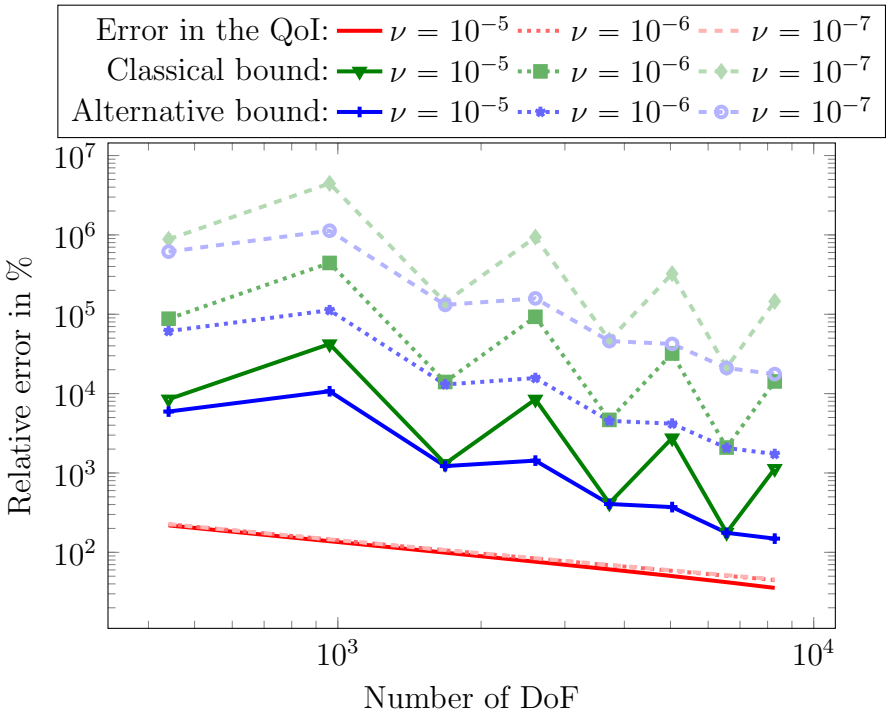

Figure 5.16.: 2D convection-dominated diffusion problem. Uniform p-refinements for different diffusion coefficients.

We now set $\nu = 10^{-4}$ and consider uniform p-refinements. Figure 5.17a

shows the following four upper bounds of the error in the QoI:

$$|l(e)| \leqslant \sum_K |\langle B_K e\,, \varepsilon\rangle| \tag{5.17}$$

$$\leqslant \sum_K (\nu \|\nabla\varepsilon\|_{L^2(K)} + \|\varepsilon\|_{L^2(K)}) \|\nabla e\|_{L^2(K)}\,, \tag{5.18}$$

and

$$|l(e)| \leqslant \sum_K \left|\left\langle \widetilde{B}_K e\,, \widetilde{\varepsilon}\right\rangle\right| \tag{5.19}$$

$$\leqslant \sum_K \|\nabla e\|_{L^2(K)} \|\nabla\widetilde{\varepsilon}\|_{L^2(K)}\,. \tag{5.20}$$

Upper bounds (5.17) and (5.19) are non-monotonous probably due to the lack of control on the angle between the errors. However, the monotonicity is recovered when considering upper bounds (5.18) and (5.20), although those upper bounds are less sharp. Nevertheless, in all cases, we observe that the alternative upper bounds are sharper than the classical ones. Moreover, if $\widetilde{B}$ also includes an L^2-inner product term as follows,

$$\left\langle \widetilde{B} w\,, z\right\rangle_{\mathbb{H}^*,\mathbb{H}} = \langle \nabla w\,, \nabla z\rangle_{L^2(\Omega)} + \langle w\,, z\rangle_{L^2(\Omega)} \quad \forall w, z \in \mathbb{H}. \tag{5.21}$$

The alternative upper bound is still sharper than the classical one. Nonetheless, the Laplace alternative operator still provides the best results (see Figure 5.17a). For h-refinements (see Figure 5.17b), we observe that upper bound (5.19) is sharper than upper bound (5.17). However, there is no oscillating behavior due to the selected mesh size. For a finer size, we would again observe the previously mentioned oscillations.

We now execute the p-adaptive process for $\nu = 10^{-7}$ with an initial mesh uniformly distributed on the log scale from the boundaries to the interior of the domain such that the boundary layers are captured. Figure 5.18 shows the evolution of the upper bounds driving the adaptivity. The classical method does not converge, whereas the alternative criterion is successful even if not very sharp at first glance. Additionally, the number of DoF needed for a given precision is lower for the adaptive discretization than for the uniform refinements case. This occurs because features of the solution are localized, unlike in the solution of the Helmholtz problem, as mentioned in Section 3.2.

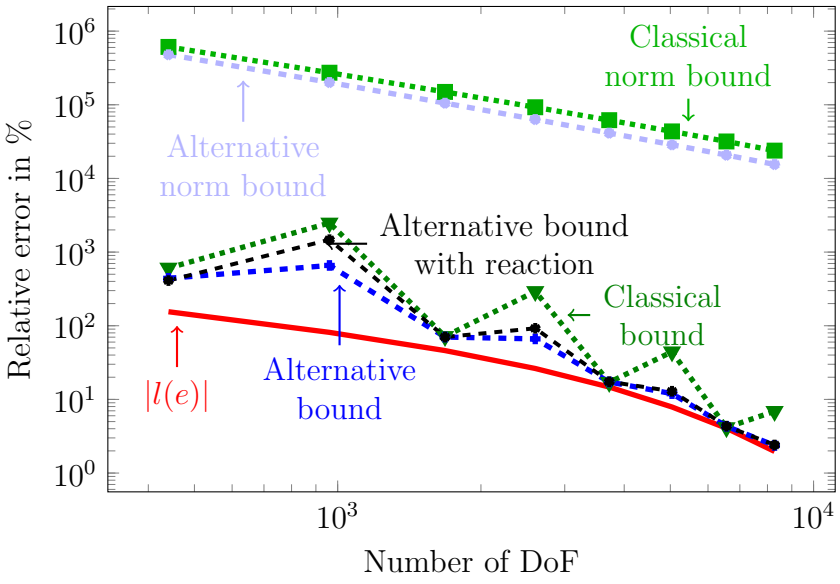

(a) Uniform p-refinement.

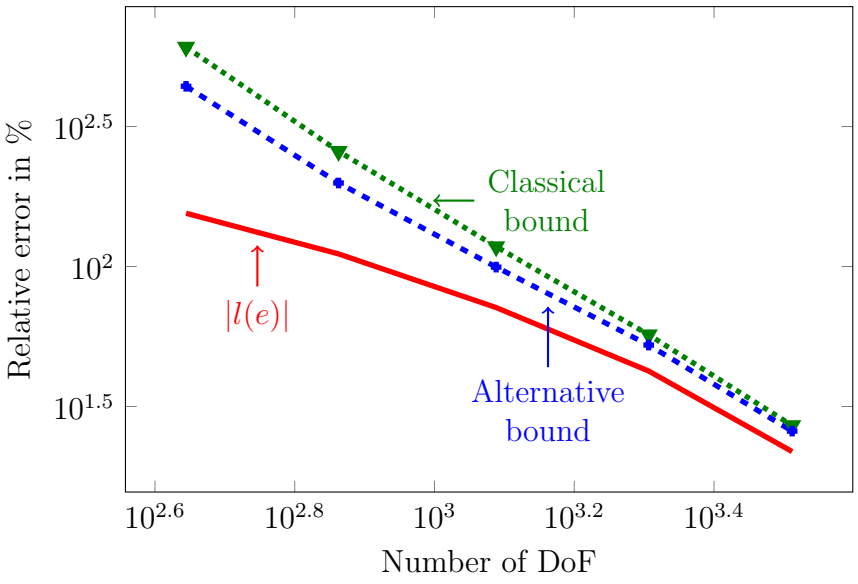

(b) Uniform h-refinements.

Figure 5.17.: 2D convection-dominated diffusion problem. Uniform refinements for $\nu = 10^{-4}$.

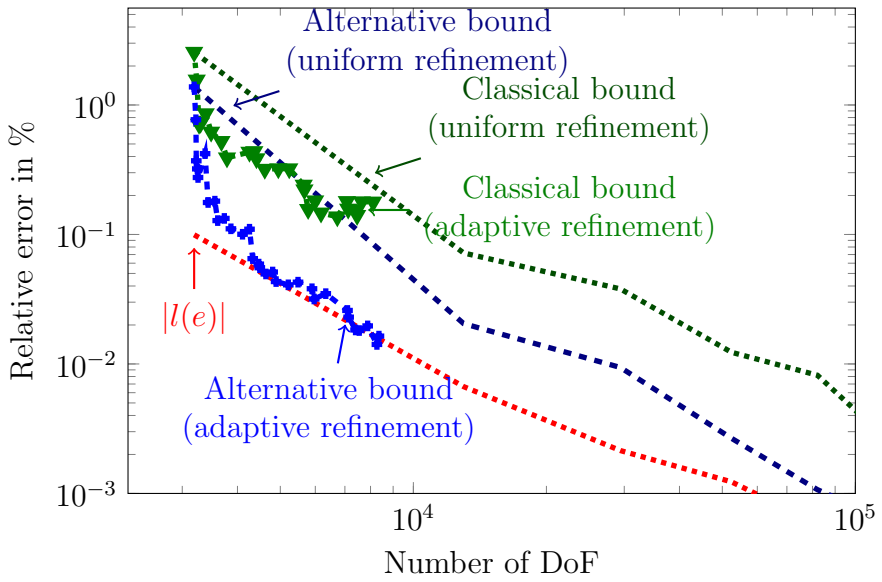

Figure 5.18.: 2D convection-dominated diffusion problem with $\nu = 10^{-7}$. Evolution of the upper bounds through p-adaptivity.

5.3. Discontinuous coefficients

5.3.1. Model problem

We consider the following general model problem governed by a diffusion-convection-reaction equation with mixed boundary conditions: For $\Omega = (0,1)^2$, with $\bar{\Gamma}_D \bigcup \bar{\Gamma}_I = \partial\Omega$, $\mathring{\Gamma}_D \bigcap \mathring{\Gamma}_I = \varnothing$.

Find u such that, for $\alpha, \beta, \gamma \in L^2(\Omega)$,

$$\begin{cases} -\nabla(\alpha \cdot \nabla u) + \beta(1,1) \cdot \nabla u + \gamma u = 1 & \text{in } \Omega, \\ u = 0 & \text{on } \Gamma_D, \\ \partial_n u + i\sqrt{|\gamma|}u = 0 & \text{on } \Gamma_I, \end{cases} \tag{5.22}$$

In particular, for $\Gamma_I = \varnothing$ and $\gamma = 0$, we recover our previous convection diffusion problem, and for $\beta = 0$ and $\gamma < 0$, we obtain the Helmholtz equation. We set $\mathbb{H} := \{u \in H^1(\Omega), u_{|\Gamma_D} = 0\}$ and $\langle \cdot, \cdot \rangle_{L^2}$ the standard L^2 scalar product. We define the QoI as the integral of $w \in \mathbb{H}$ over $\Omega_{\text{QoI}} \subset \Omega$, which is given by the functional

$$\langle l, w \rangle_{\mathbb{H}^*,\mathbb{H}} = \langle 1, w \rangle_{L^2(\Omega_{\text{QoI}})} \quad \forall w \in \mathbb{H}.$$

In the following, we set the QoI domain to $\Omega_{\text{QoI}} = (0.75, 1)^2$. Operator $B \in \mathcal{L}(\mathbb{H}, \mathbb{H}^*)$ is defined as follows,

$$\langle Bw\,,z\rangle_{\mathbb{H}^*,\mathbb{H}} = \langle \alpha\nabla w\,,\nabla z\rangle_{L^2(\Omega)} + \langle \beta(1,1)\cdot\nabla w\,,z\rangle_{L^2(\Omega)} \tag{5.23}$$

$$+ \langle \gamma w\,,z\rangle_{L^2(\Omega)} + i\left\langle \sqrt{|\gamma|}w\,,z\right\rangle_{L^2(\Gamma_I)}, \quad \forall w,z\in\mathbb{H}. \tag{5.24}$$

We define the following alternative operator: for $\widetilde{\alpha},\widetilde{\beta},\widetilde{\gamma}\in L^2(\Omega)$,

$$\left\langle \widetilde{B}w\,,z\right\rangle_{\mathbb{H}^*,\mathbb{H}} = \langle \widetilde{\alpha}\nabla w\,,\nabla z\rangle_{L^2(\Omega)} + \left\langle \widetilde{\beta}(1,1)\cdot\nabla w\,,z\right\rangle_{L^2(\Omega)} \tag{5.25}$$

$$+ \langle \widetilde{\gamma} w\,,z\rangle_{L^2(\Omega)} + i\left\langle \sqrt{|\widetilde{\gamma}|}w\,,z\right\rangle_{L^2(\Gamma_I)}, \quad \forall w,z\in\mathbb{H}. \tag{5.26}$$

The coefficients are considered to be piecewise-constant, as illustrated in Figure 5.19.

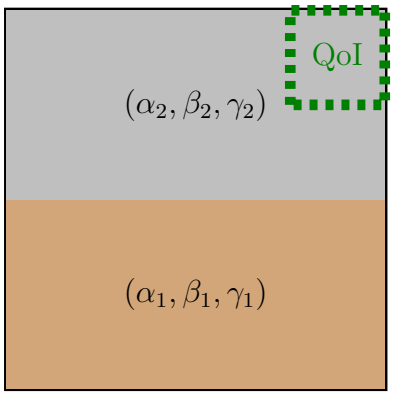

Figure 5.19.: Domain with two materials.

5.3.2. Numerical results

We first set $\Gamma_I = \varnothing$, $\gamma = 0$, $\beta = 1$ with the following piecewise-constant diffusion coefficient: $\alpha = \alpha_1 \mathbb{1}_{(0,1)\times(0,0.5)} + \alpha_2 \mathbb{1}_{(0,1)\times(0.5,1)}$ with $\mathbb{1}$ being the characteristic function. Figure 5.20 shows the upper bounds for $\alpha_1 = 10^{-4}$, $\alpha_2 = 10^{-7}$, $\widetilde{\beta} = \widetilde{\gamma} = 0$, and $\widetilde{\alpha} = \alpha$. The alternative bound is sharper than the classical one. As the discontinuity in the coefficients induces a loss of stability, both upper bounds are less effective than in the constant coefficient case. However, the alternative upper bound is less affected by the instability than the classical one.

We now consider a Helmholtz problem by setting

$$\Gamma_I = \big(\{1\}\times(0,1)\big)\bigcup\big((0,1)\times\{1\}\big),$$

$\alpha = 1$, $\beta = 0$ and a piecewise constant reaction coefficient:

$$\gamma = \gamma_1 \mathbb{1}_{(0,1)\times(0,0.5)} + \gamma_2 \mathbb{1}_{(0,1)\times(0.5,1)}.$$

Figure 5.21 shows the upper bounds for $\gamma_1 = -2842$ and $\gamma_2 = -5053$, $\widetilde{\beta} = \widetilde{\gamma} = 0$, and $\widetilde{\alpha} = \alpha$. For this case, there are no significant differences in the behavior of the upper bounds between continuous or discontinuous coefficients. The alternative method is producing sharper upper bounds for both cases, and we again observe that both upper bounds coincide in the asymptotic regime (when the error in the QoI is around 1%).

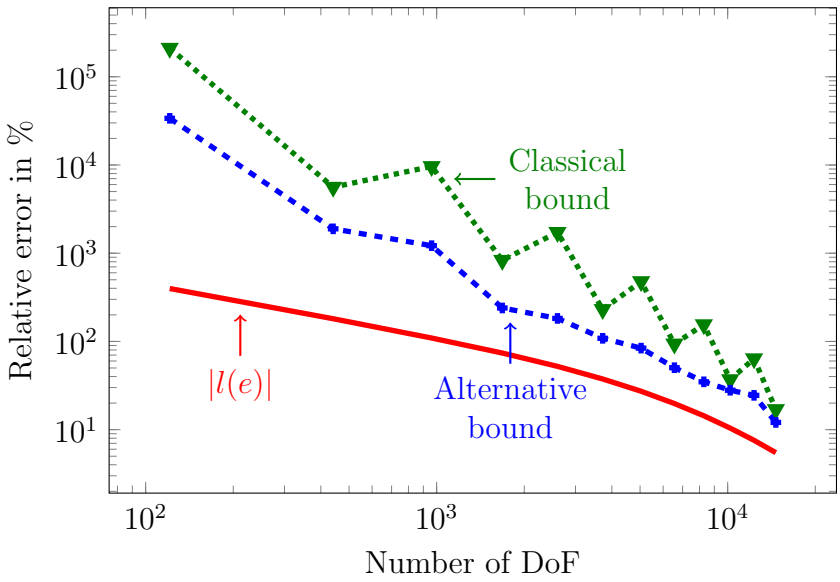

Figure 5.20.: 2D Convection-dominated diffusion problem with a discontinuous diffusion coefficient ($\alpha = 10^{-4} \cdot \mathbb{1}_{(0,1)\times(0,0.5)} + 10^{-7} \cdot \mathbb{1}_{(0,1)\times(0.5,1)}$). Upper bounds corresponding to the case of uniform p-refinements

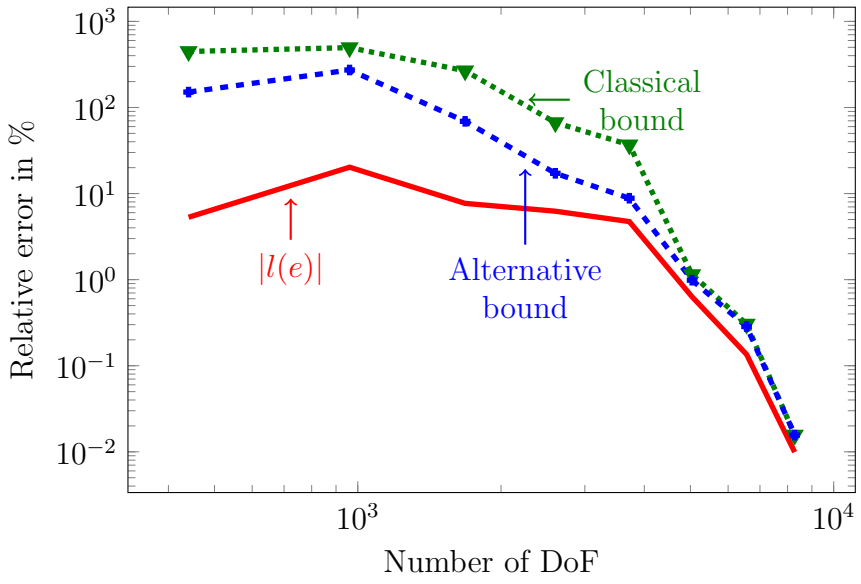

Figure 5.21.: 2D Helmholtz problem with discontinuous materials ($\gamma = 2\,842 \cdot \mathbb{1}_{(0,1)\times(0,0.5)} + 5053 \cdot \mathbb{1}_{(0,1)\times(0.5,1)}$). Upper bounds corresponding to the case of uniform p-refinements

6. Geophysical borehole application: frequency domain acoustics

In this section, we apply our adaptive strategy to the simulation of sonic Logging While Drilling (LWD) measurements, as described in [116, 117, 118]. To simplify the implementation, we focus only on a purely acoustic media (without elasticity).

6.1. Model problem

We assume axial symmetry around the center of the borehole, so we can reduce the original 3D formulation to two spatial dimensions using cylindrical coordinates. To truncate the computational domain, we employ a Perfectly Matched Layer (PML) (see [119]). The logging instrument contains a transmitter t_x and an array of 13 receivers $(r_x^i)_{i=1,13}$.

We consider the following problem with the following boundary conditions: for $\Omega \subset \mathbb{R}^2$, with boundary $\bar{\Gamma}_D \bigcup \bar{\Gamma}_{\text{axis}} = \partial\Omega$, $\mathring{\Gamma}_D \bigcap \mathring{\Gamma}_{\text{axis}} = \varnothing$, where Γ_{axis} is the boundary corresponding to the symmetry axis,

Find $\mathfrak{p}$ such that, for $c \in L^\infty(\Omega), c \neq 0, f \in \mathbb{R}^+$,

$$\begin{cases} -\Delta\mathfrak{p} - \frac{2\pi \cdot f}{c}\mathfrak{p} = \mathbb{1}_{t_x} & \text{in } \Omega \\ \mathfrak{p} = 0 & \text{on } \Gamma_D, \\ \nabla\mathfrak{p} \cdot \vec{n} = 0 & \text{on } \Gamma_{\text{axis}}, \end{cases} \tag{6.1}$$

where $\mathbb{1}_{t_x}$ is the characteristic function over the area occupied by transmitter t_x and $\vec{n}$ is the outgoing normal unit vector. We define the Quantity of Interest (QoI) as the sum over the array of receivers of the average value of the solution

at each receiver. Namely,

$$\langle l\,,\phi\rangle_{\mathbb{H}^*,\mathbb{H}} = \sum_{i=1}^{N_{r_x}} \frac{1}{\left|\Omega_{r_x^i}\right|} \int_{\Omega_{r_x^i}} \phi, \quad \forall \phi \in \mathbb{H}, \tag{6.2}$$

where $\Omega_{r_x^i}$ is the domain occupied by the i-th receiver, and N_{r_x} is the number of receivers. We set the frequency of the transmitter to $f = 20$ kHz. The material coefficient c varies throughout the domain depending on the propagation velocity of the wave in each layer. The domain is composed of three different layers: The tool (with associated velocity c_{tool}), the fluid surrounding the tool with velocity c_{fluid}, and the rock formation with velocity $c_{\text{formation}}$ (see Table 6.1). The computational domain is described in Figure 6.1.

	c_{tool}	c_{fluid}	$c_{\text{formation}}$
Velocities (m/s)	5862	1524	4354

Table 6.1.: Propagation velocities (m/s) of the materials for LWD acoustic measurements.

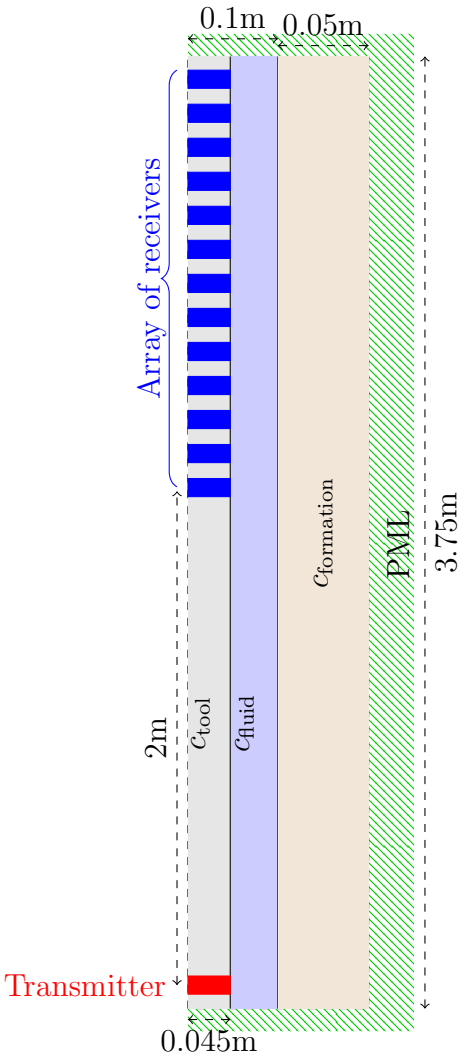

Figure 6.1.: Sketch of the computational domain for acoustic LWD measurements, composed of three different materials: The logging tool, the borehole fluid, and the rock formation. The axis of symmetry is located on the left side of the domain and coincides with the tool center. We have added a PML to truncate the computational domain. In red, we draw the transmitter and in blue the array of receivers.

6.2. Numerical Results

We select the Laplace operator with constant material coefficients as our alternative operator,

$$\left\langle \widetilde{B}w\,,z\right\rangle_{\mathbb{H}^*,\mathbb{H}} = \langle \nabla w\,,\nabla z\rangle_{L^2(\Omega)} \quad \forall w,z\in\mathbb{H}. \tag{6.3}$$

Figure 6.2 shows the evolution of the error upper bounds throughout the adaptive process. We plot the upper bounds given by Eqs. (2.8) and (2.11) both when using p-adaptivity with and without the Projection Based Interpolation (PBI) operator. Results are similar to the ones of Figure 5.8. The classical criterion fails to drive the adaptive process. On the other hand, both the alternative and the PBI criteria succeed. The resulting meshes are shown in Figure 6.3. We observe that the classical criterion (see Figure 6.3a) performs refinements only within the borehole and from which most of them are located within the area occupied by the fluid. Thus, leading to an incorrect solution. When the adaptive process is successful (see Figures 6.3b, 6.3c, and 6.3d), refinements occur almost uniformly throughout the computational domain, except on the surroundings of the junctions between the PML, the logging instrument, and the fluid. The solution at those points is probably singular due to the large variation of the coefficients, and further (possibly h-) refinements are required.

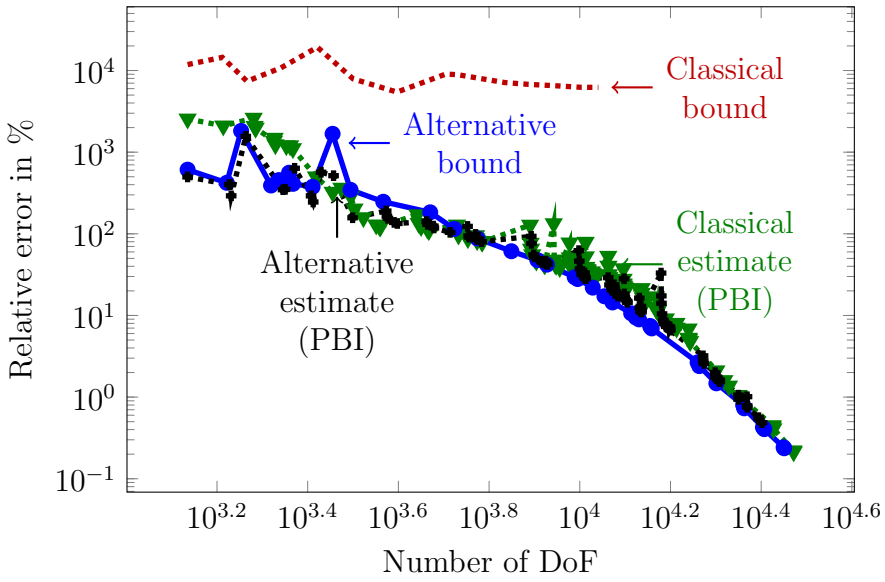

Figure 6.2.: Sonic LWD. Error representations for p-adaptivity depending on the selected criterion: classical criterion without PBI ·····, alternative criterion without PBI —●—, classical criterion using the PBI ·▼·, and alternative criterion using the PBI ·■·.

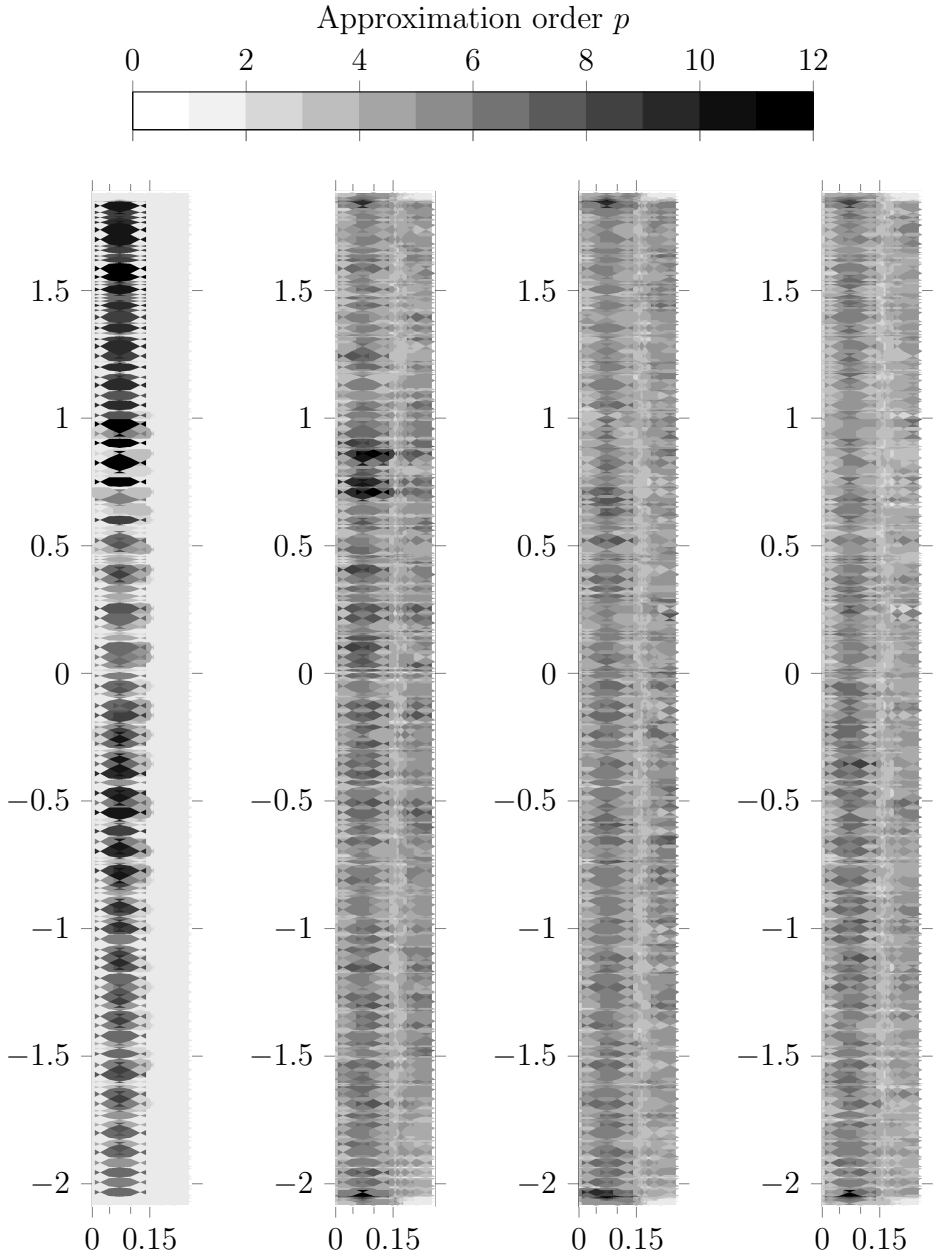

(a) Classical criterion without PBI (b) Alternative criterion without PBI (c) Classical criterion with PBI (d) Alternative criterion with PBI

Figure 6.3.: Sonic LWD. Final adapted fine meshes after p-adaptivity.

Part III.

Main achievement, conclusions and future work

7. Main achievements

7.1. Peer reviewed publications

2017 V. Darrigrand, Á. Rodríguez-Rozas, D. Pardo, I. Muga, A. Romkes, and S. Prudhomme. ***Goal-oriented adaptivity using unconventional error representations for the multi-dimensional Helmholtz equation.*** (accepted in International Journal for Numerical Methods in Engineering), 2017.

2017 V. Darrigrand, Á. Rodríguez-Rozas, D. Pardo, and I. Muga. ***Goal-oriented p-adaptivity using unconventional error representations for a 1D steady state convection-diffusion problem.*** Procedia Computer Science, 2017. doi: 10.1016/j.procs.2017.05.168

2015 V. Darrigrand, D. Pardo, and I. Muga. ***Goal-oriented adaptivity using unconventional error representations for the 1D Helmholtz equation.***
Computers & Mathematics with Applications, 69(9):964 – 979, 2015.
`http://dx.doi.org/10.1016/j.camwa.2015.03.006`.

7.2. Conferences talks

2017 V. Darrigrand, D. Pardo, I. Muga, Á. Rodríguez-Rozas.
Unconventional Error Representations for Goal-Oriented p-Adaptivity and its Applications
ADMOS 2017, Verbania, Italia.

2017 V. Darrigrand, D. Pardo, I. Muga, Á. Rodríguez-Rozas.
Goal-oriented p-adaptivity using unconventional error representations for a 1D steady state convection-diffusion problem.
ICCS, Zurich, Switzerland.

2016 V. Darrigrand, D. Pardo, I. Muga, Á. Rodríguez-Rozas.
Unconventional Error Representations for Goal-Oriented Ad-

aptivity
WCCM XII & APCOM VI, Seoul, South Korea.

2016 V. Darrigrand, D. Pardo, H. Barucq, I. Muga, Á. Rodríguez-Rozas. ***Unconventional Error Representations for Goal-Oriented Adaptivity***
ICOSAHOM 2016, Rio de Janeiro, Brazil.

2015 V. Darrigrand, D. Pardo and I. Muga. ***Goal-Oriented Adaptivity using Unconventional Error Representations***
PANACM 2015, Buenos Aires, Argentina.

7.3. Seminars & Workshops

2017 E. Alberdi, V. Darrigrand, J. Muñoz, D. Pardo, V. M. Calo, Á. Rodríguez-Rozas, I. Muga. ***Pseudo-Dual Error Representations for Goal-Oriented Adaptivity: Applications to Time-Domain and Helmholtz Problems*** Fifth International Workshop On Multiphysics, Multiscale, and Optimization Problems, Barcelona, Spain. May 2017

2016 V. Darrigrand, D. Pardo, H. Barucq, I. Muga, Á. Rodríguez-Rozas. ***Goal-Oriented Adaptivity using Unconventional Error Representations*** Fourth International Workshop On Multiphysics, Multiscale, and Optimization Problems, BCAM, Bilbao, Spain. May 2016

2016 V. Darrigrand, D. Pardo, I. Muga and Á. Rodríguez-Rozas. ***Generalised Error Representations for Goal-Oriented Adaptivity*** Seminar Caleta Numérica, Valparaiso, Chile. May 2016

2016 V. Darrigrand, D. Pardo, I. Muga, and Á. Rodríguez-Rozas. ***Generalised Error Representations for Goal-Oriented Adaptivity*** Workshop: "The Sixth Valparaíso's Mathematics and Applications Days" (V-MAD 6), Valparaiso, Chile. January 2016

2015 V. Darrigrand, D. Pardo, and I. Muga. ***Goal-Oriented Adaptivity using Unconventional Error Representations*** Workshop on Advanced Subsurface Visualization Methods: "Exploring the Earth" 2015, Pau, France. May 2015

2015 V. Darrigrand, D. Pardo and I. Muga. ***Goal-Oriented Adaptivity using Unconventional Error Representations for Wave Propagation Problems.*** Seminar at UPC, Barcelona, Spain. March 2015

2015 V. Darrigrand, D. Pardo and I. Muga. ***Goal-Oriented Adaptivity using Unconventional Error Representations for Wave Propagation Problems.*** Seminar at Kaust, Saudi Arabia. March 2015

2014 V. Darrigrand, D. Pardo, and I. Muga. ***Goal-Oriented Adaptivity for Wave Propagation Problems using Multiple Dual Problems.*** Third International Workshop On Multiphysics, Multiscale, and Optimization Problems, BCAM, Bilbao, May 2014.

2014 D. Pardo, J. Alvarez-Aramberri, V. Darrigrand, S. Bakr, and C. Torres-Verdin. ***Fast Inversion of Alternate Current (AC) Geophysical Measurements*** Third International Workshop On Multiphysics, Multiscale, and Optimization Problems, BCAM, Bilbao, May 2014.

2014 V. Darrigrand, D. Pardo, and I. Muga. ***Goal-Oriented Adaptivity using Unconventional Error Representations for Wave Propagation Problems.*** Third International Workshop On Multiphysics, Multiscale, and Optimization Problems, BCAM, Bilbao, May 2014.

7.4. Teaching

2016 Mini course (4h) : **Improving figures using TikZ/PGF for LaTeX: An Introduction.**
Valparaíso, Chile : May 2016.
Bilbao, Spain : May 2016.

2014-2015 ATER position: 192h (EqTD). *Pau, France*

7.5. Awards

2015 Best poster presentation for the doctoral school at University of Pau.
Goal-oriented adaptivity with multiple dual problems
University of Pau, France

7.6. Implemented software

The finite element library *FEM* employed in this work has been developed within the group M2SI[1]. It is written in Fortran90 and it is still under development. It allows arbitrary high-order, mixed finite element of H^1-, $H(\text{curl})$-

[1] `https://sites.google.com/site/m2sigroup/`

$H(\mathrm{div})$-, and L^2-conforming discretizations. Thus, it is suitable for solving multiphysics problems and it is also employed for the inversion of borehole resistivity measurements. The library solves 1D, 2D, and 3D problems, and it employs quadrilateral elements in 2D and hexahedral elements in 3D.

My contribution to the software has been (a) to implement the p-adaptive goal-oriented algorithm compatible with the proposed method, for H^1 discretizations. It contains a package that solves the direct and adjoint problems on both fine and coarse meshes; (b) to implement the Projection Based Interpolation (PBI) for 1D and 2D; (c) to implement a Perfectly Matched Layer (PML) for Helmholtz problems in 1D, 2D, and 3D in collaboration with Dr. Julen Álvarez-Arramberri.

We reduce the needs of computational resources by reusing the matrix LU decomposition when feasible. When possible, we also pre-compute Gauss integrations in the master element in order to accelerate the computation of the stiffness matrix. Indeed, for high-order elements, the time needed to integrate basis functions dramatically increases. However, and especially for axial symmetry (cylindrical coordinates), pre-computations comes with a cost in memory usage compensated by the saved computational time.

8. Conclusions and Future work

8.1. Conclusions

This dissertation proposes the use of operators, different from the adjoint one, to represent the error in the Quantity of Interest (QoI). Upper bounds of these error representations drive the goal-oriented (or energy-norm) adaptive process. We compared our alternative upper bound estimates vs those derived with the classical goal-oriented methodology. In particular, we have studied the behavior of a simple p-adaptive process when using both a classical error representation in the QoI (as described in [19, 17]) and an alternative error representation, for the cases of (a) a 1D Helmholtz problem,(see Section 4.1), (b) a 1D convection dominated problem,(see Section 4.2), (c) a 2D and a 3D Helmholtz problem,(see Section 5.1), (d) a 2D convection dominated problem (see Section 5.2), (e) 2D problems with discontinuous material coefficients (see Section 5.3), and (f) a geophysical application consisting of simulating sonic Logging While Drilling (LWD) measurements restrained to a purely acoustic media (see Chapter 6).

We observe that our method provides sharper upper bounds when applied to the 1D-Helmholtz equation using the 1D-Laplace operator to represent the error. The experiments performed using different alternative operators, like the L^2-scalar product or the positive definite Helmholtz equation, show that we also obtain upper bounds sharper than the classical ones. Thus, we have a set of operators that may provide sharper estimates. This, in turn, enables us to obtain more efficient adaptive algorithms.

For the 1D convection-dominated diffusion problem, we start with a very coarse initial mesh with very few Degrees of Freedom (DoF). Our alternative goal-oriented adaptive algorithm produces a final mesh that captures the boundary layer, thus, reduces significantly the spurious oscillations.

We address the question of whether we can find an operator that provides the sharpest upper bounds independently of the approximation space. However, this seems to be prohibitively expensive. We illustrate this issue with a 2D Helmholtz problem and we propose to use the Laplacian as the alternative operator in order to represent the dual residual. With that operator, we are not computing the sharpest upper bound but it represents a good trade-off between

computational feasibility and obtaining sharp upper bounds. A guideline for the choice of the alternative operator is to construct an operator that presents a better numerical stability than the original one.

In the multi-dimensional case, numerical results confirm that error bounds are sharper when using the alternative representation than with the classical one. As a result, our simple adaptive process does not need the PBI (nor any other projection) to converge when using the alternative error representation as indicators, whereas the classical representation fails to drive the algorithm to converge without the PBI. The classical and alternative bounds coincide when reaching the asymptotic regime.

One notorious advantage of our approach is its flexibility. Indeed, we can apply this technique to a wide range of problems, including adaptivity in time domain [104, 120], adaptivity in a high continuity space [121, 122, 123], or *hp*-adaptive algorithms [7, 58].

8.2. Future work

In Chapter 6, we treated the case of sonic LWD measurements restrained to acoustics media. In a near future, we plan to extend our adaptive strategy to elastoacoustics media [116, 117, 118]. The main challenge of elastoacoustics media is the presence of coupled equations. The underlying questions about the choice of the alternative operator are: (a) Should we choose an alternative operator for each medium type or a uniform one? (b) If we select a different operator for elastic and purely acoustics media, which one could provide best error distribution for elastic media? For the case of purely acoustic media, Chapter 6 provides some hints on how to address this question. Another question is how to take into account the elastoacoustic interface in the alternative error representation. Our first attempt, coming from the work developed in this dissertation, would be to select a uniform possibly vector Laplacian as the alternative operator.

We are also interested in solving multi-physics and/or multi-equation problems, such as those described in [6, 22, 124]. For instance, [124] studied a 2.5D resistivity problem governed by coupled equations. The challenges are similar to those appearing in the elastoacoustic case: Which physic(s) should we select for the alternative operator? And, how to handle the coupling?

In both developments, the aim is to "reduce" the effect of the pollution error intrinsic of wave propagation problems so that the adaptive process can lead to an adapted mesh requiring an optimum number of DoF.

In addition, we plan to implement an automatic *hp*-adaptive process for the resolution of the aforementioned applications. However, its implemen-

tation is challenging mainly due to the presence of hanging nodes that are used to guarantee the continuity of the approximations. To overcome this difficulty, we will implement a multi-level version of the *hp*-Finite Element Method (FEM) described in [125]. We expect a similar behavior of the alternative error representations when using an *hp*-adaptive process as what we observed for *p*-adaptivity.

A. Error representations in terms of bilinear forms

A.1. Definitions

We start this appendix with some definitions and notation. Let $\Omega \subset \mathbb{R}^N$ be an open domain and $\mathbb{H} := \mathbb{H}(\Omega)$ a Hilbert space on Ω.

Let $\mathcal{T}$ be a partition of Ω into open elements K such that $\bar{\Omega} = \bigcup_{K\in\mathcal{T}} \bar{K}$. For each $K \in \mathcal{T}$, we consider the space $\mathbb{H}_K$ containing the restrictions to K of functions of $\mathbb{H}$. A continuous bilinear form $a : \mathbb{H} \times \mathbb{H} \to \mathbb{R}$ is said to be *localisable* if

$$a(u, v) = \sum_{K\in\mathcal{T}} a_K(u, v), \qquad \forall u \in \mathbb{H},\ \forall v \in \mathbb{H}, \tag{A.1}$$

where a_K denotes the *restriction* of a to the space $\mathbb{H}_K \times \mathbb{H}_K$. If a is also symmetric and positive definite, then it defines a norm on $\mathbb{H}$ and semi-norms on each $\mathbb{H}_K$. We denote them by

$$\|\cdot\|_a := \sqrt{a(\cdot,\cdot)} \quad \text{and} \quad |\cdot|_{a_K} := \sqrt{a_K(\cdot,\cdot)},$$

respectively.

A.2. Variational problem

We set b to be a localizable symmetric continuous bilinear form and f a continuous linear form, both defined on $\mathbb{H}$. Let $\mathbb{V}_h \subset \mathbb{H}$ be a finite dimensional Galerkin approximation space of $\mathbb{H}$, related to the partition $\mathcal{T}$. Let us consider the following variational formulation and its discrete equivalent:

Find $u \in \mathbb{H}$, $u_h \in \mathbb{V}_h$ such that

$$b(u, \phi) = f(\phi), \qquad \forall \phi \in \mathbb{H}, \tag{A.2}$$
$$b(u_h, \phi_h) = f(\phi_h), \qquad \forall \phi_h \in \mathbb{V}_h. \tag{A.3}$$

We assume that solutions of these variational formulations are unique. Thus, we can define the error function $e := u - u_h$.

For goal-oriented approaches, we provide an output functional l that defines the Quantity of Interest (QoI) for which we want to minimise the relative error. For example, an output functional (QoI) can be the average of a function (or a derivative) over a small subset $\Omega_S \subset \Omega$, i.e.,

$$l(u) = \frac{1}{|\Omega_S|}\int_{\Omega_S} u\, dx \quad \text{or} \quad l(u) = \frac{1}{|\Omega_S|}\int_{\Omega_S} \nabla u \cdot \vec{\alpha}\, dx, \quad \text{for some } \vec{\alpha} \in \mathbb{R}^N. \tag{A.4}$$

We assume that l is a linear and continuous form on $\mathbb{H}$. The goal of computations from the engineering point of view is to accurately estimate $|l(u)|$. For that purpose, the main idea of Goal-Oriented Adaptivity (GOA) is to control the error $|l(e)|$. This can be achieved by finding a *sharp* upper bound that is expressed in terms of computable norms that are guaranteed to decrease as one performs grid refinements.

A.3. Error representations

A.3.1. Classical approach

In goal-oriented adaptivity, one employs the adjoint problems (A.2) and (A.3):

> Find $v \in \mathbb{H}$ and $v_h \in \mathbb{V}_h$ such that
>
> $$b(\phi, v) = l(u), \qquad \forall \phi \in \mathbb{H}, \tag{A.5}$$
> $$b(\phi_h, v_h) = l(u_h), \qquad \forall \phi_h \in \mathbb{V}_h. \tag{A.6}$$

We assume that problems (A.5) and (A.6) are well posed so the dual error function $\varepsilon := v - v_h$ is well defined. Let $\hat{b}$ be a localisable symmetric positive definite bilinear form on $\mathbb{H}$ such that:

$$|b_K(\phi, \psi)| \leqslant |\phi|_{\hat{b}_K} |\psi|_{\hat{b}_K}, \quad \forall \phi, \psi \in \mathbb{H}. \tag{A.7}$$

We use $\hat{b}$ since the b form may not be positive definite and therefore we may not be able to define a norm or semi-norm from it. For instance, if b is the weak form of Helmholtz operator $(-\Delta - k^2)(\cdot)$, then $\hat{b}$ may be selected as the weak form of operator $(-\Delta + k^2)(\cdot)$.

By plugging solutions u and u_h into (A.5) and (A.6) respectively, and using the *localisable* property of b, we obtain the following local estimation:

$$|l(e)| = |b(e, v)| \leqslant \sum_{K \in \mathcal{T}} |b_K(e, v)| \leqslant \sum_{K \in \mathcal{T}} |e|_{\hat{b}_K} |v|_{\hat{b}_K}. \tag{A.8}$$

We observe that v is independent of the discretization and does not decrease with mesh refinements. However, the error e of the direct problem is b-orthogonal to $\mathbb{V}_h$. In particular $b(e, v) = b(e, \varepsilon)$. Therefore, we can improve the upper bound of $|l(e)|$ by introducing a quantity that decreases faster with mesh refinements:

$$|l(e)| = |b(e, \varepsilon)| \leqslant \sum_{K \in \mathcal{T}} |b_K(e, \varepsilon)| \leqslant \sum_{K \in \mathcal{T}} |e|_{\hat{b}_K} |\varepsilon|_{\hat{b}_K}. \tag{A.9}$$

A.3.2. Alternative approach

The objective of our new approach is to improve the upper bound of the error in the QoI $|l(e)|$ by obtaining sharper upper bounds.

Let $\widetilde{b}$ be an arbitrary localisable symmetric, elliptic, and continuous bilinear form. We define our elliptic representation of the dual residual error functional as the solution of the problem:

> Find $\widetilde{\varepsilon} \in \mathbb{H}$ such that:
>
> $$\widetilde{b}(\phi, \widetilde{\varepsilon}) = l(\phi) - b(\phi, v_h), \quad \forall \phi \in \mathbb{H}. \tag{A.10}$$

By the Lax-Milgram theorem (or Riesz representation), the variational formulation (A.10) has a unique solution on $\mathbb{H}$. A similar idea called *elliptic error representation* was introduced by A. Romkes & J.T. Oden [115] in the context of modelling error analysis for adaptive modelling.

$\widetilde{\varepsilon}$ must decrease with mesh refinements since it represents an error functional that depends continuously on the error ε. Moreover, $\widetilde{\varepsilon}$ is $\widetilde{b}$-orthogonal to $\mathbb{V}_h$:

$$\widetilde{b}(\phi_h, \widetilde{\varepsilon}) = l(\phi_h) - b(\phi_h, v_h) = 0, \quad \text{for all } \phi_h \in \mathbb{V}_h.$$

By introducing (A.10), we can represent the error in the QoI as:

$$l(e) = b(e, \varepsilon) = l(e) - b(e, v_h) = \widetilde{b}(e, \widetilde{\varepsilon}).$$

Hence, we obtain the new estimate:

$$|l(e)| = \left|\widetilde{b}(e, \widetilde{\varepsilon})\right| \leqslant \sum_{K \in \mathcal{T}} \left|\widetilde{b}_K(e, \widetilde{\varepsilon})\right| \leqslant \sum_{K \in \mathcal{T}} |e|_{\widetilde{b}_K} |\widetilde{\varepsilon}|_{\widetilde{b}_K}, \tag{A.11}$$

If problem (A.10) is well-posed but the $\widetilde{b}$ form is non-elliptic, then only the last inequality in (A.11) is false. In that case, we would need to make use of an inequality such as (A.7). Thus, our method generalises the existing ones.

In this Dissertation, we have shown numerically that there often exists a $\widetilde{b}$ so that estimate (A.11) is sharper than estimate (A.9).

Bibliography

[1] Ihlenburg F, Babuška I. Finite element solution of the Helmholtz equation with high wave number. II. The *h-p* version of the FEM. *SIAM J. Numer. Anal.* 1997; **34**(1):315–358, doi:10.1137/S0036142994272337. URL `http://dx.doi.org/10.1137/S0036142994272337`. (cited in page(s) 1, 6, 49)

[2] Melenk JM, Schwab C. An *hp* finite element method for convection-diffusion problems in one dimension. *IMA J. Numer. Anal.* 1999; **19**(3):425–453, doi:10.1093/imanum/19.3.425. URL `http://dx.doi.org/10.1093/imanum/19.3.425`. (cited in page(s) 1, 6)

[3] Carstensen C, Schröder A, Wiedemann S. An optimal adaptive finite element method for elastoplasticity. *Numer. Math.* 2016; **132**(1):131–154, doi:10.1007/s00211-015-0714-9. URL `http://dx.doi.org/10.1007/s00211-015-0714-9`. (cited in page(s) 1)

[4] Babuška I, Rheinboldt WC. A-posteriori error estimates for the finite element method. *International Journal for Numerical Methods in Engineering* 1978; **12**(10):1597–1615. (cited in page(s) 1)

[5] Babuška I, Rheinboldt W. Adaptive approaches and reliability estimations in finite element analysis. *Computer Methods in Applied Mechanics and Engineering* 1979; **17**:519 – 540, doi:http://dx.doi.org/10.1016/0045-7825(79)90042-2. URL `http://www.sciencedirect.com/science/article/pii/0045782579900422`. (cited in page(s) 1)

[6] Pardo D. Integration of *hp*-adaptivity with a two grid solver: applications to electromagnetics. PhD Thesis, The University of Texas at Austin 2004. URL `https://www.lib.utexas.edu/etd/d/2004/pardod042/pardod042.pdf`. (cited in page(s) 1, 84)

[7] Pardo D, Demkowicz L, Torres-Verdín C, Paszynski M. Two-dimensional high-accuracy simulation of resistivity logging-while-drilling (LWD) measurements using a self-adaptive goal-oriented *hp* finite element method. *SIAM J. Appl. Math.* 2006; **66**(6):2085–2106, doi:10.1137/050631732.

URL http://dx.doi.org/10.1137/050631732. (cited in page(s) 1, 2, 3, 84)

[8] Becker R, Rannacher R. A feed-back approach to error control in finite element methods: basic analysis and examples. *East-West J. Numer. Math.* 1996; **4**(4):237–264. (cited in page(s) 1)

[9] Becker R, Rannacher R. *Weighted a posteriori error control in FE methods*. IWR, 1996. (cited in page(s) 1)

[10] Rannacher R, Suttmeier FT. A posteriori error control in finite element methods via duality techniques: application to perfect plasticity. *Comput. Mech.* 1998; **21**(2):123–133, doi:10.1007/s004660050288. URL http://dx.doi.org/10.1007/s004660050288. (cited in page(s) 1)

[11] Paraschivoiu M, Peraire J, Patera AT. A posteriori finite element bounds for linear-functional outputs of elliptic partial differential equations. *Comput. Methods Appl. Mech. Engrg.* 1997; **150**(1-4):289–312, doi:10.1016/S0045-7825(97)00086-8. URL http://dx.doi.org/10.1016/S0045-7825(97)00086-8, symposium on Advances in Computational Mechanics, Vol. 2 (Austin, TX, 1997). (cited in page(s) 1, 5)

[12] Paraschivoiu M, Patera AT. A hierarchical duality approach to bounds for the outputs of partial differential equations. *Comput. Methods Appl. Mech. Engrg.* 1998; **158**(3-4):389–407, doi:10.1016/S0045-7825(99)00270-4. URL http://dx.doi.org/10.1016/S0045-7825(99)00270-4. (cited in page(s) 1, 5)

[13] Peraire J, Patera AT. Bounds for linear-functional outputs of coercive partial differential equations: local indicators and adaptive refinement. *Advances in adaptive computational methods in mechanics (Cachan, 1997)*, *Stud. Appl. Mech.*, vol. 47. Elsevier Sci. B. V., Amsterdam, 1998; 199–216, doi:10.1016/S0922-5382(98)80011-1. URL http://dx.doi.org/10.1016/S0922-5382(98)80011-1. (cited in page(s) 1, 5)

[14] Maday Y, Patera AT, Peraire J. A general formulation for a posteriori bounds for output functionals of partial differential equations; application to the eigenvalue problem. *C. R. Acad. Sci. Paris Sér. I Math.* 1999; **328**(9):823–828, doi:10.1016/S0764-4442(99)80279-1. URL http://dx.doi.org/10.1016/S0764-4442(99)80279-1. (cited in page(s) 1, 5)

[15] Peraire J, Patera AT. Asymptotic a posteriori finite element bounds for the outputs of noncoercive problems: the Helmholtz and Burgers equations. *Comput. Methods Appl. Mech. Engrg.* 1999; **171**(1-2):77–86, doi:10.1016/S0045-7825(98)00244-8. URL `http://dx.doi.org/10.1016/S0045-7825(98)00244-8`. (cited in page(s) 1, 5)

[16] Sarrate J, Peraire J, Patera A. A posteriori finite element error bounds for non-linear outputs of the Helmholtz equation. *Internat. J. Numer. Methods Fluids* 1999; **31**(1):17–36, doi:10.1002/(SICI)1097-0363(19990915)31:1⟨17::AID-FLD953⟩3.0.CO;2-X. URL `http://dx.doi.org/10.1002/(SICI)1097-0363(19990915)31:1<17::AID-FLD953>3.0.CO;2-X`, tenth International Conference on Finite Elements in Fluids (Tucson, AZ, 1998). (cited in page(s) 1, 5)

[17] Prudhomme S, Oden JT. On goal-oriented error estimation for elliptic problems: application to the control of pointwise errors. *Comput. Methods Appl. Mech. Engrg.* 1999; **176**(1-4):313–331, doi:10.1016/S0045-7825(98)00343-0. URL `http://dx.doi.org/10.1016/S0045-7825(98)00343-0`. (cited in page(s) 1, 2, 5, 6, 83)

[18] Oden JT, Prudhomme S. New approaches to error estimation and adaptivity for the Stokes and Oseen equations. *Internat. J. Numer. Methods Fluids* 1999; **31**(1):3–15, doi:10.1002/(SICI)1097-0363(19990915)31:1⟨3::AID-FLD952⟩3.3.CO;2-2. URL `http://dx.doi.org/10.1002/(SICI)1097-0363(19990915)31:1<3::AID-FLD952>3.3.CO;2-2`, tenth International Conference on Finite Elements in Fluids (Tucson, AZ, 1998). (cited in page(s) 1)

[19] Oden JT, Prudhomme S. Goal-oriented error estimation and adaptivity for the finite element method. *Comput. Math. Appl.* 2001; **41**(5-6):735–756, doi:10.1016/S0898-1221(00)00317-5. URL `http://dx.doi.org/10.1016/S0898-1221(00)00317-5`. (cited in page(s) 1, 2, 83)

[20] Prudhomme S, Oden JT. Computable error estimators and adaptive techniques for fluid flow problems. *Error estimation and adaptive discretization methods in computational fluid dynamics*, *Lect. Notes Comput. Sci. Eng.*, vol. 25. Springer, Berlin, 2003; 207–268, doi:10.1007/978-3-662-05189-4_5. URL `http://dx.doi.org/10.1007/978-3-662-05189-4_5`. (cited in page(s) 1)

[21] Pardo D, Demkowicz L, Torres-Verdín C, Tabarovsky L. A goal-oriented *hp*-adaptive finite element method with electromagnetic applications. I.

Electrostatics. *Internat. J. Numer. Methods Engrg.* 2006; **65**(8):1269–1309, doi:10.1002/nme.1488. URL `http://dx.doi.org/10.1002/nme.1488`. (cited in page(s) 2, 3, 14)

[22] Pardo D, Demkowicz L, Torres-Verdín C, Paszynski M. A self-adaptive goal-oriented *hp* finite element method with electromagnetic applications. II. Electrodynamics. *Comput. Methods Appl. Mech. Engrg.* 2007; **196**(37-40):3585–3597, doi:10.1016/j.cma.2006.10.016. URL `http://dx.doi.org/10.1016/j.cma.2006.10.016`. (cited in page(s) 2, 3, 14, 84)

[23] Pardo D. Multigoal-oriented adaptivity for *hp*-finite element methods. *Procedia Computer Science* 2010; **1**(1):1953 – 1961, doi:http://dx.doi.org/10.1016/j.procs.2010.04.219. URL `http://www.sciencedirect.com/science/article/pii/S1877050910002206`. (cited in page(s) 2, 3, 5)

[24] Alvarez-Aramberri J, Pardo D, Barucq H. Inversion of magnetotelluric measurements using multigoal oriented *hp*-adaptivity. *Procedia Computer Science* 2013; **18**:1564 – 1573, doi:http://dx.doi.org/10.1016/j.procs.2013.05.324. URL `http://www.sciencedirect.com/science/article/pii/S1877050913004675`. (cited in page(s) 2, 3)

[25] Panetier J, Ladevèze P, Chamoin L. Strict and effective bounds in goal-oriented error estimation applied to fracture mechanics problems solved with XFEM. *Internat. J. Numer. Methods Engrg.* 2010; **81**(6):671–700, doi:10.1002/nme.2705. URL `http://dx.doi.org/10.1002/nme.2705`. (cited in page(s) 2)

[26] Waeytens J, Chamoin L, Ladevèze P. Guaranteed error bounds on pointwise quantities of interest for transient viscodynamics problems. *Comput. Mech.* 2012; **49**(3):291–307, doi:10.1007/s00466-011-0642-1. URL `http://dx.doi.org/10.1007/s00466-011-0642-1`. (cited in page(s) 2)

[27] Jhurani C, Demkowicz L. Multiscale modeling using goal-oriented adaptivity and numerical homogenization. Part II: Algorithms for the Moore-Penrose pseudoinverse. *Comput. Methods Appl. Mech. Engrg.* 2012; **213/216**:418–426, doi:10.1016/j.cma.2011.06.003. URL `http://dx.doi.org/10.1016/j.cma.2011.06.003`. (cited in page(s) 2)

[28] Jhurani C, Demkowicz L. Multiscale modeling using goal-oriented adaptivity and numerical homogenization. Part I: Mathematical formulation and numerical results. *Comput. Methods Appl. Mech. Engrg.*

2012; **213/216**:399–417, doi:10.1016/j.cma.2011.06.011. URL `http://dx.doi.org/10.1016/j.cma.2011.06.011`. (cited in page(s) 2)

[29] Verdugo F, Díez P. Computable bounds of functional outputs in linear visco-elastodynamics. *Comput. Methods Appl. Mech. Engrg.* 2012; **245/246**:313–330, doi:10.1016/j.cma.2012.06.016. URL `http://dx.doi.org/10.1016/j.cma.2012.06.016`. (cited in page(s) 2)

[30] Van der Zee KG, Van Brummelen EH, Akkerman I, de Borst R. Goal-oriented error estimation and adaptivity for fluid-structure interaction using exact linearized adjoints. *Comput. Methods Appl. Mech. Engrg.* 2011; **200**(37-40):2738–2757, doi:10.1016/j.cma.2010.12.010. URL `http://dx.doi.org/10.1016/j.cma.2010.12.010`. (cited in page(s) 2, 4)

[31] Van der Zee KG, Oden JT, Prudhomme S, Hawkins-Daarud A. Goal-oriented error estimation for Cahn-Hilliard models of binary phase transition. *Numer. Methods Partial Differential Equations* 2011; **27**(1):160–196, doi:10.1002/num.20638. URL `http://dx.doi.org/10.1002/num.20638`. (cited in page(s) 2, 4)

[32] Van der Zee KG, Verhoosel CV. Isogeometric analysis-based goal-oriented error estimation for free-boundary problems. *Finite Elem. Anal. Des.* 2011; **47**(6):600–609, doi:10.1016/j.finel.2010.12.013. URL `http://dx.doi.org/10.1016/j.finel.2010.12.013`. (cited in page(s) 2, 4)

[33] Günther A, Hinze M, Tber MH. A posteriori error representations for elliptic optimal control problems with control and state constraints. *Constrained optimization and optimal control for partial differential equations*, *Internat. Ser. Numer. Math.*, vol. 160. Birkhäuser/Springer Basel AG, Basel, 2012; 303–317, doi:10.1007/978-3-0348-0133-1_17. URL `http://dx.doi.org/10.1007/978-3-0348-0133-1_17`. (cited in page(s) 2, 4)

[34] Hintermüller M, Hoppe R, Löbhard C. Dual-weighted goal-oriented adaptive finite elements for optimal control of elliptic variational inequalities. *ESAIM: Control, Optimisation and Calculus of Variations* 4 2014; **20**:524–546, doi:10.1051/cocv/2013074. URL `http://www.esaim-cocv.org/article_S1292811913000742`. (cited in page(s) 2, 4)

[35] Hintermüller M, Hoppe RH. Goal-oriented adaptivity in pointwise state constrained optimal control of partial differential equations. *SIAM Journal on Control and Optimization* 2010; **48**(8):5468–5487, doi:10.1137/

090761823. URL http://dx.doi.org/10.1137/090761823. (cited in page(s) 2, 4)

[36] Pollock S. Convergence of Goal-Oriented Adaptive Finite Element Methods. PhD Thesis 2012. URL http://gateway.proquest.com/openurl?url_ver=Z39.88-2004&rft_val_fmt=info:ofi/fmt:kev:mtx:dissertation&res_dat=xri:pqm&rft_dat=xri:pqdiss:3509792, thesis (Ph.D.)–University of California, San Diego. (cited in page(s) 2, 5)

[37] Holst M, Pollock S, Zhu Y. Convergence of goal-oriented adaptive finite element methods for semilinear problems. *Computing and Visualization in Science* 2015; **17**(1):43–63, doi:10.1007/s00791-015-0243-1. URL http://dx.doi.org/10.1007/s00791-015-0243-1. (cited in page(s) 2, 5)

[38] Holst M, Pollock S. Convergence of goal-oriented adaptive finite element methods for nonsymmetric problems. *Numerical Methods for Partial Differential Equations* 2016; **32**(2):479–509, doi:10.1002/num.22002. URL http://dx.doi.org/10.1002/num.22002. (cited in page(s) 2, 5)

[39] Mommer MS, Stevenson R. A goal-oriented adaptive finite element method with convergence rates. *SIAM J. Numer. Anal.* 2009; **47**(2):861–886, doi:10.1137/060675666. URL http://dx.doi.org/10.1137/060675666. (cited in page(s) 2, 5)

[40] Feischl M, Praetorius D, Van der Zee KG. An abstract analysis of optimal goal-oriented adaptivity. *SIAM Journal on Numerical Analysis* 2016; **54**(3):1423–1448, doi:10.1137/15M1021982. URL http://dx.doi.org/10.1137/15M1021982. (cited in page(s) 2, 5)

[41] Oden J, Vemaganti KS. Estimation of local modeling error and goal-oriented adaptive modeling of heterogeneous materials: I. Error estimates and adaptive algorithms. *Journal of Computational Physics* 2000; **164**(1):22 – 47, doi:http://dx.doi.org/10.1006/jcph.2000.6585. URL http://www.sciencedirect.com/science/article/pii/S0021999100965859. (cited in page(s) 2)

[42] Vemaganti KS, Oden JT. Estimation of local modeling error and goal-oriented adaptive modeling of heterogeneous materials. II. A computational environment for adaptive modeling of heterogeneous elastic solids. *Comput. Methods Appl. Mech. Engrg.* 2001; **190**(46-47):6089–6124, doi:10.1016/S0045-7825(01)00217-1. URL http://dx.doi.org/10.1016/S0045-7825(01)00217-1. (cited in page(s) 2)

[43] Oden JT, Prudhomme S, Bauman P. On the extension of goal-oriented error estimation and hierarchical modeling to discrete lattice models. *Comput. Methods Appl. Mech. Engrg.* 2005; **194**(34-35):3668–3688, doi:10.1016/j.cma.2004.08.010. URL `http://dx.doi.org/10.1016/j.cma.2004.08.010`. (cited in page(s) 2)

[44] Fuentes D, Littlefield D, Oden JT, Prudhomme S. Extensions of goal-oriented error estimation methods to simulations of highly-nonlinear response of shock-loaded elastomer-reinforced structures. *Comput. Methods Appl. Mech. Engrg.* 2006; **195**(37-40):4659–4680, doi:10.1016/j.cma.2005.10.027. URL `http://dx.doi.org/10.1016/j.cma.2005.10.027`. (cited in page(s) 2)

[45] Romkes A, Oden JT, Vemaganti K. Multi-scale goal-oriented adaptive modeling of random heterogeneous materials. *Mechanics of Materials* 2006; **38**(8–10):859 – 872, doi:http://dx.doi.org/10.1016/j.mechmat.2005.06.028. URL `http://www.sciencedirect.com/science/article/pii/S0167663605001675`, advances in Disordered Materials. (cited in page(s) 2)

[46] Ladevèze P. Upper error bounds on calculated outputs of interest for linear and nonlinear structural problems. *Comptes Rendus Mécanique* 2006; **334**(7):399 – 407, doi:http://dx.doi.org/10.1016/j.crme.2006.04.004. URL `http://www.sciencedirect.com/science/article/pii/S1631072106000702`. (cited in page(s) 2)

[47] Ladevèze P. Strict upper error bounds on computed outputs of interest in computational structural mechanics. *Computational Mechanics* 2008; **42**(2):271–286, doi:10.1007/s00466-007-0201-y. URL `http://dx.doi.org/10.1007/s00466-007-0201-y`. (cited in page(s) 2)

[48] Chamoin L, Ladevèze P. Bounds on history-dependent or independent local quantities in viscoelasticity problems solved by approximate methods. *Internat. J. Numer. Methods Engrg.* 2007; **71**(12):1387–1411, doi:10.1002/nme.1978. URL `http://dx.doi.org/10.1002/nme.1978`. (cited in page(s) 2)

[49] Chamoin L, Ladevèze P. A non-intrusive method for the calculation of strict and efficient bounds of calculated outputs of interest in linear viscoelasticity problems. *Comput. Methods Appl. Mech. Engrg.* 2008; **197**(9-12):994–1014, doi:10.1016/j.cma.2007.09.021. URL `http://dx.doi.org/10.1016/j.cma.2007.09.021`. (cited in page(s) 2)

[50] Chamoin L, Ladevèze P. Strict and practical bounds through a non-intrusive and goal-oriented error estimation method for linear viscoelasticity problems. *Finite Elements in Analysis and Design* 2009; **45**(4):251 – 262, doi:http://dx.doi.org/10.1016/j.finel.2008.10.003. URL `http://www.sciencedirect.com/science/article/pii/S0168874X08001571`, the Twentieth Annual Robert J. Melosh Competition. (cited in page(s) 2)

[51] Ladevèze P, Chamoin L. Calculation of strict error bounds for finite element approximations of non-linear pointwise quantities of interest. *Internat. J. Numer. Methods Engrg.* 2010; **84**(13):1638–1664, doi:10.1002/nme.2957. URL `http://dx.doi.org/10.1002/nme.2957`. (cited in page(s) 2)

[52] Ladevèze P, Pled F, Chamoin L. New bounding techniques for goal-oriented error estimation applied to linear problems. *Internat. J. Numer. Methods Engrg.* 2013; **93**(13):1345–1380, doi:10.1002/nme.4423. URL `http://dx.doi.org/10.1002/nme.4423`. (cited in page(s) 2)

[53] Šolín P, Demkowicz L. Goal-oriented *hp*-adaptivity for elliptic problems. *Comput. Methods Appl. Mech. Engrg.* 2004; **193**(6-8):449–468, doi:10.1016/j.cma.2003.09.015. URL `http://dx.doi.org/10.1016/j.cma.2003.09.015`. (cited in page(s) 3, 21)

[54] Paszyński M, Demkowicz L, Pardo D. Verification of goal-oriented *hp*-adaptivity. *Comput. Math. Appl.* 2005; **50**(8-9):1395–1404, doi:10.1016/j.camwa.2005.03.018. URL `http://dx.doi.org/10.1016/j.camwa.2005.03.018`. (cited in page(s) 3)

[55] Pardo D, Demkowicz L, Torres-Verdín C, Michler C. PML enhanced with a self-adaptive goal-oriented *hp*-finite element method: simulation of through-casing borehole resistivity measurements. *SIAM J. Sci. Comput.* 2008; **30**(6):2948–2964, doi:10.1137/070689796. URL `http://dx.doi.org/10.1137/070689796`. (cited in page(s) 3, 5)

[56] Calo VM, Pardo D, Paszyński MR. Goal-oriented self-adaptive *hp* finite element simulation of 3D DC borehole resistivity simulations. *Procedia Computer Science* 2011; **4**(0):1485 – 1495, doi:http://dx.doi.org/10.1016/j.procs.2011.04.161. URL `http://www.sciencedirect.com/science/article/pii/S1877050911002195`, proceedings of the International Conference on Computational Science, ICCS 2011. (cited in page(s) 3, 5)

[57] Paszyński M, Pardo D, Calo V. Parallel simulations of 3D DC borehole resistivity measurements with goal-oriented self-adaptive *hp* finite element method. *Journal of the Serbian Society for Computational Mechanics/Vol* 2012; **6**(2):1–18. (cited in page(s) 3)

[58] Pardo D, García-Castillo L, Demkowicz L, Torres-Verdín C. A two-dimensional self-adaptive *hp* finite element method for the characterization of waveguide discontinuities. II. Goal-oriented *hp*-adaptivity. *Comput. Methods Appl. Mech. Engrg.* 2007; **196**(49-52):4811–4822, doi:10.1016/j.cma.2007.06.023. URL `http://dx.doi.org/10.1016/j.cma.2007.06.023`. (cited in page(s) 3, 5, 84)

[59] García-Castillo LE, Pardo D, Gómez-Revuelto I, Demkowicz LF. A two-dimensional self-adaptive *hp* finite element method for the characterization of waveguide discontinuities. I. Energy-norm based automatic *hp*-adaptivity. *Comput. Methods Appl. Mech. Engrg.* 2007; **196**(49-52):4823–4852, doi:10.1016/j.cma.2007.06.024. URL `http://dx.doi.org/10.1016/j.cma.2007.06.024`. (cited in page(s) 3, 28)

[60] Garcia-Castillo LE, Pardo D, Demkowicz LF. Energy-norm-based and goal-oriented automatic adaptivity for electromagnetics: Application to waveguide discontinuities. *Microwave Theory and Techniques, IEEE Transactions on* 2008; **56**(12):3039–3049. (cited in page(s) 3, 5, 28)

[61] Gomez-Revuelto I, Garcia-Castillo LE, Salazar-Palma M. Goal-oriented self-adaptive hp-strategies for finite element analysis of electromagnetic scattering and radiation problems. *Progress In Electromagnetics Research* 2012; **125**. (cited in page(s) 3)

[62] Key K, Ovall J. A parallel goal-oriented adaptive finite element method for 2.5-D electromagnetic modelling. *Geophysical Journal International* 2011; **186**(1):137–154. (cited in page(s) 3)

[63] Steffens LM, Parés N, Díez P. Goal-oriented *h*-adaptivity for the Helmholtz equation: error estimates, local indicators and refinement strategies. *Comput. Mech.* 2011; **47**(6):681–699, doi:10.1007/s00466-010-0557-2. URL `http://dx.doi.org/10.1007/s00466-010-0557-2`. (cited in page(s) 3, 49)

[64] Steffens LM, Díez P. A simple strategy to assess the error in the numerical wave number of the finite element solution of the Helmholtz equation. *Comput. Methods Appl. Mech. Engrg.* 2009; **198**(15-16):1389–1400, doi:10.1016/j.cma.2008.12.005. URL `http://dx.doi.org/10.1016/j.cma.2008.12.005`. (cited in page(s) 3, 49)

[65] Dunne T. An Eulerian approach to fluid-structure interaction and goal-oriented mesh adaptation. *Internat. J. Numer. Methods Fluids* 2006; **51**(9-10):1017–1039, doi:10.1002/fld.1205. URL `http://dx.doi.org/10.1002/fld.1205`. (cited in page(s) 3)

[66] Grätsch T, Bathe KJ. Goal-oriented error estimation in the analysis of fluid flows with structural interactions. *Comput. Methods Appl. Mech. Engrg.* 2006; **195**(41-43):5673–5684, doi:10.1016/j.cma.2005.10.020. URL `http://dx.doi.org/10.1016/j.cma.2005.10.020`. (cited in page(s) 3)

[67] Van der Zee KG. Goal-adaptive discretization of fluid–structure interaction. PhD Thesis, Delft University of Technology, http://repository.tudelft.nl June 2009. (cited in page(s) 3, 21, 55)

[68] Van der Zee KG, Van Brummelen EH, de Borst R. Goal-oriented error estimation for stokes flow interacting with a flexible channel. *International Journal for Numerical Methods in Fluids* 2008; **56**(8):1551–1557, doi:10.1002/fld.1652. URL `http://dx.doi.org/10.1002/fld.1652`. (cited in page(s) 3)

[69] Fick PW, Van Brummelen EH, Van der Zee KG. On the adjoint-consistent formulation of interface conditions in goal-oriented error estimation and adaptivity for fluid-structure interaction. *Comput. Methods Appl. Mech. Engrg.* 2010; **199**(49-52):3369–3385, doi:10.1016/j.cma.2010.07.009. URL `http://dx.doi.org/10.1016/j.cma.2010.07.009`. (cited in page(s) 3)

[70] Van der Zee KG, Van Brummelen EH, de Borst R. Goal-oriented error estimation and adaptivity for free-boundary problems: the domain-map linearization approach. *SIAM J. Sci. Comput.* 2010; **32**(2):1064–1092, doi:10.1137/080741227. URL `http://dx.doi.org/10.1137/080741227`. (cited in page(s) 4)

[71] Van der Zee KG, Van Brummelen EH, de Borst R. Goal-oriented error estimation and adaptivity for free-boundary problems: the shape-linearization approach. *SIAM J. Sci. Comput.* 2010; **32**(2):1093–1118, doi:10.1137/080741239. URL `http://dx.doi.org/10.1137/080741239`. (cited in page(s) 4)

[72] Becker R, Kapp H, Rannacher R. Adaptive finite element methods for optimal control of partial differential equations: basic concept. *SIAM J. Control Optim.* 2000; **39**(1):113–132 (electronic),

doi:10.1137/S0363012999351097. URL `http://dx.doi.org/10.1137/S0363012999351097`. (cited in page(s) 4)

[73] Bangerth W, Rannacher R. *Adaptive finite element methods for differential equations*. Lectures in Mathematics ETH Zürich, Birkhäuser Verlag, Basel, 2003. (cited in page(s) 4)

[74] Vexler B, Wollner W. Adaptive finite elements for elliptic optimization problems with control constraints. *SIAM J. Control Optim.* 2008; **47**(1):509–534, doi:10.1137/070683416. URL `http://dx.doi.org/10.1137/070683416`. (cited in page(s) 4)

[75] Hintermüller M, Hoppe RH. Goal-oriented adaptivity in control constrained optimal control of partial differential equations. *SIAM Journal on Control and Optimization* 2008; **47**(4):1721–1743. (cited in page(s) 4)

[76] Hintermüller M, Hoppe RHW, Iliash Y, Kieweg M. An a posteriori error analysis of adaptive finite element methods for distributed elliptic control problems with control constraints. *ESAIM Control Optim. Calc. Var.* 2008; **14**(3):540–560, doi:10.1051/cocv:2007057. URL `http://dx.doi.org/10.1051/cocv:2007057`. (cited in page(s) 4)

[77] Günther A, Hinze M. A posteriori error control of a state constrained elliptic control problem. *J. Numer. Math.* 2008; **16**(4):307–322, doi:10.1515/JNUM.2008.014. URL `http://dx.doi.org/10.1515/JNUM.2008.014`. (cited in page(s) 4)

[78] Meidner D, Rannacher R, Vihharev J. Goal-oriented error control of the iterative solution of finite element equations. *J. Numer. Math.* 2009; **17**(2):143–172, doi:10.1515/JNUM.2009.009. URL `http://dx.doi.org/10.1515/JNUM.2009.009`. (cited in page(s) 4)

[79] Besier M, Rannacher R. Goal-oriented space-time adaptivity in the finite element Galerkin method for the computation of nonstationary incompressible flow. *Internat. J. Numer. Methods Fluids* 2012; **70**(9):1139–1166, doi:10.1002/fld.2735. URL `http://dx.doi.org/10.1002/fld.2735`. (cited in page(s) 4)

[80] Hintermüller M, Hoppe RH. Goal oriented mesh adaptivity for mixed control-state constrained elliptic optimal control problems. *Applied and Numerical Partial Differential Equations*. Springer Netherlands, 2010; 97–111. (cited in page(s) 4)

[81] Dahmen W, Kunoth A, Vorloeper J. *Convergence of adaptive wavelet methods for goal-oriented error estimation*. Springer, 2006. (cited in page(s) 4)

[82] Moon KS, von Schwerin E, Szepessy A, Tempone R. Convergence rates for an adaptive dual weighted residual finite element algorithm. *BIT Numerical Mathematics* 2006; **46**(2):367–407. (cited in page(s) 5)

[83] Sauer-Budge AM, Bonet J, Huerta A, Peraire J. Computing bounds for linear functionals of exact weak solutions to Poisson's equation. *SIAM J. Numer. Anal.* 2004; **42**(4):1610–1630, doi:10.1137/S0036142903425045. URL `http://dx.doi.org/10.1137/S0036142903425045`. (cited in page(s) 5)

[84] Sauer-Budge AM, Peraire J. Computing bounds for linear functionals of exact weak solutions to the advection-diffusion-reaction equation. *SIAM J. Sci. Comput.* 2004; **26**(2):636–652, doi:10.1137/S1064827503427121. URL `http://dx.doi.org/10.1137/S1064827503427121`. (cited in page(s) 5)

[85] Demkowicz L, Kurtz J, Pardo D, Paszyński M, Rachowicz W, Zdunek A. *Computing with hp-adaptive finite elements. Vol. 2. Frontiers: three dimensional elliptic and Maxwell problems with applications*. Applied Mathematics and Nonlinear Science Series, Chapman & Hall/CRC, Boca Raton, FL, 2008. (cited in page(s) 5, 6)

[86] Ovall JS. Asymptotically exact functional error estimators based on superconvergent gradient recovery. *Numerische Mathematik* 2006; **102**(3):543–558, doi:10.1007/s00211-005-0655-9. URL `http://dx.doi.org/10.1007/s00211-005-0655-9`. (cited in page(s) 5)

[87] Darrigrand V, Pardo D, Muga I. Goal-oriented adaptivity using unconventional error representations for the 1D Helmholtz equation. *Computers & Mathematics with Applications* 2015; **69**(9):964 – 979, doi:http://dx.doi.org/10.1016/j.camwa.2015.03.006. URL `http://www.sciencedirect.com/science/article/pii/S0898122115001017`. (cited in page(s) 6, 44)

[88] Darrigrand V, Rodríguez-Rozas A, Pardo D, Muga I, Romkes A, Prudhomme S. Goal-oriented adaptivity using unconventional error representations for the multi-dimensional Helmholtz equation 2017. (accepted in International Journal for Numerical Methods in Engineering). (cited in page(s) 6)

[89] Darrigrand V, Rodríguez-Rozas A, Pardo D, Muga I. Goal-oriented p-adaptivity using unconventional error representations for a 1D steady state convection-diffusion problem. *Procedia Computer Science* 2017; doi:10.1016/j.procs.2017.05.168. (cited in page(s) 6)

[90] Cao W, Demkowicz L. Optimal error estimate of a projection based interpolation for the p-version approximation in three dimensions. *Computers & Mathematics with Applications* 2005; **50**(3):359–366. (cited in page(s) 6)

[91] Demkowicz L. *Computing with hp-adaptive finite elements. Vol. 1. One and two dimensional elliptic and Maxwell problems*. Chapman & Hall/CRC Applied Mathematics and Nonlinear Science Series, Chapman & Hall/CRC, Boca Raton, FL, 2007, doi:10.1201/9781420011692. URL `http://dx.doi.org/10.1201/9781420011692`. (cited in page(s) 6, 21, 23)

[92] Ihlenburg F, Babuška I. Finite element solution of the Helmholtz equation with high wave number. I. The h-version of the FEM. *Comput. Math. Appl.* 1995; **30**(9):9–37, doi:10.1016/0898-1221(95)00144-N. URL `http://dx.doi.org/10.1016/0898-1221(95)00144-N`. (cited in page(s) 6, 49)

[93] Ihlenburg F, Babuška I. Dispersion analysis and error estimation of Galerkin finite element methods for the Helmholtz equation. *Internat. J. Numer. Methods Engrg.* 1995; **38**(22):3745–3774, doi:10.1002/nme.1620382203. URL `http://dx.doi.org/10.1002/nme.1620382203`. (cited in page(s) 6, 49)

[94] Babuška I, Ihlenburg F, Strouboulis T, Gangaraj SK. A posteriori error estimation for finite element solutions of Helmholtz' equation. I. The quality of local indicators and estimators. *Internat. J. Numer. Methods Engrg.* 1997; **40**(18):3443–3462, doi:10.1002/(SICI)1097-0207(19970930)40:18⟨3443::AID-NME221⟩3.3.CO;2-T. URL `http://dx.doi.org/10.1002/(SICI)1097-0207(19970930)40:18<3443::AID-NME221>3.3.CO;2-T`. (cited in page(s) 6, 49)

[95] Babuška I, Ihlenburg F, Strouboulis T, Gangaraj SK. A posteriori error estimation for finite element solutions of Helmholtz' equation. II. Estimation of the pollution error. *Internat. J. Numer. Methods Engrg.* 1997; **40**(21):3883–3900, doi:10.1002/(SICI)1097-0207(19971115)40:21⟨3883::AID-NME231⟩3.0.CO;2-V. URL `http://dx.doi.org/10.1002/(SICI)`

1097-0207(19971115)40:21<3883::AID-NME231>3.0.CO;2-V. (cited in page(s) 6, 49)

[96] Babuška IM, Sauter SA. Is the pollution effect of the FEM avoidable for the Helmholtz equation considering high wave numbers? *SIAM Rev.* 2000; **42**(3):451–484 (electronic), doi:10.1137/S0036142994269186. URL http://dx.doi.org/10.1137/S0036142994269186, reprint of SIAM J. Numer. Anal. *34* (1997), no. 6, 2392–2423 [MR1480387 (99b:65135)]. (cited in page(s) 6, 49)

[97] Oden JT, Prudhomme S, Demkowicz L. A posteriori error estimation for acoustic wave propagation problems. *Arch. Comput. Methods Engrg.* 2005; **12**(4):343–389, doi:10.1007/BF02736190. URL http://dx.doi.org/10.1007/BF02736190. (cited in page(s) 6, 22, 55)

[98] Barucq H, Chaumont-Frelet T, Gout C. Stability analysis of heterogeneous Helmholtz problems and finite element solution based on propagation media approximation. *Math. Comp.* 2017; **86**(307):2129–2157, doi:10.1090/mcom/3165. URL http://dx.doi.org/10.1090/mcom/3165. (cited in page(s) 6)

[99] Barucq H, Bendali A, Fares M, Mattesi V, Tordeux S. A symmetric Trefftz-DG formulation based on a local boundary element method for the solution of the Helmholtz equation. *J. Comput. Phys.* 2017; **330**:1069–1092, doi:10.1016/j.jcp.2016.09.062. URL http://dx.doi.org/10.1016/j.jcp.2016.09.062. (cited in page(s) 6)

[100] Ferreri JC. A note on the steady-state advection-diffusion equation. *International Journal for Numerical Methods in Fluids* 1985; **5**(6):593–596, doi:10.1002/fld.1650050608. URL http://dx.doi.org/10.1002/fld.1650050608. (cited in page(s) 6)

[101] Kuzmin D, Korotov S. Goal-oriented a posteriori error estimates for transport problems. *Mathematics and Computers in Simulation* 2010; **80**(8):1674–1683. (cited in page(s) 6)

[102] Almeida RC, Oden JT. Solution verification, goal-oriented adaptive methods for stochastic advection-diffusion problems. *Comput. Methods Appl. Mech. Engrg.* 2010; **199**(37-40):2472–2486, doi:10.1016/j.cma.2010.04.001. URL http://dx.doi.org/10.1016/j.cma.2010.04.001. (cited in page(s) 6)

[103] Parés N, Díez P, Huerta A. Computable exact bounds for linear outputs from stabilized solutions of the advection-diffusion-reaction equation. *Internat. J. Numer. Methods Engrg.* 2013; **93**(5):483–509, doi:10.1002/nme.4396. URL `http://dx.doi.org/10.1002/nme.4396`. (cited in page(s) 6)

[104] Collier N, Radwan H, Dalcin L, Calo VM. Time adaptivity in the diffusive wave approximation to the shallow water equations. *Journal of Computational Science* 2013; **4**(3):152–156. (cited in page(s) 6, 84)

[105] Gedicke J, Carstensen C. A posteriori error estimators for convection-diffusion eigenvalue problems. *Comput. Methods Appl. Mech. Engrg.* 2014; **268**:160–177, doi:10.1016/j.cma.2012.09.018. URL `http://dx.doi.org/10.1016/j.cma.2012.09.018`. (cited in page(s) 6)

[106] Balay S, Abhyankar S, Adams MF, Brown J, Brune P, Buschelman K, Dalcin L, Eijkhout V, Gropp WD, Kaushik D, *et al.*. PETSc Web page. `http://www.mcs.anl.gov/petsc` 2015. URL `http://www.mcs.anl.gov/petsc`. (cited in page(s) 19)

[107] Babuška I, Rheinboldt WC. Error estimates for adaptive finite element computations. *SIAM Journal on Numerical Analysis* 1978; **15**(4):736–754, doi:10.1137/0715049. URL `http://dx.doi.org/10.1137/0715049`. (cited in page(s) 21)

[108] Becker R, Rannacher R. An optimal control approach to a posteriori error estimation in finite element methods. *Acta Numer.* 2001; **10**:1–102, doi:10.1017/S0962492901000010. URL `http://dx.doi.org/10.1017/S0962492901000010`. (cited in page(s) 21)

[109] Giles MB, Süli E. Adjoint methods for PDEs: a posteriori error analysis and postprocessing by duality. *Acta Numer.* 2002; **11**:145–236, doi:10.1017/S096249290200003X. URL `http://dx.doi.org/10.1017/S096249290200003X`. (cited in page(s) 21)

[110] Gaspoz FD, Morin P. Convergence rates for adaptive finite elements. *IMA J. Numer. Anal.* 2009; **29**(4):917–936, doi:10.1093/imanum/drn039. URL `http://dx.doi.org/10.1093/imanum/drn039`. (cited in page(s) 21)

[111] Becker R, Estecahandy E, Trujillo D. Weighted marking for goal-oriented adaptive finite element methods. *SIAM J. Numer. Anal.* 2011; **49**(6):2451–2469, doi:10.1137/100794298. URL `http://dx.doi.org/10.1137/100794298`. (cited in page(s) 21)

[112] Demkowicz L, Babuška I. p interpolation error estimates for edge finite elements of variable order in two dimensions. *SIAM J. Numer. Anal.* 2003; **41**(4):1195–1208, doi:10.1137/S0036142901387932. URL `http://dx.doi.org/10.1137/S0036142901387932`. (cited in page(s) 21, 23)

[113] Steffens LM, Parés N, Díez P. Estimation of the dispersion error in the numerical wave number of standard and stabilized finite element approximations of the Helmholtz equation. *Internat. J. Numer. Methods Engrg.* 2011; **86**(10):1197–1224, doi:10.1002/nme.3104. URL `http://dx.doi.org/10.1002/nme.3104`. (cited in page(s) 49)

[114] Ainsworth M. Discrete dispersion relation for *hp*-version finite element approximation at high wave number. *SIAM J. Numer. Anal.* 2004; **42**(2):553–575, doi:10.1137/S0036142903423460. URL `http://dx.doi.org/10.1137/S0036142903423460`. (cited in page(s) 55)

[115] Romkes A, Oden J. Adaptive modeling of wave propagation in heterogeneous elastic solids. *Computer Methods in Applied Mechanics and Engineering* 2004; **193**(6–8):539 – 559, doi:http://doi.org/10.1016/j.cma.2003.10.014. URL `http://www.sciencedirect.com/science/article/pii/S0045782503005772`. (cited in page(s) 60, 89)

[116] Pardo D, Matuszyk P, Muga I, Torres-Verdín C, Mora A, Calo VM. Simulation of wireline sonic logging measurements acquired with borehole–eccentered tools using a high-order adaptive finite-element method. *Journal of Computational Physics* 2011; **230**(16):6320 – 6333, doi:http://dx.doi.org/10.1016/j.jcp.2011.04.028. URL `http://www.sciencedirect.com/science/article/pii/S0021999111002762`. (cited in page(s) 71, 84)

[117] Matuszyk PJ, Torres-Verdín C, Pardo D. Frequency-domain finite-element simulations of 2D sonic wireline borehole measurements acquired in fractured and thinly bedded formations. *Geophysics* 2013; **78**(4):D193–D207, doi:10.1190/geo2012-0397.1. URL `http://dx.doi.org/10.1190/geo2012-0397.1`. (cited in page(s) 71, 84)

[118] Matuszyk PJ, Torres-Verdín C. Frequency-domain simulation of logging-while-drilling borehole sonic waveforms. *Geophysics* 2014; **79**(2):D99–D113, doi:10.1190/geo2013-0279.1. URL `http://dx.doi.org/10.1190/geo2013-0279.1`. (cited in page(s) 71, 84)

[119] Alvarez-Aramberri J, Pardo D, Barucq H. A secondary field based *hp*-Finite Element Method for the simulation of magnetotelluric

measurements. *Journal of Computational Science* 11 2015; **11**:137–144, doi:http://doi.org/10.1016/j.jocs.2015.02.005. URL `http://www.sciencedirect.com/science/article/pii/S1877750315000150`. (cited in page(s) 71)

[120] Verdugo F, Parés N, Díez P. Goal-oriented space-time adaptivity for transient dynamics using a modal description of the adjoint solution. *Comput. Mech.* 2014; **54**(2):331–352, doi:10.1007/s00466-014-0988-2. URL `http://dx.doi.org/10.1007/s00466-014-0988-2`. (cited in page(s) 84)

[121] Bazilevs Y, Calo VM, Cottrell JA, Evans JA, Hughes T, Lipton S, Scott M, Sederberg T. Isogeometric analysis using T-splines. *Computer Methods in Applied Mechanics and Engineering* 2010; **199**(5):229–263. (cited in page(s) 84)

[122] Dedè L, Santos H. B-spline goal-oriented error estimators for geometrically nonlinear rods. *Computational Mechanics* 2012; **49**(1):35–52, doi:10.1007/s00466-011-0625-2. URL `http://dx.doi.org/10.1007/s00466-011-0625-2`. (cited in page(s) 84)

[123] Kuru G, Verhoosel CV, Van der Zee KG, van Brummelen EH. Goal-adaptive Isogeometric Analysis with hierarchical splines. *Comput. Methods Appl. Mech. Engrg.* 2014; **270**:270–292, doi:10.1016/j.cma.2013.11.026. URL `http://dx.doi.org/10.1016/j.cma.2013.11.026`. (cited in page(s) 84)

[124] Rodríguez-Rozas Á, Pardo D. A priori Fourier analysis for 2.5D finite elements simulations of Logging-While-Drilling (LWD) resistivity measurements. *Procedia Computer Science* 2016; **80**:782 – 791, doi:http://dx.doi.org/10.1016/j.procs.2016.05.368. URL `http://www.sciencedirect.com/science/article/pii/S1877050916308432`. (cited in page(s) 84)

[125] D'Angella D, Zander N, Kollmannsberger S, Frischmann F, Rank E, Schröder A, Reali A. Multi-level *hp*-adaptivity and explicit error estimation. *Advanced Modeling and Simulation in Engineering Sciences* 2016; **3**(1):33, doi:10.1186/s40323-016-0085-5. URL `http://dx.doi.org/10.1186/s40323-016-0085-5`. (cited in page(s) 85)

Acronyms

FEM Finite Element Method

PDE Partial Differential Equation

GOA Goal-Oriented Adaptivity

DWR Dual Weighted Residual

DoF Degrees of Freedom

QoI Quantity of Interest

PBI Projection Based Interpolation

LWD Logging While Drilling

PML Perfectly Matched Layer